University of Cape Town

Department of Electrical Engineering

INDUCTION MOTOR VARIABLE SPEED DRIVE PERFORMANCE AND IMPACT ON ENERGY SAVINGS

Prepared by : Siboniso T. Khumalo (candidate)

Prepared for : Prof. P. Pillay (supervisor)

Report submitted to the University of Cape Town in fulfillment of the degree of Master of Science in Engineering

December 2001

Declaration

I, Siboniso T. Khumalo, submit this thesis in fulfillment of the requirements of the degree of Master of Science in Engineering. I claim that this is my original work and that it has not been submitted in this or in a similar form for a degree at any other University.

signature removed

Mr. Siboniso.T. Khumalo BSc.(ENG) UCT

...FRI...day of ...14/12/...200..1...

Acknowledgements

The author wishes to thank the following people for their invaluable contribution towards the success of this project:

- Prof Pragasen Pillay, my thesis project supervisor for his support, supervision and for making this project possible,
- UCT Machines Research Group: Azeem, Huey, Marubini, Dave, Lotten and the Chief Technical Officer Chris, who were always willing to help when needed and who made my time spent at UCT pleasant.
- My best friends: Buhle, Mavo, Sipho and Craig who always provided good support and courage.
- My family at home for their continuous warm support and comfort they provided during the project period and
- To ESKOM for their continuous financial support.

Terms Of Reference

This project was commissioned by Prof. Pragasen Pillay, Department of Electrical Engineering, University of Cape Town. Prof. Pillay requested a study of the impact of unbalance voltage supplies with under or overvoltages on induction motor drives, to aid ESKOM's Demand Side Management and Power Quality studies.

The project was undertaken according to the following specifications:

1. Construct and commission two test beds for Induction Motor VSD performance testing.

2. Develop PSpice models for the test beds.

3. Determine and document the effects of unbalanced supplies on induction machine VSDs.

4. Evaluate the correct method of calculating energy savings for the application of VSDs to centrifugal loads.

5. Quantify the effects of cable mismatch on VSDs.

SYNOPSIS

ESKOM, together with Municipalities distribute power at a line-to-line voltage of 400+/-10%. Hence in theory, the user ends up with a voltage of 340 to 440. In urban areas 2% voltage unbalance is considered acceptable, while 3% voltage unbalance is considered acceptable for rural areas. The combined effects of under or overvoltages coupled with "acceptable maximum" voltage unbalance is not understood or documented.

This project is a comprehensive study of the effects of voltage unbalance in combination with under or overvoltages on induction machines (IM) variable speed drives. In addition the performance with PWM inverters connected to IM via long cables is also studied. The project starts by an evaluation of previous work on the subject and related topics. Relevant conclusions are made based on the literature review in Chapter One. The second step of the project was to develop two test beds in the UCT Machine's Laboratory. The test beds are for performance testing of low (up to 15kW) and medium (up to 75kW) power IM and their VSDs. The test bed losses are determined at 4 different operating points and documented.

Several tests such as the blocked rotor and no load tests were undertaken to determine the machine parameters. A PSpice simulation model was developed and tested for the low voltage test bed. The test results compared well to simulation predictions.

Furthermore, tests under unbalanced and overvoltage conditions were performed and the results verified with simulations. This proves that the developed PSpice model can reliably simulate the actual test bed for both balanced and unbalanced conditions.

SYNOPSIS

Moreover, it can be easily applied to model different size machines and drives. The information required includes: the motor parameters, drive dc-link parameters, modulation ratio (ma) and the switching frequency.

The impact of voltage unbalance in drives with long cables between the inverter and motor is examined. A 36m long, 4-core, PVC insulated cable is used on the low voltage test bed for a case study. The model used for the cable is a lumped parameter model. The IM model is also taken from the literature to include a high frequency branch, to model the reflected voltage wave phenomenon.

A basic analysis of energy savings in pumps and fans load associated with the application of variable speed drives is also done. Boiler feed-pumps from Tutuka power station are used as a case study that may be replicated for other applications in utilities or industry. The developed Excel Spreadsheet program to project the value of savings and determine the payback period is compared to an ABB program. The two results agree within an acceptable range. Therefore, the knowledge of the pumping system specifications and the cost of energy in kWh with the Energy Savings Program would enable one to project energy savings.

List of Figures

Page

Figure 1.1: Drive elements 2
Figure 1.2: NEMA motor design curve 6
Figure 2.1: Low power machine test bed 17
Figure 2.2 AC drive with measuring instruments 18
Figure 2.3: Four-quadrant dc drive for the dc-dynamometer 18
Figure 2.4: 3kW IM Test Bed 19
Figure 2.5: IM Equivalent per phase circuit 20
Figure 2.6: Torque-Speed curves for a 3kW EE IM 21
Figure 2.7: Voltage boost to compensate for the stator drop 25
Figure 2.8: IM T-Speed characteristics with voltage boost 25
Figure 2.9: Impact of voltage boost at 25Hz 26
Figure 2.10: Test bed efficiency curves 27
Figure 2.11: Medium power test bed 29
Figure 2.12 Induction motor, 75kW VSD on the supply panel 29
Figure 2.13: Schematic representation of the 75kW drive set 30
Figure 2.14: Armature voltage vs. Current 31
Figure 2.15: Mechanical losses of the large test bed machines 35
Figure: 2.16 Torque-Speed characteristic of a 75kW IM 36
Figure 3.1: PSpice model block diagram 37
Figure 3.2: IM drive system 38
Figure 3.3: The effect of *ma* on voltage control 40
Figure 3.4: Mains three-phase line-to-line voltage supply 42
Figure 3.5: Rectifier currents, simulated and measured, respectively 43
Figure 3.6: Simulated dc-link voltage at balanced conditions 44
Figure 3.7: Measured dc-link voltage at balanced conditions 44
Figure 3.8: Measured and simulated inverter currents 45
Figure 3.9: Measured inverter voltage waveform 45
Figure 3.10: Simulated inverter output voltage 46
Figure 3.11: Machine's lab generated three-phase line-to-line voltage supply 47
Figure 3.12: Mains three-phase voltage supply with unbalance 50
Figure 3.13: Measured rectifier current waveform 52
Figure 3.14: Simulated rectifier current waveform 52

List of Figures

Page

Figure 3.15: Measured dc-link voltage showing effects of unbalance 54
Figure 3.16: Simulated dc-link voltage showing effects of unbalance 54
Figure 3.18: Measured inverter output voltage waveform 55
Figure 3.19: Simulated inverter output voltage waveform 56
Figure 3.20: Rectifier currents, measured and simulated, respectively 57
Figure 3.21: Supply voltage peaks for zero, 1%, 3% and 5% voltage unbalance 58
Figure 3.22: Dc-link voltage for balanced voltage supply up-to 5% voltage unbalances . 59
Figure 3.23: Three-phase diode rectifier 60
Figure 3.24: Forward biased rectifier diodes conducting 61
Figure 3.25: Dc-link voltage for balanced and 1% unbalance voltage supply 62
Figure 3.26: Diode currents for 1% unbalanced voltage supply 63
Figure 3.27: 2% Voltage unbalance, resultant dc-link voltage and currents 63
Figure 3.28: Current through Diode 1, 3 and 5 65
Figure 3.29: Inverter output peak voltage 67
Figure 4.1: Inverter output voltage "Train of pulses" 71
Figure 4.2: Transient over-voltage at switching for one phase 71
Figure 4.3: Voltage reflection diagram 72
Figure 4.4: Voltage at induction motor terminals 73
Figure 4.5: General supply-drive-motor layout 75
Figure 4.6: Per phase cable parameter model 76
Figure 4.7: Dc-voltage step response waveforms 77
Figure 4.8: Differential mode motor model 79
Figure 4.9: Measured inverter output and IM terminal voltage 81
Figure 4.10: Measured inverter output and IM terminal line-to-line voltages 84
Figure 4.11: A closer view of Figure 4.10 84
Figure 4.12: Simulated inverter output and IM terminal line-to-line voltages 85
Figure 4.13: Simulated IM line current 85
Figure 4.14 Measured IM line current 86
Figure 4.15: Modified cable model 87
Figure 4.16: RLC high frequency branch 88
Figure 4.17: Simulated volt-drop across the cable 89
Figure 4.18: Measured volt-drop across the cable 90

List of Figures

Page

Figure 4.19: Simulated IM line current 91
Figure 4.20: Measured IM current 91
Figure 4.21: Simulated rectifier current for line A 95
Figure 4.22: Measured rectifier current for line A 95
Figure 4.23: Measured dc-link voltage waveform 96
Figure 4.24: Simulated dc-link voltage waveform 96
Figure 4.25: Simulated inverter output current 97
Figure 4.26: Measured inverter output current 98
Figure 4.27: Simulated IM terminal current 98
Figure 4.28: Measured IM terminal current 98
Figure 4.29: Reflected voltage peak 99
Figure 4.30: Average dc-link voltage and ripple 100
Figure 4.31: Percentage voltage drop along the cable 101
Figure 4.32: First three reflected wave peaks 103
Figure 5.1: Annual duty cycle of a water pumping plant 108
Figure 5.2: Pump curve showing operating point 110
Figure 5.3: Shaft power curve superimposed on pump characteristic curves 115
Figure 5.4: Operating point by valve flow control 116
Figure 5.5: Pump curve showing three operating points 116
Figure 5.6: Design system curve and operating point affinity curve 118

APPENDICES

Figure A3.1: Three-Phase Induction Motor in Star Connection load mode I137
Figure A3.2: Diode D1 current from zero to 5% LVUR 139
Figure A3.3: Diode D3 current from zero to 5% LVUR 139
Figure A3.4: Diode D5 current from zero to 5% LVUR 139
Figure A4.1: Dc-step response test schematic 140
Figure A4.2: Line-to-neutral three-phase unbalanced supply voltage 140

List of Tables

Page

Table 2.1: Predicted and actual operating points 22
Table 2.2: Calculated rotor current and stator volt-drop 24
Table 2.3 Motor terminal voltages with and without V-boost 24
Table 2.4: Mechanical power losses [W] 27
Table 2.5: Power flow 27
Table 2.6: Measured voltage drop over armature 31
Table 2.7: Galvanometer results of armature resistance 32
Table 2.8: Medium power test bed mechanical loss data for the cold state 33
Table 2.9: Medium power test bed mechanical loss data for the warm state 33
Table 2.10: Medium power test bed mechanical loss data with one motor decoupled 34
Table 2.11: Parameters for the 75kW IM 35
Table 3.1: PSpice input parameters 40
Table 3.2: Rectifier current comparison 43
Table 3.3: Dc-link voltage comparison 43
Table 3.4: Inverter current comparison 44
Table 3.5: Inverter output line-to-line voltage comparison 45
Table 3.6: Rectifier current harmonic comparison for the mains supply 46
Table 3.7: Comparison of simulated and measured results for the lab voltage supply 48
Table 3.8: Rectifier current harmonic comparison for the big generator set 49
Table 3.9: Unbalance line-to-neutral voltages 51
Table 3.10: Rectifier line currents showing the effect of unbalance 53
Table 3.11: Dc-link voltage showing the effects of voltage unbalance 53
Table 3.12: Inverter output line-to-line voltage 55
Table 3.13: Inverter output line currents 56
Table 3.14: Average dc-link voltage 59
Table 3.15: Rectifier line currents as a function of LUVR 65
Table 3.16: Inverter line-to-line voltage 66
Table 3.17: Induction motor line currents 68
Table 4.1: Cable specifications 76
Table 4.2: Cable parameters 79
Table 4.3: Motor model parameters 83
Table 4.4: Balanced voltage supply reflected voltage 83

List of Tables

Page

Table 4.5: Balanced supply IM line currents 85
Table 4.6: Balanced voltage supply reflected voltage 89
Table 4.7: IM terminal current 90
Table 4.8: Improved cable model reflected voltage summary 92
Table 4.9: Dc-link voltage with modified model 93
Table 4.10: Revised cable inverter and IM currents 93
Table 4.11: Rectifier line currents 94
Table 4.12: Dc-link voltage analysis 96
Table 4.13: Inverter and IM currents 97
Table 4.14: Reflected peak voltages 99
Table 4.15: Percentage ripple with increasing %LUVR 100
Table 4.16: Supply voltage with 5% LUVR and 10% overvoltage 102
Table 4.17: Supply voltage with 5% LUVR and 10% undervoltage 102
Table 4.18: pu reflected voltage 103
Table 4.19: Dc-link voltage (10% overvoltage and 5% LUVR) 104
Table 4.20: Dc-link voltage (10% undervoltage and 5% LUVR) 104
Table 4.21: Inverter and IM currents 105
Table 5.1: Energy cost based on ESKOM's 2000 tariffs 120
Table 5.2 Electrical energy cost per annum: Constant speed operation 120
Table 5.3: Electrical power cost per annum: Variable speed operation 121
Table 5.4: Energy and cost savings 122
Table 5.5: ABB and ESS program result comparison 122
Table 5.6: Electrical energy cost per annum: Constant speed operation 124
Table 5.7: Electrical power cost per annum: Variable speed operation 125
Table 5.8: Energy and cost savings 126

APPENDICES

Table A2.1: AC circuit nameplate 135
Table A2.2: DC circuit nameplate 135
Table A2.3: Load cell nameplate 135
Table A2.4: IM Nameplate 136

List of Tables

Page

Table A2.5: 75kW IM drive nameplate 136
Table A3.1: Three-phase line-to-line voltages as a function of unbalance 138
TABLE A5.1: Parameter input window 143
Table A5.2: Spreadsheet LDC input table 143
TABLE A5.4: Equipment costs for the first case study 144
TABLE A5.5: Equipment log for the second case study 144

TABLE OF CONTENTS

Page

Acknowledgements ..... *iii*

Terms of Reference ..... *iv*

Synopsis ..... *v*

List of Figures ..... *vii*

List of Tables ..... *x*

CHAPTER ONE Literature Review

1.1 INTRODUCTION 1

1.2 VARIABLE SPEED CLASSIFICATION 2

1.2.1Machine type 2

1.2.2Power rating 3

1.2.3Power source 3

1.2.4Control strategy 3

1.3 PWM (Pulse Width Modulation) 3

1.4 VARIABLE SPEED DRIVE APPLICATIONS 3

1.4.1 Process control 4

1.4.2 Energy savings 4

1.4.3 VSD application in power stations 4

1.5 BENEFITS OF USING VARIABLE SPEED DRIVES 5

1.6 INDUCTION MOTOR DRIVE PERFORMANCE 6

1.6.1 Symptoms of voltage unbalance 6

1.6.2 Effect of PWM on low voltage induction machines 6

1.6.3Harmonics 7

1.7 POWER QUALITY 7

1.7.1 Power quality measurable quantities 7

1.7.2 Sequence components 8

1.7.3 Unsymmetrical voltage conditions 10

1.7.4 Voltage unbalance definitions 10

1.8 SOURCES OF POWER QUALITY PROBLEMS 11

1.9 LITERATURE SEARCH FINDINGS 13

1.10 CONTRIBUTION OF THIS THESIS 14

TABLE OF CONTENTS

Page#

CHAPTER TWO Test Bed Development

2.1 INTRODUCTION 15
2.2 TEST BEDS OBJECTIVES 15
2.3 TEST BED CHARACTERISTIC 16
2.4 LOW POWER TEST DRIVE 16
2.4.1 System overview 16
2.4.2 System components 17
2.4.3 Basic instrumentation 17
2.5 TEST BED DESCRIPTION 19
2.5.1 Circuit description 19
2.5.2 Circuit operation 19
2.6 OPERATING POINT DETERMINATION 20
2.7 VOLTAGE BOOST REQUIRED AT LOW FREQUENCIES 22
2.7.1 Voltage boost for the pump curve 23
2.7.2 IM torque-speed characteristics with voltage boost 25
2.8 TEST RESULTS 26
2.8.1 Power losses of the 3kW-Test bed 26
2.8.2 Efficiency 27
2.9 MEDIUM POWER INDUCTION MOTOR DRIVE TEST BED 28
2.9.1 System equipment 28
2.10 DESCRIPTION OF THE 75 KW IM AND VSD TEST BED 29
2.11 TEST RESULTS 30
2.11.1 I^2R and brush losses of 250 kW dc machine 30
2.11.2 Mechanical losses of the 250kW dc and sync machines 32
2.12 INDUCTION MOTOR (75KW) INSTALLATION 35
2.13 CONCLUSION 36

TABLE OF CONTENTS

Page

CHAPTER THREE Drive Model Development and Simulation

3.1 INTRODUCTION 37
3.2 DRIVE MODEL DEVELOPMENT 37
3.2.1 Simulation model 37
3.2.2 Load model 38
3.3 MODEL PARAMETERS 39
3.4 EXPERIMENTAL PROCEDURE 41
3.5 CORRELATION OF TEST BED AND SIMULATION FOR THE MAINS VOLTAGE SUPPLY 41
3.5.1 Current and voltage comparison 42
3.5.2 Rectifier current harmonics comparison 46
3.6 CORRELATION OF TEST BED AND SIMULATION FOR THE LAB GENERATED VOLTAGE SUPPLY 47
3.6.1 Current and voltage comparison 47
3.6.2 Rectifier current harmonics comparison 49
3.7 CORRELATION OF TEST BED AND SIMULATION FOR AN UNBALANCE MAINS VOLTAGE SUPPLY 50
3.71 Impact of voltage unbalance on rectifier current 52
3.7.2 Impact of voltage unbalance on dc-link voltage 53
3.7.3 Impact of voltage unbalance on inverter output voltage 55
3.7.4 Impact of voltage unbalance on inverter output current 56
3.8 VOLTAGE UNBALANCE SIMULATION OF IM VSD 57
3.8.1 Three-phase voltage supply 57
3.8.2 Dc-link voltage 58
3.9 RECTIFIER CURRENT EVALUATION 60
3.9.1 Peak to peak rectifier current 60
3.9.2 Impact of unbalance voltage on rectifier current waveform 64
3.10 INVERTER OUTPUT VOLTAGE AND CURRENT 66
3.10.1 Inverter line-to-line output voltage 66
3.10.2 Inverter line current 68
3.11CONCLUSION 68

TABLE OF CONTENTS

Page

CHAPTER FOUR Impact Of Long Cables In PWM Drives

4.1 INTRODUCTION 70
4.2 REFLECTED WAVE PHENOMENON (RWP) 70
4.2.1 RWP analysis 70
4.2.2 Causes of reflected waves in cable leads 73
4.2.3 Variables affecting reflected wave magnitude 74
4.3 CABLE CHARACTERISTIC IMPEDANCE 74
4.3.1 Cable parameters 75
4.4 MOTOR MODEL 79
4.5 MOTOR PARAMETERS 80
4.6 SIMULATED AND MEASURED TEST RESULTS 83
4.6.1 Cable voltage drop and IM line currents comparison 83
4.6.2 Discussion 86
4.7 CABLE MODEL REVISION/ MODIFICATION 86
4.8 ANALYSIS OF THE REVISED CABLE MODEL FOR A BALANCED VOLTAGE SUPPLY 89
4.9 PARAMETRIC STUDY BASED ON THE MODIFIED CABLE MODEL 91
4.9.1 Analysis of the 36m-cable test and simulation result 92
4.10 IMPACT OF CABLE LENGTH UNDER UNBALANCED SUPPLIES 93
4.10.1 Rectifier current 94
4.10.2 Dc-link voltage 95
4.10.3 Inverter output and IM currents 97
4.11 PARAMETRIC STUDY FOR INCREASING %LUVR 99
4.12 WORST CASE CONSIDERATION 101
4.12.1 Reflected voltage peaks 102
4.12.2 Effect of 10% overvoltage with 5% LUVR on dc-link voltage 103
4.12.3 Effect of 10% undervoltage with 5% LUVR on dc-link voltage 104
4.12.4 Inverter and IM currents 104
4.13 CONCLUSION 105

CHAPTER FIVE Energy Savings of a Pump Drive

5.1 INTRODUCTION 107
5.2 VSD BENEFITS 107
5.3 VSD CANDIDATE IDEMTIFICATION 108
5.4 JUSTIFICATION FOR VSD INVESTMENT 109
5.5 ENERGY UTILIZATION POINT 109
5.6 HOW VSDs SAVE ENERGY 110
5.7 PROCESS SYSTEM MODELING 111
5.7.1 Pump performance curve 111
5.7.2 Process lines 112
5.7.3 Affinity curve 113
5.7.4 Shaft power curve 114
5.8 APPLICATION OF AFFINITY LAWS 115
5.9 RAND ENERGY SAVINGS 118
5.9.1 Cost of energy for constant speed operation 120
5.9.2 Cost of energy for variable speed operation 121
5.9.3 Energy saved 121
5.10 ABB AND ESS ENERGY SAVINGS PROGRAM COMPARISON 122
5.11 INVESTMENT PAYBACK PERIOD FOR TUTUKA P/S 123
5.12 EXAMPLE TO VERIFY THE ENERGY SAVINGS SPREADSHEET 124
5.12.1 Cost of energy for constant speed operation 124
5.12.2 Cost of energy for variable speed operation 125
5.12.3 ABB and ESS energy savings program comparison 125
5.12.4 Investment payback period for the selected example 126
5.13 CONCLUSION 126

CHAPTER SIX Conclusions and Recommendations

6.1 Conclusions 128
6.2 Recommendations 131
REFERENCES 132
APPENDICES 135
APPENDIX A2 135
APPENDIX A3 137
APPENDIX A4 140
APPENDIX A5 141

CHAPTER ONE

Literature Review

1.1 INTRODUCTION

The three-phase supply to industrial, commercial and residential power systems, where induction machines are widely used, should ideally be balanced. Electrical power is generated at power stations and transformed to high voltage for transmission. The transmission and subsequent distribution process introduces unsymmetrical conditions to the power supply. Hence, unbalanced voltages and under or overvoltage are present at the point of common coupling and/ or at the loads. Additional power quality problems are introduced by current harmonics due to variable speed drives (VSD's) and other nonlinear loads. Induction motors, which use up to 64% of generated electricity in the US and SA, are subjected to these unbalanced and/ or distorted voltage conditions [1]. This can result in increased thermal stresses and rotor losses followed by loss of life of the motors. Moreover, the presence of voltage unbalance can cause control circuits to malfunction.

The analysis of the operation of rectifiers and their effects on power systems can be found in standard textbooks. However, most analyses are conducted with the assumption of a balanced input power supply [2]. This condition is not necessarily true in many practical industrial systems, particularly in the presence of the nonlinear loads.

The percentage of industrial motors operated from variable speed drives is steadily increasing. A drive consists of the motor, power electronics, control electronics and transducers, which is used to control the speed, torque or position of a motor. Figure 1.1 illustrates the drive elements. This includes,

- The load, e.g. conveyor belt system or feed water pumps
- Electrical machine, e.g. induction motor
- Power electronic converter
- Controller

- Power source

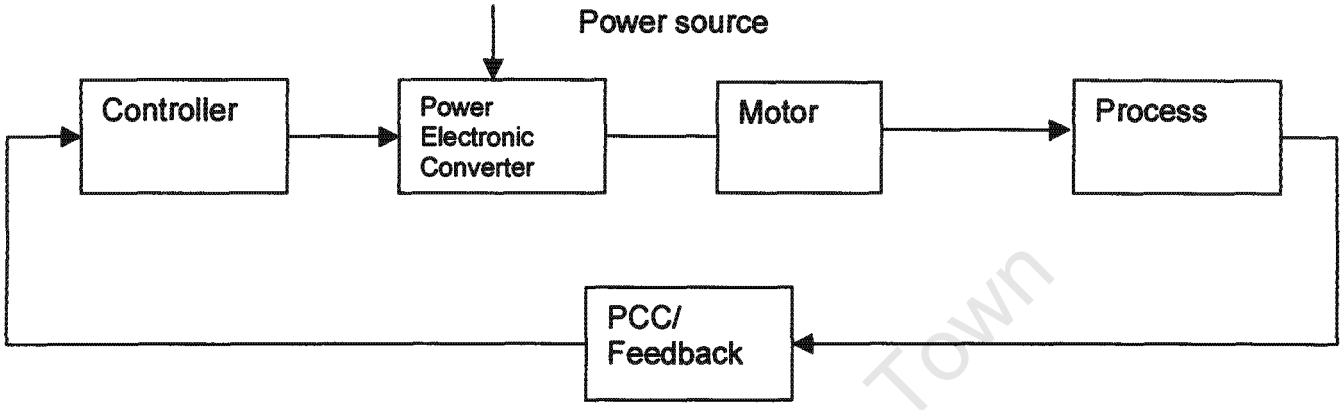

Figure 1.1: Drive elements

Drives may use various techniques to control motor speed, torque or position. A moderate low-cost drive makes use of several types of power transistors (IGBTs). These transistors are switched rapidly On and Off in a technique known as Pulse Width Modulation (PWM). The voltage source inverters (VSI) with PWM switching are at present most widely used. The PWM inverter is controlled such that it supplies a sequence of pulses, which as far as possible simulates a sine wave of the desired frequency.

1.2 VARIABLE SPEED DRIVE CLASSIFICATION

Variable speed drives are classified in a number of ways, this could include their design topology, the type of machine they drive and/ or power rating.

1.2.1 Machine type

VSDs could be classified according to the type of electrical machine they drive. The most common drives are:

- DC machine's drive (DCMD)
- Induction machine drives (IMD)

- Synchronous machine drives (SMD)
- Switched reluctance machine drives (SRMD)

1.2.2 Power rating

This classification includes,

- Small drives (up to 75kW)
- Medium size drives (from +75kW to 600kW)
- Large drives (greater than 0.6 MW) [3]

1.2.3 Converter topology

- Voltage source converters
- Current source converters

1.2.4 Control strategy

- Open loop PWM
- Space vector
- Direct torque control

1.3 PULSE WIDTH MODULATION (PWM)

A transistor allows a precise amount of current to flow through to the motor. As this transistor is rapidly switched On and Off, the amount of current, which flows through the motor, is dependent upon the ratio between on-time and off-time. This ratio is known as the Duty ratio. The larger this ratio the more current will flow. The power electronic device is pulsed, hence the term PWM.

1.4 VARIABLE SPEED DRIVE APPLICATIONS

The use of VSDs differs from industry to industry, depending on the production process and the requirements of the particular plant or system.

1.4.1 Process control

One of the fundamental purposes of VSDs is to achieve improved process control without compromising the output quality. This is achieved by controlling the speed of the load.

1.4.2 Energy savings

The potential for reduced energy consumption, lies in the retrofitting of variable speed drives (VSD), so as to eliminate the significant auxiliary mechanical losses which apply to fixed speed drives. Each installation needs a detailed account of the benefits and disadvantages of VSD [4]. Benefits are more noticeable or significant in applications where pumps, fans and compressors are the driven loads. This is because when a pump speed is changed and the affinity laws are correctly applied, the pump efficiency stays approximately constant. Furthermore, these energy and costs savings are more apparent in large rated drives in the order of 2MW [4], although they can be attractive even in medium and small size applications.

1.4.3 VSD applications in power stations

The synchronous motor and the squirrel cage induction motor drive are the dominant contenders for new power station drives. [4] lists the advantages and disadvantages of VSDs in power stations. The most prominent advantage is energy savings. This depends heavily on system head/ flow characteristics, generator duty cycle, fuel costs, excess capacity and maintenance. In some cases, energy savings may not be the significant factor. Secondary factors may have to be considered all of which should be accounted for in a consistent manner.

1.5 BENEFITS OF USING VARIABLE SPEED DRIVES [4]

Advantages

(i) There are no inrush currents, thus allowing a reduction in the capacity of the auxiliary power supply system.

(ii) Startups are smoother resulting in lower mechanical impact on the motor and pump system and reduced maintenance. There is no limit to the number of allowable repetitive startups.

(iii) There is longer pump seal life and reduced impeller wear.

(iv) Reliability is high (MTBF of 50 000hrs) and there is a low mean time to repair.

(v) Ride through capability with short time power interruptions is now possible.

(vi) Control can be local or communicated to a remote control point. The integration of the pump into the overall plant is achieved with ease.

(vii) Regeneration capability allows rapid controlled deceleration, allowing for emergency stops of ID fans without risk of boiler implosion.

(viii) Gearbox can be eliminated on high-speed drives.

Disadvantages

(i) The iron and copper losses are higher than expected for sinusoidal waveforms of the same RMS value. The motor may need derating by as much as 10% to allow for this.

(ii) At low frequencies, harmonics in the motor current waveform cause pulsating torque, which can cause annoying audible noise, mechanical fatigue and degradation in the load performance.

(iii) Depending on the type of rectifier, which is usually either the diode or SCR rectifier, the supply side will contain harmonics and can have a poor power factor.

(iv) All converters produce large voltage excursions with respect to ground. This may require special isolation techniques and careful layout of the dc-link reactors.

1.6 INDUCTION MOTOR DRIVE PERFORMANCE

VSDs can provide many advantages to industry depending on the make, model, installation and the control strategy. However, they can create problems with respect to the quality of electrical power, sometimes tripping and interrupting the very process they are designed to control [5]. The rectifier current waveform drawn by the diode rectifier is far from sinusoidal. This alone introduces unwanted current harmonics, which are reflected back to the supply. The current harmonics can be aggravated by the presence of voltage unbalance.

1.6.1 Symptoms of voltage unbalance

VSDs show symptoms of overload by tripping overload protection circuits. This may be the result of unbalanced phase currents. Even a small voltage unbalance can cause severe current unbalance.

1.6.2 Effect of PWM on low voltage induction machines

Low voltage induction motor designs are based on constant voltage and frequency supplied power. When considering the operation of a low voltage induction motor on a PWM inverter, it is necessary to consider the motor's NEMA design, figure 1.2, which defines its speed-torque characteristics [6].

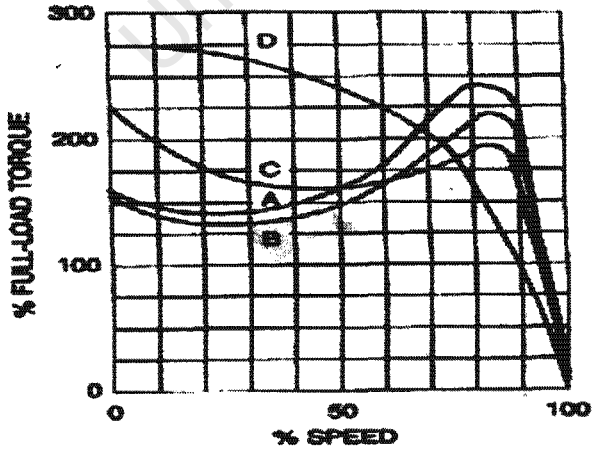

Figure 1.2: NEMA motor design curves [6]

The electrical characteristics of a particular NEMA design will produce different operating characteristics for a given application. For example, a Class C or D motor typically has high rotor resistance, in order to develop the torque defined by NEMA. This is undesirable for a PWM inverter-fed motor because it results in a higher power loss and temperature rise than for a Class A or B PWM inverter-fed motor. The amount of starting torque that the PWM inverter and IM combination can provide, is limited by the amount of current that the PWM inverter can provide to the motor.

1.6.3 Harmonics

A 'pure' sine wave, by definition, would have no harmonic content. Harmonics are defined as the sum of all components generated as a percentage of the fundamental waveform. These harmonics can be found at the motor terminals (inverter output) and generally create no useful torque at the motor shaft. Instead, they result in additional heat losses to the machines. On the other hand, the rectifier also generates a current waveform rich in harmonics.

1.7 POWER QUALITY

As industry continues to use sensitive equipment for increased productivity and efficiency, the issue of power quality has become an important requirement.

1.7.1 Power quality measurable quantities

- ***Voltage dip*** **(sag)** is a reduction in the RMS voltage in the range of 0.1 to 0.9 pu for periods greater than half the mains cycle and less than a minute. Possible causes could be faults, an increased load demand and transitional events such as motor starting.
- ***Voltage swell*** is an increase in the RMS voltage in the range of 1.1 to 1.8 pu for a duration greater than half a mains cycle and less than a minute. Caused by system faults, load switching and capacitor switching.

- ***A transient*** is an undesirable momentary deviation of the supply voltage or load current. There are two classifications, impulsive and oscillatory.
- ***Harmonics*** are periodic sinusoidal distortions of the supply voltage or load current caused by nonlinear loads. Inter-harmonics are harmonics with a harmonic order, which is not an integer-multiple of the fundamental.
- ***Flicker*** is a term used to describe the visual effects of small voltage variations on electrical lighting equipment, within the frequency range of 1-30Hz detectable by the human eye.
- ***Voltage imbalance*** is a deviation in the magnitude and/ or phase of one or more of the phases, of a three-phase supply.
- ***Frequency deviation*** is a variation in frequency from nominal supply frequency above/ below a predetermined level, normally +/-0.1%.
- *Transient interruption* is a reduction in the supply voltage, or load current, to a level, less than 0.1pu for a time of not more than 1 minute.
- ***An outage*** is an interruption that has a duration lasting in excess of one minute [7].

1.7.2 Sequence components

- Zero sequence components consist of three phasors with equal magnitudes and zero phase displacement,
- Positive sequence components consist of three phasors with equal magnitudes, +/- 120° phase displacement, with a sequence a-b-c.
- Negative sequence components, consist of three phasors with equal magnitudes, +/- 120° phase displacement, with a sequence a-c-b. [8].

Let Vab, Vbc, and Vca, be a set of unbalanced voltages.

$V_L \rightarrow$ A column vector of phase voltages

$V_s \rightarrow$ A column vector of sequence voltages

$A \rightarrow$ A transformation matrix

$A^{-1} \rightarrow$ An inverse of A

Therefore:

$$V_L = AV_s \tag{1.1}$$

It can be shown that:

$A^{-1}A = I$, Where I is a unit matrix

In Equation (1.1) multiply both sides by A^{-1}

$$A^{-1}V_L = A^{-1}AV_s$$

$$\Rightarrow V_s = A^{-1}V_L \tag{1.2}$$

Writing as separate sequence voltage equations

$$V_o = \frac{1}{3}(V_{ab} + V_{bc} + V_{ca}) \tag{1.3}$$

$$V_p = \frac{1}{3}(V_{ab} + aV_{bc} + a^2V_{ca}) \tag{1.4}$$

$$V_n = \frac{1}{3}(V_{ab} + a^2V_{bc} + aV_{ca}) \tag{1.5}$$

These are therefore, the positive V_p and negative V_n sequence voltages.

Where $a = -0.5 + j0.866$ (1.6)

$a^2 = -0.5 - j0.866$ (2.7)

Equation (1.3) shows that there is no zero sequence voltage in balanced three-phase systems. This is because the sum of the three balanced phasors is zero. In an unbalanced three-phase system, line-to-neutral voltages may have a zero sequence component. However, line-to-line voltages never have a zero sequence component, since by KVL their sum is always zero [8] except when there is a fault. The same analysis is also true for line currents.

1.7.3 Unsymmetrical voltage conditions

- Unbalanced voltage
- Undervoltage (An undervoltage is defined as unbalance due to positive sequence voltage lower than the rated voltage magnitude)
- Overvoltage (An overvoltage unbalance is defined as unbalance due to positive-sequence voltage higher than the rated voltage magnitude [9].

1.7.4 Voltage unbalance definitions

There are three definitions of voltage unbalance,

(a) The line voltage unbalance rate *(LVUR)* as defined by the National Electrical Manufactures Association (NEMA).

$$LVUR = \frac{\max.-voltage-deviation-from-average-line-voltage-magnitude}{average-line-voltage-magnitude} * 100$$

$$= Max\left[\left|V_{ab} - V_{avg}\right| or \left|V_{bc} - V_{avg}\right| or \left|V_{ca} - V_{avg}\right|\right] * \frac{100}{V_{avg}} \qquad (1.10)$$

Where, $V_{avg} = \frac{V_{ab} + V_{bc} + V_{ca}}{3}$ (1.11)

(b)The phase voltage unbalance rate (*PVUR*) as defined in IEEE Std. 141,

$$PVUR(\%) = \frac{\max.-voltage-deviation-fom-average-phase-voltage-magnitude}{average-phase-voltage-magnitude} * 100$$

$$= \frac{Max\left[\left|V_a - V_{avg}\right| * \left|V_b - V_{avg}\right| * \left|V_c - V_{avg}\right|\right]}{V_{avg}} * 100 \qquad (2.12)$$

Where, $V_{avg} = \frac{V_a + V_b + V_c}{3}$ (2.13)

(c)The voltage unbalance factor (*VUF*) defined as the ratio of the negative-sequence voltage component to the positive-sequence voltage component.

$$VUF(\%) = \frac{negative-sequence-voltage-component}{positive-sequence-voltage-component} * 100$$

$$= \frac{V_n}{V_p} * 100 \qquad (2.14)$$

Where, Vp and Vn are obtained by symmetrical component transformation [9].

1.8 SOURCES OF POWER QUALITY PROBLEMS

- ***Variable speed drives***: The most common 'economically damaging' power quality problem encountered.
- ***IT and office equipment***: IT equipment power supplies consist of a switched mode power supply (SMPS) and are the cause of a significant increase in the level of 3rd, 5th and 7th harmonic voltage distortion.
  The third harmonic is a 'triplen' harmonic. It is of zero order phase sequence and therefore adds in the neutral of the balanced three-phase system. This may lead to overloading of neutral conductors and overheating of transformers.
- ***Arcing devices***: These devices consist of electric arc furnaces, arc welders and electric discharge lamps. All arcing devices are sources of harmonic distortion.
- ***Load switching 'single phase loads'***: Heavy load switching on the local network is a common problem causing transients to propagate through to 'electrically close' equipment. These transients may have large voltage magnitudes, but low energy due to their short duration in milliseconds.
- ***Large motor starting***: During startup, induction machines can draw up-to six times their rated current. This increase in loading on the local network

has an effect of causing a voltage dip, the magnitude of which is dependent on the system impedance.

- ***Embedded 'dispersed' generation***: Increased levels of dispersed generation predicted in the future are likely to have an effect on power quality. Although it cannot be stated yet, this may degrade or improve power quality.
- ***Sensitive equipment***: Equipment manufacturers are designing and manufacturing ever more sophisticated equipment, much of which is more susceptible to variations in power quality. The result may be a combination of,

  (a) Catastrophic equipment malfunction
  (b) Data corruption
  (c) Reduced equipment operating life
  (d) Reduced process quality, hence product quality
  (e) Increase scrap material produced in production process
  (f) Process stoppage
  (g) Equipment damage
  (h) Safety issues

This may be a result of the standards that the electricity distributors adhere to, different from that of the end-user. This leaves a grey area between the two different standards.

- ***Storm and environment related damage:*** Lightning strikes, high winds and storm conditions, snow and ice build-up, sea mists, dust and heavy dew in hot and humid climates, tree branches touching overhead lines and birds colliding with overhead lines [7].

1.9 LITERATURE SEARCH FINDINGS

Findings relevant to this topic, voltage unbalance on VSDs, are listed, together with their corresponding sources.

- In some VSDs the current unbalance can be 20 times as high as the voltage unbalance [5].
- Excessive current unbalance increases current harmonic distortion, which can overload building wiring and transformers. This can trip protection circuits, even though the average current is well below the current rating of the VSD [7].
- Non-characteristic third harmonic currents and poor power factor are typical consequences of unbalanced VSD line currents [5].
- As the %LVUR increases, the double-pulse rectifier current waveform, characteristic of VSDs, will change to a single pulse waveform [5].
- NEMA Class C and Class D motors are not recommended for use on PWM inverters when selecting a PWM inverter and motor for a new application [6].
- A given value of percentage unbalance may correspond to at least eight voltage unbalance cases yielding different temperature rises in induction machines [9].
- Voltage unbalance causes additional loads on utilities resulting in additional charges for consumers [9]. Therefore, reducing system unbalance to decrease loads on the power system, improves capacity of the power system to meet its load.

1.10 CONTRIBUTION OF THIS THESIS

The main contributions and objectives of this thesis are:

- Construction and commissioning of two test beds for VSD performance testing.
- To develop PSpice models for the two test beds.
- To determine and document the effects of unbalanced supplies on induction machine VSDs.
- Evaluate the correct method of calculating energy savings for the application of VSDs to centrifugal loads.
- Quantify the effects of cable mismatch with the motor impedance.

CHAPTER TWO

Test Bed Development

2.1 INTRODUCTION

The University of Cape Town has a unique electrical machine's laboratory. In addition to a flexible distribution system with the capability of various dc and ac supplies, the laboratory is also home to two, 250kW 4-quadrant dc machines and drives, fed directly from the University 11kV ring mains through 11kV to 500V three-phase transformers. This includes a three-phase, 6.6kV, 520kW alternator and a 75kW induction motor with a 75kW drive. One of the purposes of this project is the upgrading of the laboratory to be able to test three-phase induction motor drives as an aid to ESKOM's Demand Side Management program.

This chapter describes the development of test beds for 3 and 75 kW induction motor drives sets. The test beds are developed with the intention of imposing fan or pump type loads and the ability to measure current harmonics, power flow from the utility supply through the converter and to the induction motor and hence, efficiency. The test beds are intended to have the capability to introduce voltage unbalance on the supply voltage, so as to determine the effects of voltage unbalance on induction machine drives. Mechanical losses of the test beds are determined and documented in this chapter.

2.2 TEST BEDS OBJECTIVES (low and medium power)

- To study and measure the performance of induction machines and variable speed drives operating under balanced voltage supplies,
- To study and measure the performance of induction machines and variable speed drives under unbalanced voltage supplies,
- To model industrial loads such as fans and pumps, driven by induction machine and VSD sets,
- To determine the current harmonics due to voltage unbalance on VSDs,
- To determine the effect of these harmonic currents on the performance of the VSDs,
- To study the effect of voltage unbalance on induction machines and drives due to reflected waves associated with long cables.

- To determine energy savings associated with VSDs in industry.

2.3 TEST BED CHARACTERISTICS [11]

The ideal test bed should include the following features:

- Industrially relevant power rating capability;
- Wide range of service voltage, with capability for under-, over- and unbalanced voltage supplies;
- Wide range of machine frame sizes, with the capability to accommodate unusual geometries;
- Wide range of machine speeds, with capability for locked-rotor tests and dynamic speed changes;
- The ability to test both motors and generators, while minimizing the dissipated energy;
- Ability to test power electronics converters, with investigations of non-sinusoidal and high frequency effects;
- Ability to make accurate measurements of the above.

2.4 LOW POWER TEST DRIVE

The term, low power, in this context refers to machines and drives rated at below 20kVA.

2.4.1 System overview

Figure 2.1, shows the low power test bed, including an energy efficient induction motor, coupled to dc machine. The load cell and its mounting frame can be seen on the left of the dc machine.

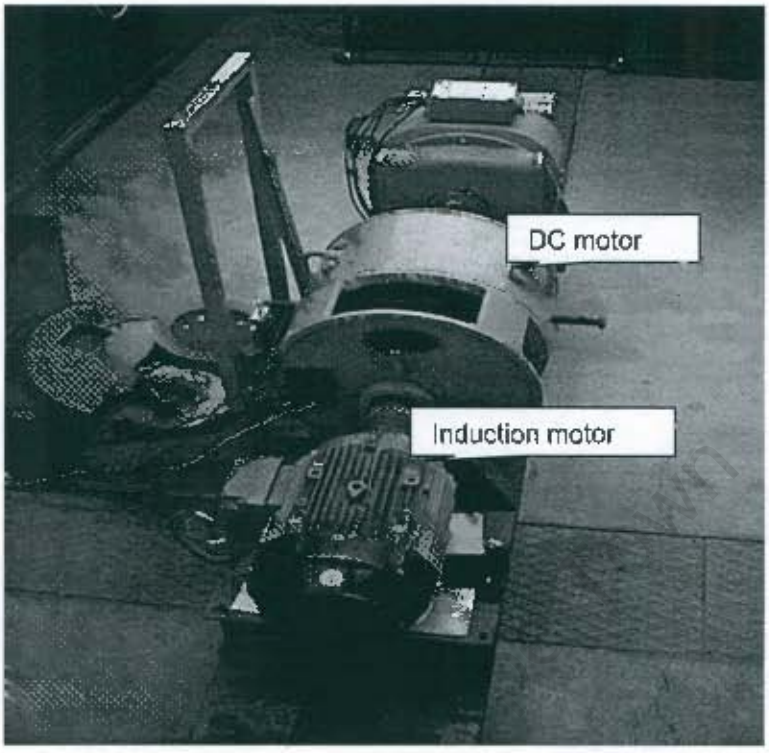

Figure 2.1: Low power machine test bed

2.4.2 System components *(see Figure 2.1-3)*

The components assembled to build the complete power circuit are listed below,

- Three phase voltage supply, 380V line-to-line
- Variable voltage transformers
- Induction motor drive
- Induction motor
- DC machine
- Four-quadrant thyristor rectifier

2.4.3 Basic instrumentation

The required instrumentation for system study and analysis are:

- Oscilloscope
- Power analyzer
- Torque meter

Figure 2.2, shows the AC side of the test bed circuit. The VSD, can be seen on the left as indicated. Single-phase variable voltage transformers are also visible including a power analyzer on the right.

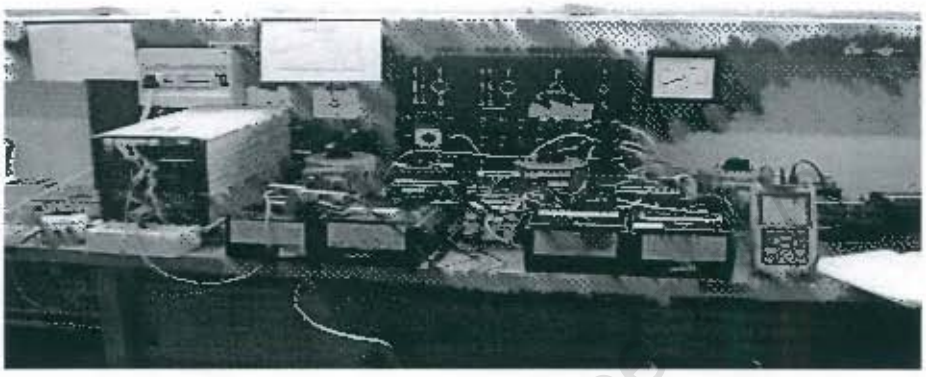

Figure 2.2: AC drive with measuring instruments

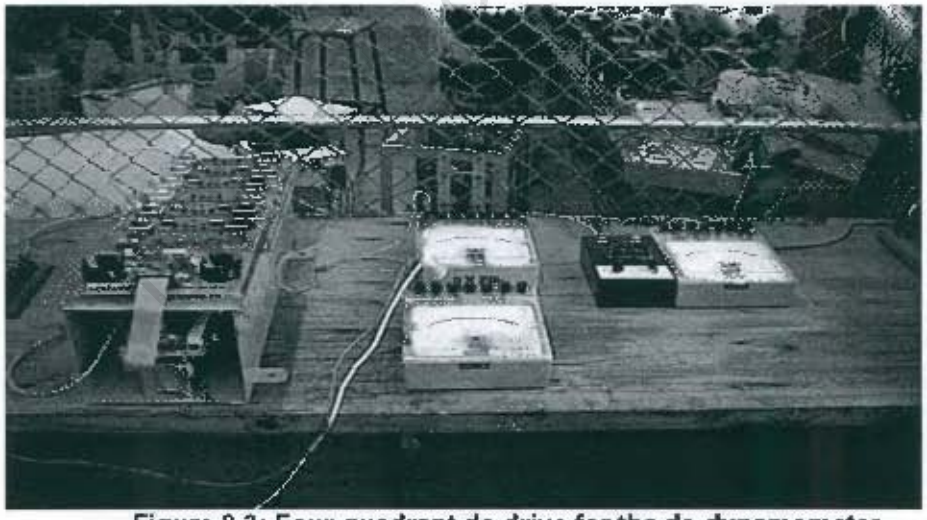

Figure 2.3: Four-quadrant dc drive for the dc-dynamometer

Figure 2.3 shows the dc side of the test bed circuit for the dc machine speed control. A rectifier is visible on the left hand side; it is used to adjust the load on the induction motor by varying the armature current.

2.5 TEST BED DESCRIPTION

A short circuit description is given below, describing the connection among the various circuit components.

2.5.1 Circuit description

The utility three-phase voltage supply is connected to the IM VSD via three single-phase Variable Voltage Transformers (VVT). The output of the ac VSD is fed to the energy efficient (EE) induction motor. Coupled to the IM is a dc machine via a flexible joint coupling. A four quadrant-thyristor rectifier is connected to the input of the dc motor. A load cell is attached to dc-motor stator for torque measurements. Figure 2.4 is a schematic representation of the test bed. Torque is displayed by a digital torque meter, which converts the current signals from the load cell transducer to Newton meters (Nm).

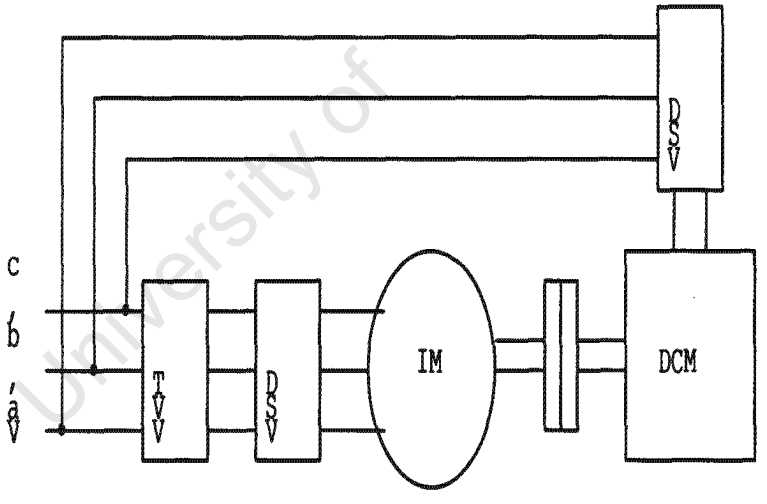

Figure 2.4: 3kW IM Test Bed

2.5.2 Circuit operation

The three-phase voltage supply from the mains is fed through VVT's to the motor. Depending on the test in progress, for example, for balanced voltage tests, the VVT's are bypassed. In the case where unbalanced voltage is required, the VVT's are connected. VVT's enable only per phase voltage amplitude variation to be introduced to produce voltage unbalance. The IM VSD varies the induction

machine speed to the required magnitude depending on the load and type of test. Either of the two machines can be used as the driver or load. When the induction machine is the driver, the dc-machine can be used to represent different industrial loads, such as pumps and constant conveyor belt loads. The nameplates of the different components of the circuit are listed in Appendix A2.1.

2.6 OPERATING POINT DETERMINATION

The no-load and blocked rotor tests are undertaken for the induction motor. The motor parameters are computed using the IEEE equivalent circuit for induction motors, Figure 2.5.

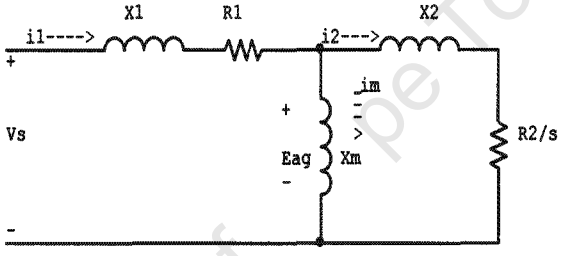

Figure 2.5: IM equivalent per phase circuit

Induction motor capability curves are developed using the characteristic equations, (2.1), (2.2) and (2.3).

$$T_d = \frac{3 * I_2^2 R_2}{s * \omega_s} \tag{2.1}$$

$$I_2^2 = \frac{E_{ag}^2}{\left(R_1 + \frac{R_2}{s}\right)^2 + (X_1 + X_2)^2} \tag{2.2}$$

$$E_{ag} = V_1 \frac{jX_m}{R_1 + j(X_m + X_1)} \tag{2.3}$$

The pump-load curve is also developed based on the rated torque and speed of the induction motor as described by Equation (2.4).

$$T_L = k_1 \omega_r^2 \qquad (2.4)$$

The pump-load curve is superimposed on the induction machine torque-speed capability curves in Figure (2.3). In this example, the motor is modeled at four operating speeds, which are at 15Hz, 25Hz, 40Hz and 50Hz. The intersection of the pump-load curve with the induction motor torque-speed curve is the operating point. That is, if the 3kW IM were to drive a pump or similar load, it would operate at the intersection of the two curves depending on the speed required.

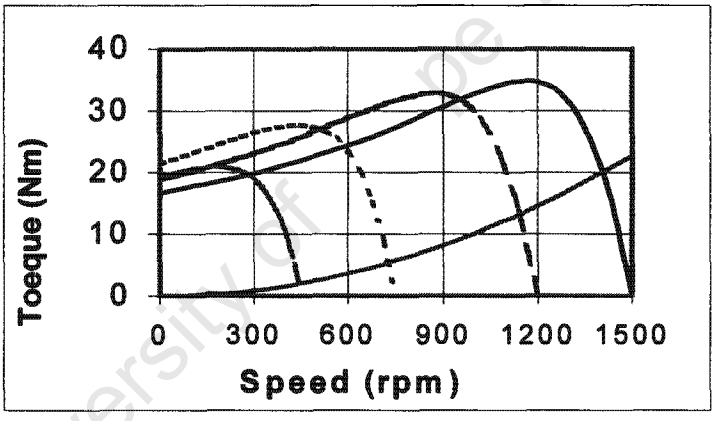

Figure 2.6: Torque-Speed curves for a 3kW EE IM

Tests on the test bed are undertaken to verify that this exercise does predict the operating point in terms of shaft speed and load torque. The induction motor is set to the required speed via the ac drive, e.g. corresponding to 25Hz. The resulting speed of rotation would be close to synchronous speed, since it is at no load. The load is imposed to represent a fan or pump load, which is 5.4Nm at 25HZ. This is achieved by setting the torque of the dc-machine by increasing the armature current. Increasing the load has an effect of increasing the slip, hence resulting in a decrease in the operating speed.

The procedure is repeated for 15Hz, 40Hz and at rated conditions (50Hz). Table 2.1 shows that the actual speed of the motor shaft correlates with the graphical synthesis of the IM-Load combination. Therefore it can be concluded that when the machine parameters and the load curve are known, the exact operating points can be computed. This can be used to calculate the energy savings that could be achieved by varying the operating speed of the motor shaft instead of throttling using valves for example. Moreover, this information can also be used to specify an appropriate variable speed drive for a particular application.

Table 2.1: Predicted and actual operating points

	Predicted Point		Actual Point		% Error	
f[Hz]	ω[rpm]	T [Nm]	ω[rpm]	T [Nm]	ω	T
50	1406.5	20	1416	17	0.7	17.6
40	1142.1	13.2	1143	13.2	0.1	0
25	727.5	5.4	730.2	5.4	0.4	0
15	441.6	2	443.4	2	0.4	0

2.7 VOLTAGE BOOST REQUIRED AT LOW FREQUENCIES

In induction motor drives, at low frequencies the effect of stator resistance cannot be neglected, even at small slip frequencies. This can be determined if the following observation is made; induction motors of normal design, $X_2 = 2\pi f L_{lr}$, is negligible compared to R_2/s in the equivalent circuit of Figure 2.2 [10]. Therefore, I_2 will be in phase with E_{ag}. Taking E_{ag} as the reference voltage,

$$Vs \cong \left[E_{ag} + X_1 I_m + R_1 I_2\right] + j\left[X_1 I_2 - R_1 I_m\right] \qquad (2.5)$$

The second term in Equation (2.5) corresponds to a phasor, which is almost perpendicular to V_s, and small in magnitude. Therefore its influence on the magnitude of V_s can be neglected, and

$$V_s \approx E_{ag} + X_1 I_m + R_1 I_2 \qquad (2.6)$$

When the air gap flux (Φ_{ag}) is kept constant, I_m is also constant and E_{ag} varies linearly with the supply frequency f. Therefore the additional voltage required due to X_1 in Equation (2.6) is also proportional to the operating frequency f. As a result, for constant Φ_{ag}, Equation (2.6) can be written as:

$$V_s \approx k_2 f + R_1 I_2 \qquad (2.7)$$

Equation (2.7) shows that the additional voltage required to compensate for the voltage drop across R_1 to keep Φ_{ag} constant does not depend on the frequency, f, but depends on I_2. It is important to note that I_2, the rotor current, is proportional to the electromechanical torque developed T_{em}. Therefore, the voltage boost required in a pump-type load increases with an increase in speed.

2.7.1 Voltage boost for the pump curve

In pump load applications, the slip frequency, f_{sl} increases with increased operating frequency. Therefore, I_2 increases in proportion to speed. Consider a 3 kW IM with R_1 = 2.2Ω and I_2 = 5.64A at some operating condition. The estimated voltage boost magnitude is:

$$V_s boost = R_1 * I_2 \qquad (2.8)$$
$$= 2.2 * 5.64$$
$$= 12.41 \text{ V}$$

Voltage boost required for constant torque operation and pump load is tabulated in Table 2.2. Table 2.3, below tabulates per phase line-to-neutral terminal voltage with and without voltage boost and Figure 2.7 displays the corresponding curves. Voltage boost is computed based on a theoretical IM model. At constant torque

operation the voltage boost is a constant, which is 12.41V in this case. However, with the pump load operation, voltage boost is a function of the rotor current.

Table 2.2: Calculated rotor currents and stator volt-drop

Motor supply	Rotor current and voltage boost			
	Constant torque		Pump load	
f[Hz]	I_2	V_b	I_2	V_b
0	5.64	12.41	0.00	0.00
15	5.64	12.41	0.50	1.10
25	5.64	12.41	1.30	2.86
40	5.64	12.41	3.50	7.70
50	5.64	12.41	5.64	12.41

Where, V_b is the voltage boost

Table 2.3: Motor terminal voltage with and without V-boost

Motor supply	IM terminal voltage		
	Vs/f	Constant torque	Pump load
f[Hz]	V_s	V_{sb1}	V_{sb2}
0	0	12.41	0
15	65.82	78.23	66.92
25	109.70	122.10	112.56
40	175.51	187.92	183.21
50	206.99	219.39	219.39

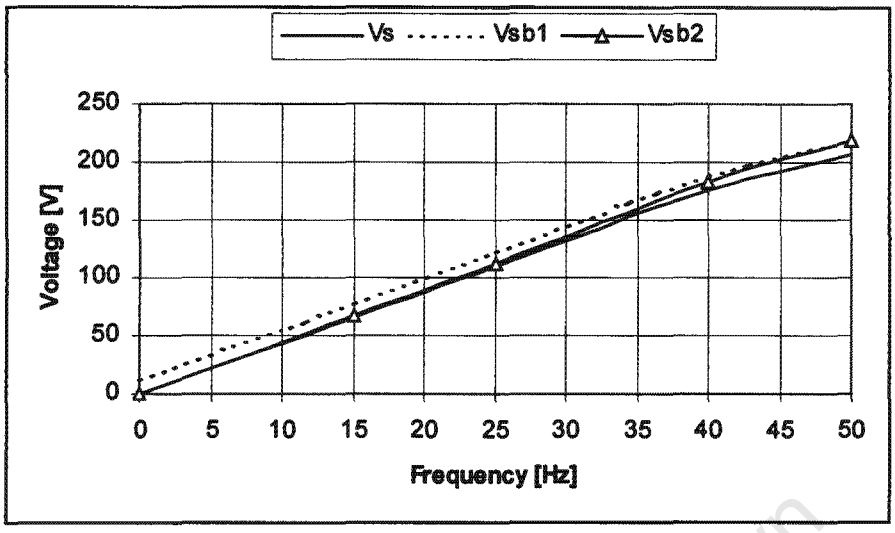

Figure 2.7: Voltage boost to compensate for the stator drop

2.7.2 IM torque-speed characteristics with voltage boost

Voltage boost is added at 15Hz, 25Hz and 40Hz and the T-Speed curves redrawn for these new conditions. The load torque curve is superimposed to determine the operating points.

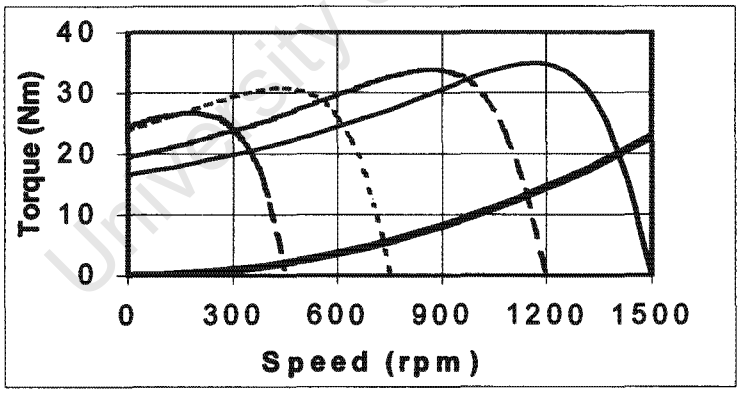

Figure 2.8: IM T-Speed characteristics with voltage boost

The starting torque is greater under voltage boost conditions. This is desired for high inertia loads requiring large starting torque to accelerate. At rated speed and load, voltage boost is not required because it has been included, e.g., an induction machine with the voltage rating of 380V, has voltage boost already included in the 380V line-to-line.

To demonstrate the impact of voltage boost at low speeds, consider Figure 2.9, the torque-speed curves at 25Hz. The starting torque is 21Nm when there is no voltage boost, this value increases to 26Nm when voltage boost is added.

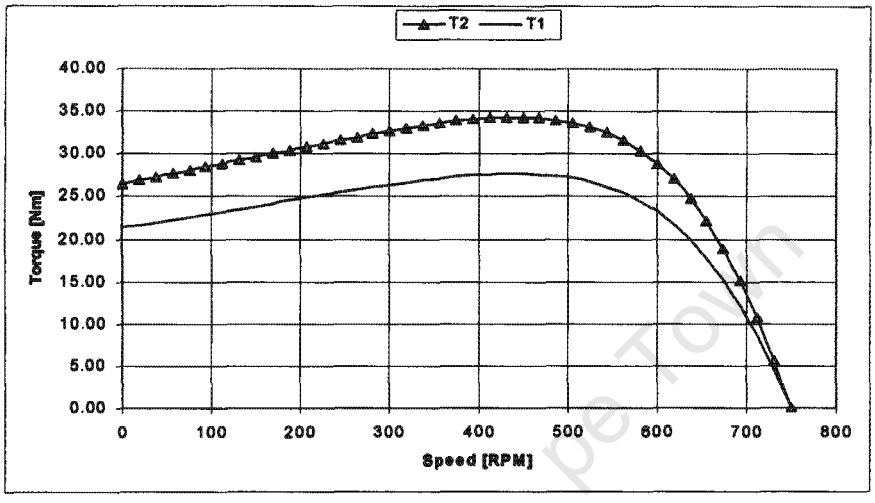

Figure 2.9: Impact of voltage boost at 25Hz

Where, T1 is the speed/torque curve without voltage boost,
T2 is the speed/torque curve with voltage boost.

2.8 TEST RESULTS

Some basic machine tests are undertaken to document the test bed characteristics.

2.8.1 Power losses of the 3kW-test bed

The mechanical losses of the test bed are determined by driving the induction motor using the dc motor. The mechanical losses incorporate friction and windage. The dc machine is run at four operating speeds corresponding to the operating points of the induction motor with pump loads. Speed, armature voltage and current are recorded for each operating point. Table 2.4 lists the power losses for each operating speed.

Table 2.4: Mechanical power losses [W]

f [Hz]	*ω [rpm]*	*Total-mechanical losses*	*Dc-machine losses*	*IM losses*
50	1416	548.39	446.76	101.63
40	1143	426.75	354.00	72.75
25	730	245.70	199.54	46.16
15	443	135.12	109.70	25.42

2.8.2 Efficiency

There are three efficiency quantities of interest; the converter efficiency, induction machine efficiency and the overall drive efficiency. Table 2.5 tabulates the power flow from the utility supply through the converter, to the motor. Figure 4.10 is a graphical representation of the efficiency. The drive maintains constant efficiency. The induction motor efficiency improves with increasing operating speed.

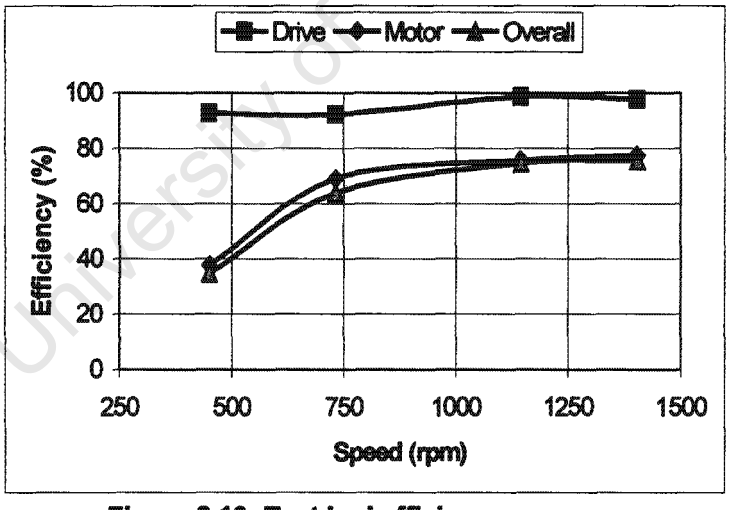

Figure 2.10: Test bed efficiency curves

Table 2.5: Power flow

f [Hz]	*α[rpm]*	*Drive P_{in}*	*IM P_{in}*	*IM P_{out}*	*Drive η*	*IM η*	*Overall η*
f = 50	1404	3.91	3.82	2.96	97.70	77.36	75.58
f = 40	1144	2.12	2.09	1.58	98.58	75.66	74.59
f = 25	732	0.65	0.6	0.41	92.31	68.99	63.68
f = 15	449.9	0.27	0.25	0.09	92.59	37.69	34.90

+

Where, P_{in} is the power input to a machine,

P_{out} is the power output of a machine.

A closer look at Table 2.5 and Figure 2.10 shows that the induction motor drive has an almost constant efficiency curve throughout the increasing speed range from 15Hz to 50Hz. The induction machine starts with very low efficiency in the region of 30% at 15Hz. It gets better as the speed increases and levels off in the 40Hz region with an efficiency of 73 %.

2.9 MEDIUM POWER INDUCTION MOTOR DRIVE TEST BED

In parallel with the construction of the low power test bed, a medium power drive-motor test bed was also developed.

2.9.1System equipment

Figure 2.11, shows the 75kW induction motor coupled to an ac generator and Figure 2.12 shows the 75kW drive installed at the lab. The ac generator is coupled to a dc generator on the other side. The ratings of the machines are as follows:

- 250 kW, 460 V, 543A dc machine
- 520 kW, 6.6kV (Y connected) synchronous generator
- 75 kW induction motor
- 75kW ac VSD
- 250kW four quadrant thyristor drive

Figure 2.11: Medium power test bed

Figure 2.12: Induction motor, 75 kW VSD on the supply panel

2.10 DESCRIPTION OF THE 75 kW IM AND VSD TEST BED

The test bed is designed with flexibility in the types of tests to be undertaken and the type of loads to be modeled. For example, the induction motor could be used

to simulate a turbine driving the alternator. The alternator can then feed an electrical load via a 6.6kV to 380V transformer. Varying the induction motor speed via the VSD can vary the output frequency of the alternator. Moreover, for any test on the induction motor and drive, the dc-motor could be the load. The machines can be decoupled depending on the type of test. Figure 2.13 is the schematic representation of the medium power machine and drive test bed.

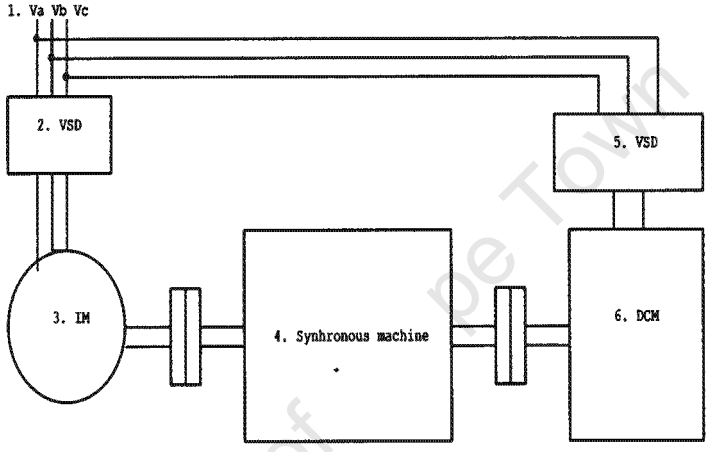

Figure 2.13: Schematic representation of the 75kW drive set

2.11 TEST RESULTS

The mechanical losses in the medium size test bed are determined and documented. The locked-rotor and no-load tests for the 75kW induction motor are undertaken and its parameters computed for simulation purposes.

2.11.1 I^2R and brush losses of the 250 kW dc machine

The dc machine is run at a constant speed of 200 rpm and armature voltage is applied to determine the brush-drop and armature resistance. The volt drop over the armature and the brushes is measured with a calibrated digital voltmeter. The voltage is allowed to stabilize, and then voltage and current are recorded. The supply is switched off and the back emf recorded. The back emf is subtracted from the measured voltage to determine the actual volt drop. The results are tabulated in Table 2.6.

Table 2.6: Measured voltage drop over armature

Current [A]	*Voltage [V]*	*Residual back emf [V]*	*Actual Volt drop [V]*	*Resistance [mΩ]*
50	4.63	1.41	3.22	64.4
100	6.63	1.41	5.22	52.2
150	8.52	1.39	7.13	47.5
200	10.11	1.35	8.76	43.8

Plotting these values on a graph and extrapolating the values to the zero Amp line (see Figure 2.14), yields the actual volt drop over the brushes of 1.37 V.

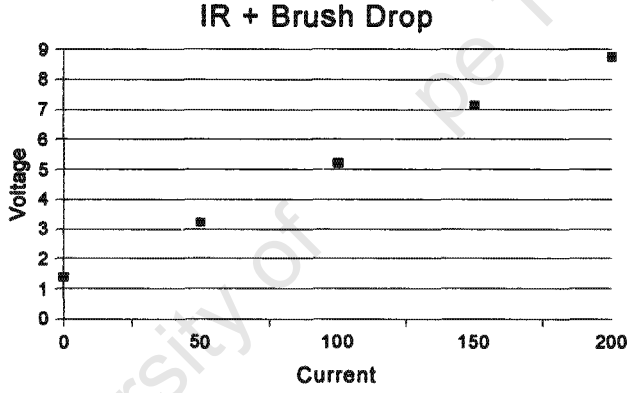

Figure 2.14: Armature voltage vs. Current

The slope of the above graph represents the resistance of the armature, i.e. 36,9 mΩ. This value is verified by taking measurements directly across the armature with the brushes disengaged. The resulting values, listed in Table 2.7, show the resistance across one set of brushes and the probes. The difference gives the armature resistance between one set of brushes and has to be halved to get the actual armature resistance.

Table 2.7: Galvanometer results of armature resistance

Position	*Resistance [mΩ]*
Resistance over 2 adjacent brushes	110.0
Resistance of the probes	37.0
Resistance of the armature	36.5

This value correlates with that of the first method, with a difference of 0.4 mΩ.

2.11.2 Mechanical losses of the 250kW dc-machine and synchronous machine

Initially the medium power test bed consisted of two 250kW dc-machines with four quadrant thyristor drives. These dc machines are coupled to either side of the alternator. The alternator is then connected to the 6.6kV/380V step-down transformer. One of the dc-machines is used to drive the other machines to determine the mechanical losses of the dc machine-alternator combination.

The dc machine is run at increasing speeds with 100rpm increments up to 1000 rpm, the rated speed. The corresponding input power, armature voltage and current are recorded. The results are tabulated in Table 2.8, 2.9 and 2.10 below. The tests are undertaken for the three conditions,

- Dc motor cold
- Dc motor warm
- Dc motor decoupled from the other machines

Table 2.8: Large test bed mechanical loss data for the cold states

Speed	V_{tacho}	*Real Speed*	V_a *[V]*	I_{lem} *[mA]*	I_a *[A]*	*Power [W]*
100	0.6	102	48.9	2.25	11.25	550.1
200	1.2	207.4	97.8	2.45	12.25	1198.1
300	1.8	312.8	145.9	2.65	13.25	1933.2
400	2.4	409.7	190.7	2.95	14.75	2812.8
500	3	504.9	235	3.37	16.85	3959.8
600	3.6	605.2	282.7	3.93	19.65	5555.1
700	4.1	703.8	327	4.57	22.85	7472
800	4.8	807.5	376.1	5.38	26.9	10117
900	5.2	875.5	409.7	5.95	29.75	12189
1000	5.9	996.2	456.7	7.1	35.5	16213

Table2.9: Large test bed mechanical loss data for the warm states

Speed	V_{tacho}	*Real Speed*	V_a *[V]*	I_{lem} *[mA]*	*I [A]*	*Power [W]*
100	0.5	91.8	44.4	2.2	11	488.4
200	1.2	195.5	91.8	2.35	11.75	1078.7
300	1.8	299.2	138.8	2.55	12.75	1769.7
400	2.4	401.2	186.6	2.9	14.5	2705.7
500	2.9	496.4	230.2	3.35	16.75	3855.9
600	3.6	603.5	279.6	3.9	19.5	5452.2
700	4.1	698.7	322.8	4.5	22.5	7263
800	4.7	802.4	370.7	5.3	26.5	9823.6
900	5.3	894.2	413.8	6.15	30.75	12724
1000	5.8	989.4	455.2	7.1	35.5	16160

Table 2.10: Large test bed mechanical loss data for dc machine decoupled

Speed	V_{tacho}	*Real Speed*	V_a *[V]*	I_{lem} *[mA]*	*I [A]*	*Power [W]*
100	-	-	48.6	1.75	8.75	425.3
200	-	-	96.5	1.85	9.25	892.6
300	-	-	143.1	2.05	10.25	1466.8
400	-	-	188.4	2.25	11.25	2119.5
500	-	-	233.5	2.6	13	3035.5
600	-	-	279.8	2.95	14.75	4127.1
700	-	-	326.4	3.45	17.25	5630.4
800	-	-	371.4	4	20	7428
900	-	-	417.2	4.65	23.25	9699.9
1000	-	-	456.8	5.4	27	12334

Figure 2.15 is a plot of input power vs. speed for the dc-synchronous machine set. This is the power consumed by the dc motor that is driving the dc machine-alternator combination. Therefore the load losses consist of bearing friction, inertia of the three machine's rotors and windage. The power difference curve represents the difference between the power when the dc machine is warm and coupled and when it is warm but decoupled (running at no load) from other machines. These power differences are the mechanical power losses of the test bed machines, attributed to bearing friction and windage losses. It can be noted that at 1000rpm, which is the rated speed for this particular dc motor, the mechanical losses are 3,826 kW. The dc machine total losses are 12,33 kW including the field winding copper losses. This totals 16,159 kW power losses for the test bed.

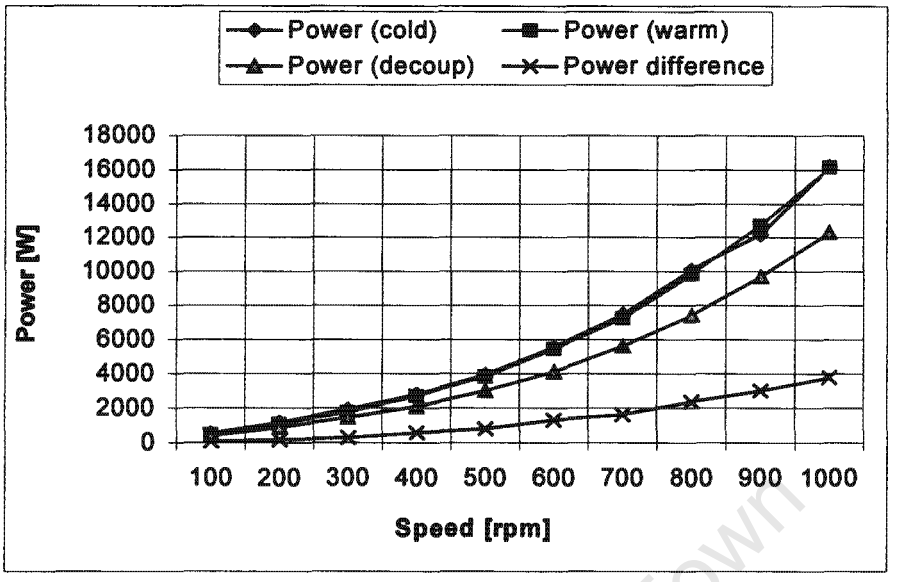

Figure 2.15: Mechanical losses of the large test bed machines set

2.12 INDUCTION MOTOR (75kW) INSTALLATION

The medium power test bed is upgraded by retrofitting one of the 250kW dc machines with a 75kW induction motor supplied via a 75kW drive. Figure 2.11 displays the actual test bed (see Appendix A2.2 for the IM and drive nameplate). The blocked rotor and no-load tests are undertaken to determine the motor's parameters. The results are tabulated in Table 2.11.

Table 2.11: Parameters for the 75kW IM

R_1 =	0.1Ω
R_2 =	0.1Ω
$X_1 = X_2$ =	0.53Ω
X_m =	14.45Ω

Similarly, the torque-speed characteristic curve is generated using Equations (2.1), (2.2) and (2.3), as illustrated in Figure 2.16.

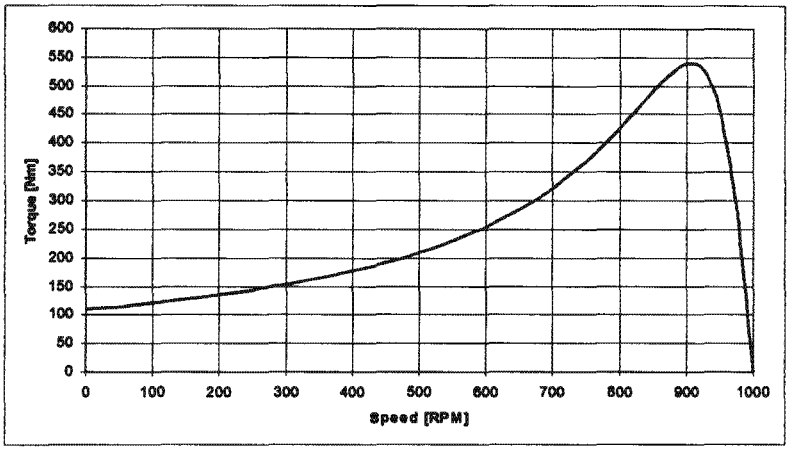

Figure 2.16: Torque-Speed characteristic of a 75kW IM

The starting torque is projected to be 109Nm and pullout torque is 540Nm. The torque of the 75kW based on the rated speed and power is 746Nm. While the torque output at rated speed from Figure 2.16 is 450Nm.

2.13 CONCLUSION

Two test beds were constructed and commissioned. Tests to determine system parameters, such as the blocked rotor and no-load tests were performed for both tests beds. The machine's parameters are computed for both test beds. Furthermore, four operating points are analytically computed and verified by measurements. Therefore, induction motor performance curves can be used to accurately determine the shaft torque for given a speed. Moreover the system losses are measured and documented.

CHAPTER THREE

Drive Model Development and Simulation

3.1 INTRODUCTION

Commercially available induction motors have been designed for operation on sine-wave power. Similarly, IM VSDs are tested under 'clean' supply conditions. The performance characteristics under these conditions are well documented. This chapter develops a PSpice simulation model, which allows the performance to be predicted under balanced conditions. The simulation model agrees with the measured results. The model is then used to determine the drive performance under unbalanced voltages to predict the impact of voltage unbalance on induction machine's variable speed drives.

3.2 DRIVE MODEL DEVELOPMENT

The high risk of undertaking tests without first predicting the result is unjustifiable. Therefore, a model correctly predicting the actual performance has to be developed.

3.2.1 Simulation model

Figure 3.1 illustrates the interconnection of the various components forming the model.

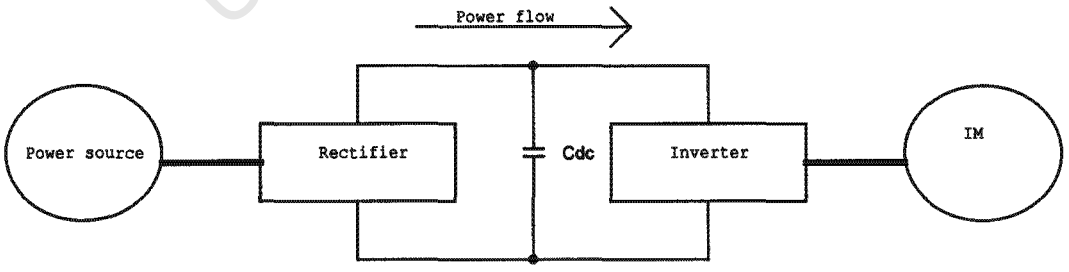

Figure 3.1: PSpice model block diagram

CHAPTER THREE

Drive Model Development and Simulation

A three-phase diode bridge rectifier is connected to a PWM switched inverter, via a dc-link circuit with smoothing capacitor and dc-bus impedance as shown in Figure 3.2. The output of the inverter is fed to a 3kW energy efficient induction motor. The induction motor in this example is operated at full-load and half rated speed. The nameplate ratings of the drive and the motor are listed in Appendix A2.1. Small inductances and resistances in series model the supply impedance. The dc link circuit consists of a dc-link series impedance and a smoothing capacitor.

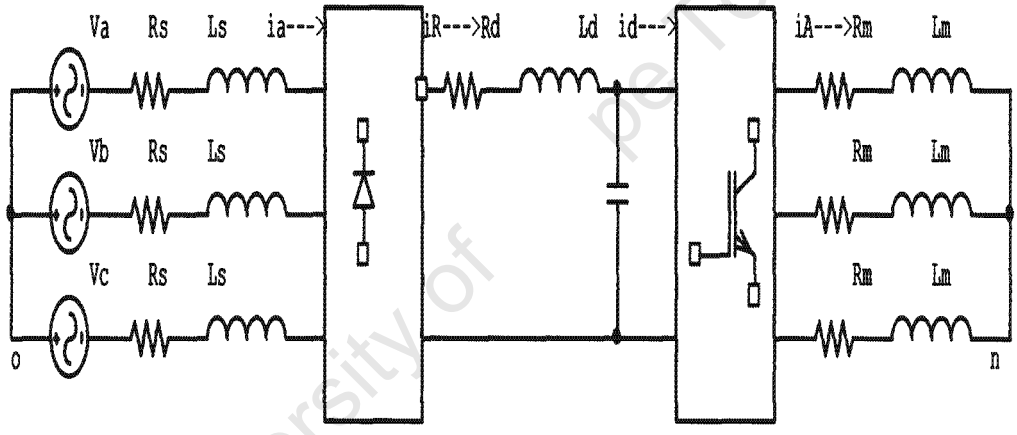

Figure 3.2: IM drive system

The inverter circuit consists of 'S-break' switches to eliminate commutation delay. Comparing the three sinusoidal waveforms at the required output frequency, to a continuous triangular waveform, generates the switching pulses. This output is fed to the inverter switches for control.

3.2.2 Load model

The induction motor is seen as an electrical load from the converter side. This is modeled as a balanced three-phase RL circuit connected in star. The effect of

the load on the slip has been taken into consideration. The complete model diagram is in Appendix A3.1.

3.3 MODEL PARAMETERS

The slip (s) of an induction machine is a function of the load torque on the output shaft.

$$\therefore \text{ s (slip)} \propto T_{LOAD} \qquad (3.1)$$

The 3kW motor test bed is run at 25Hz, that is, at half the rated speed, but at a full load of 20Nm. The speed is set such that the VSD operates in the linear region. This is because within the linear region the modulation ratio m_a can be calculated analytically. The line-to-line voltage and the line currents at the supply point and motor terminals (drive's output) are measured. The corresponding FFT's are captured via an oscilloscope. The RMS value of the fundamental voltage is extracted. The line-to-line RMS voltage, line current and the power factor at which the power is drawn by the motor are used to compute the impedance as seen by the converter. Furthermore, the amplitude modulation ratio is determined as defined by Equation (3.2) below.

$$m_a = \frac{2\sqrt{2} * V_{LL\,RMS}}{\sqrt{3} * V_{DC-LINK}} \qquad (3.2)$$

Figure 3.3 displays the RMS value of the supply line-to-line voltage as function of m_a. The three modulation regions are clearly illustrated, linear, over-modulation and square-wave region.

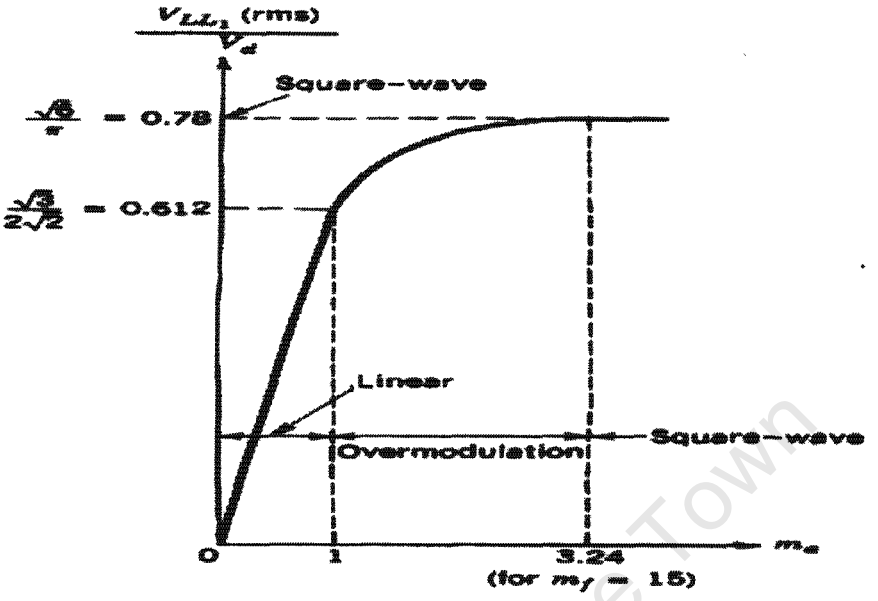

Figure 3.3: The effect of ma on voltage control

From the set points tabulated in Table 3.1, the drive is operating within the linear region. The linear region of operation is one where the modulation ratio m_a is less than one. These parameters form the inputs to the drive model in PSpice.

$$m_a \leq 1 \qquad (3.3)$$

Table 3.1: PSpice input parameters

Quantity	Magnitude
f_{supply} [Hz] =	50
f_{out} [Hz] =	25
M_a =	0.6
Z_t [Ω] =	13.74+j6.66
C_{dc} [uF] =	1000

CHAPTER THREE

Drive Model Development and Simulation

3.4 EXPERIMENTAL PROCEDURE

In the first phase of the model development, all tests and simulations are undertaken with balanced supply voltage conditions.

These conditions are summarized as:

- Balanced 380V line-to-line voltage supply,
- VSD set to 25Hz output frequency,
- Switching frequency of 2kHz
- Induction machine fully loaded

The following quantities of interest are measured, for both the supply to the rectifier and to the motor.

- Current and voltage,
- Rectifier current harmonics

Two power sources are used. The first is the mains supply from the ESKOM grid (Electricity Supply Commission). The second voltage supply is generated using the machine's lab 500kVA, 6.6kV alternator, which is transformed down to 380V line-to-line. The harmonic content of the supplies differs drastically. Hence the performance of the drive under these different conditions will test the capability of the model.

3.5 CORRELATION OF TEST BED AND SIMULATION FOR THE MAINS VOLTAGE SUPPLY

The measured and simulated results are first correlated for the mains voltage supply.

3.5.1 Current and voltage comparison

Figure 3.4 displays the actual grid, 380V line-to-line voltage supply captured from Machine's Laboratory at the University of Cape Town. This voltage is fed to the 3kW test bed machines. The quantities of interest are measured and recorded. The same three-phase line-to-line voltage supply is captured as a CVS file and fed into PSpice. It can be seen from inspection of the voltage waveform in Figure 3.4, that it is highly distorted.

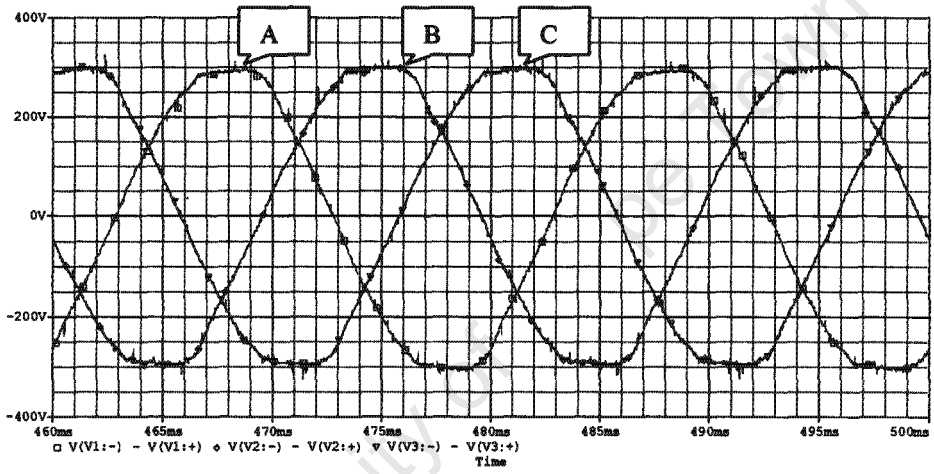

Figure 3.4: Mains three-phase line-to-line voltage supply

The term, rectifier current refers to the current drawn by the diode bridge rectifier and inverter current refers to the current drawn by the IM from the inverter. Tables 3.2 to 3.5 tabulate the results of current and voltage, for simulation and the performance test under mains three-phase line-to-line voltage supply. The corresponding waveforms are included, Figures 3.5 To 3.9. This comparison is given for amplitudes and RMS values of voltage and current.

Table 3.2: Rectifier currents comparison

	I_{peak} (A)	I_{RMS} (A)
Simulated	23	6.4
Measured	23.6	6.53
% Error	2.5	2.0

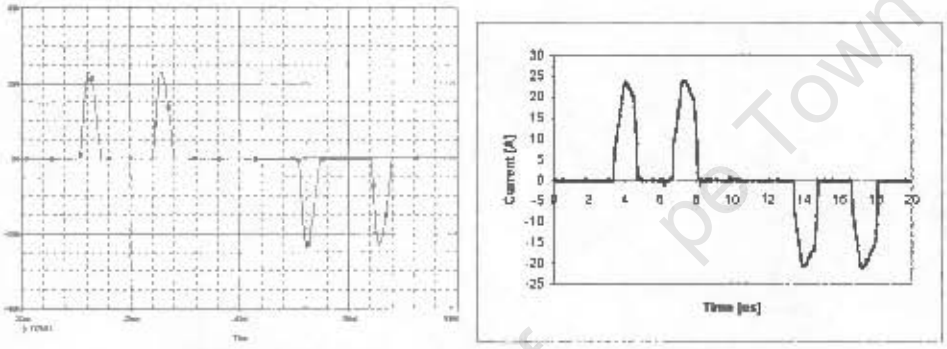

Figure 3.5: Rectifier current, simulated and measured, respectively

Table 3.3: Dc-link voltage comparison

	V_{ave} (V)	V_{pp} (V)	% Ripple
Simulated	544	12	2.2
Measured	557	10.7	1.9
% Error	2.3	12	16

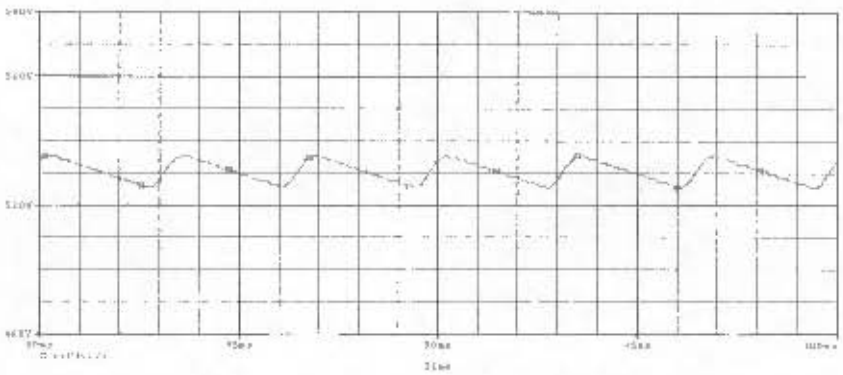

Figure3.6: Simulated Dc-link voltage at balanced conditions

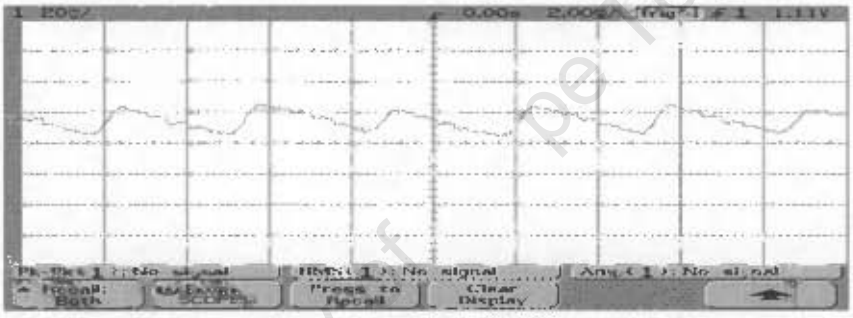

Figure 3.7: Measured Dc-link voltage at balanced conditions

Table 3.4: Inverter current comparison

	I_{peak} (A)	I_{rms} (A)
Simulated	10.5	7.2
Measured	10.6	7.1
% Error	0.9	1.4

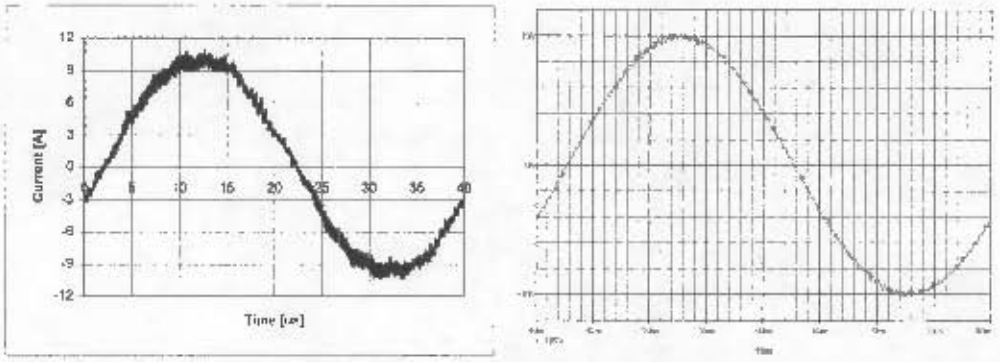

Figure 3.8: Measured and simulated inverter currents, respectively

Table 3.5: Inverter output line-to-line voltage comparison

	V_m (V)	V_{RMS} (V)
Simulated	548	305
Measured	556	311
% Error	1.4	1.9

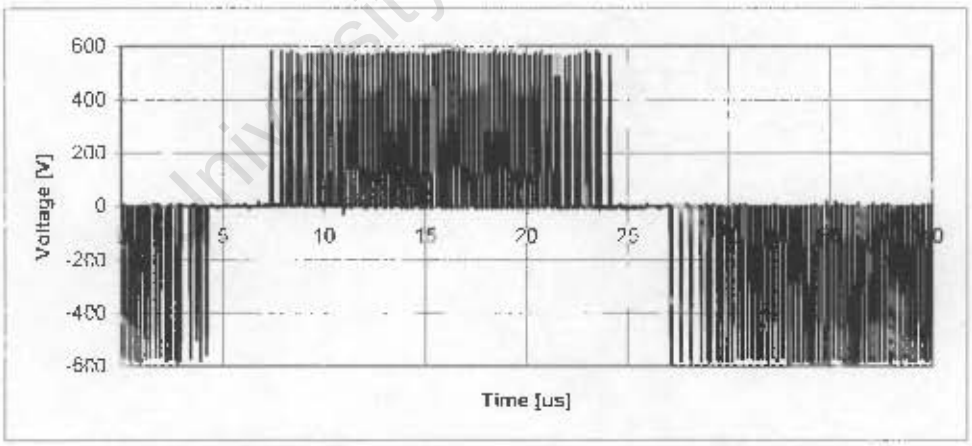

Figure 3.9: Measured inverter voltage waveform

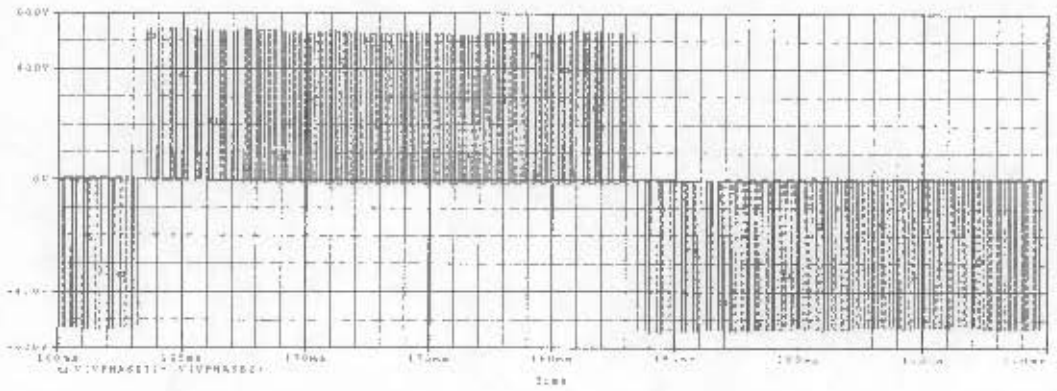

Figure 3.10: Simulated inverter output voltage

It is observed from Table 3.2 to 3.5 that the simulated result correlates with the test bed results. The percentage error for each quantity is also computed. This correlation is for amplitudes and RMS values of voltage and current. The errors are acceptable for testing purposes.

3.5.1 Rectifier current harmonics comparison

The rectifier current is characteristically rich in harmonics; therefore it is fundamentally important that the drive be capable of predicting these harmonics. The harmonic components correlate very well with a maximum difference of 0.25A at the fundamental component.

Table 3.6: Rectifier current harmonics for the mains supply

	Fundamental	5th	7th	11th	13th	17th	19th
Test Harmonics							
I_m[A]	4.55	4.23	3.94	3.06	2.85	1.66	1.44
I_m[A] pu	1.00	0.93	0.87	0.67	0.63	0.37	0.32
I_m[A] % of f1	100.00	93.11	86.60	67.30	62.66	36.52	31.62
Simulation Harmonics							
I_m[A]	4.8	4.36	3.98	2.92	2.4	1.3	0.89
I_m[A] pu	1.00	0.91	0.83	0.61	0.50	0.27	0.19
I_m[A] % of f1	100.00	90.83	82.92	60.83	50.00	27.08	18.54
% Error on I_m	5.5	3.1	1.0	4.6	15.8	21.7	38.2

The current amplitude of the fundamental, 5th through to the 19th harmonic, for the test and simulation, are compared in Table 3.6. The 5th, 7th and 11th harmonics correlate well. Larger error in the higher order harmonics are acceptable because lower order harmonics have a more significant impact.

3.6 CORRELATION OF TEST BED AND SIMULATION FOR THE LAB GENERATED VOLTAGE SUPPLY

The laboratory generator set voltage supply is used from the UCT's lab. The objective is to show that the developed drive model is robust enough to work with voltage supplies with high distortion.

3.6.1 Current and voltage comparison

Industrial voltage supplies can be 'dirty', that is, rich in undesirable harmonics due to, among other things to nonlinear loads in the three phases. This supply was made available by driving the 500kVA, 6.6kV alternator with a 75kW induction machine via an IM drive. Similarly, the objective is to determine base reference quantities while proving that the developed model accurately models the test beds. Figure 3.11 displays the three-phase voltage waveform (380V line-to-line).

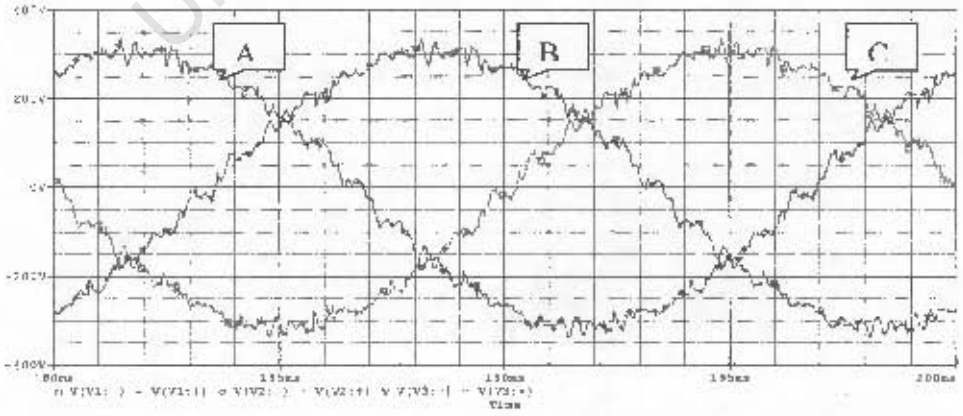

Figure 3.11: Machine's lab generated three-phase line-to-line voltage supply

The output of the alternator is fed to the test bed drive via a 6.6kV to 380V line-to-line transformer. The supply voltage is captured in a CSV file, which is then fed into the PSpice model. Again voltages and currents are recorded for both the simulation and the test bed in Table 3.7 (a)-to- (d).

Table 3.7: Comparison of simulated and test bed measured results for the laboratory generated voltage supply

(a) Rectifier currents

	I_{peak} (A)	I_{rms} (A)
Simulated	23.5	5.7
Measured	25.2	5.8
% Error	6.7	1.7

(b) DC-Link voltage

	V_{ave} (V)	V_{pp} (V)	% Ripple
Simulated	525	9.1	1.7
Measured	534.6	8.9	1.7
	1.8	2.2	0

(c) Inverter current

	I_{peak} (A)	I_{RMS} (A)
Simulated	10	7
Measured	10.6	7.1
	5.6	1.4

(d) Inverter output line-to-line voltage

	V_m (V)	V_{RMS} (V)
Simulated	528	295
Measured	531	274
% Error	0.6	7.7

It can be seen from Table 3.7 (a)-to-(d) that the simulated result correlates with the test bed result. This result further validates the developed model, that is, any industrial three-phase supply can be used and voltages and currents predicted. Although the model is developed for a 3kW induction motor, with the parameter knowledge of other machines e.g. 75kW, it can be modified accordingly and upgraded to the required power rating.

3.6.2 Rectifier current harmonics comparison

Again the model predicts the rectifier current harmonics within acceptable accuracy (+/- 10% of the measured value). The exception is at the 17th and 19th harmonics, where the predicted magnitudes are 0.69A and 0.4A respectively. The actual magnitudes are, 1.17A and 1.12A respectively, with errors of 61.2% for the 17th harmonic and 64.3% for the 19th harmonic.

Table 3.8: Rectifier current harmonics for the lab generator

	Fundamental (f_1)	5th	7th	11th	13th	17th	19th
Test Harmonics							
I_m [A]	4.55	3.80	2.85	2.38	1.44	1.78	1.12
I_m [A] pu	1.00	0.84	0.63	0.52	0.32	0.39	0.25
I_m [A] % of f_1	100.00	83.56	62.66	52.36	31.62	39.27	24.60
Simulation Harmonics							
I_m [A]	4.59	3.43	2.62	1.41	1.12	0.69	0.4
I_m [A] pu	1.00	0.75	0.57	0.31	0.24	0.15	0.09
I_m [A] % of f_1	100.00	74.73	57.08	30.72	24.40	15.03	8.71
% Error on I_m	0.9	9.7	8.1	40.8	22.2	61.2	64.3

The fundamental, 5th through to the 19th harmonic amplitudes are compared. Generally the simulation results are an under-estimate. That is, the measured 5th harmonic amplitude is 83.56% of the fundamental. The predicted 5th harmonic amplitude is only 74.73%, resulting in a difference of almost 9%. This trend is also observed at other harmonic orders.

3.7 CORRELATION OF TEST BED AND SIMULATION FOR AN UNBALANCED MAINS VOLTAGE SUPPLY

An arbitrary voltage unbalance setting is chosen, and a test run at this setting. The resulting voltages are recorded for both the test bed and simulation. The two measurements are compared to show that the developed drive model can be used to predict the impact of unbalanced voltage supplies on induction motor drives. Figure 3.12 displays the unbalanced line-to-neutral mains supply voltages and the corresponding RMS and amplitude magnitudes in Table 3.9. The unbalance introduced is only magnitude unbalance, because the laboratory currently does not have the capability of introducing phase unbalance.

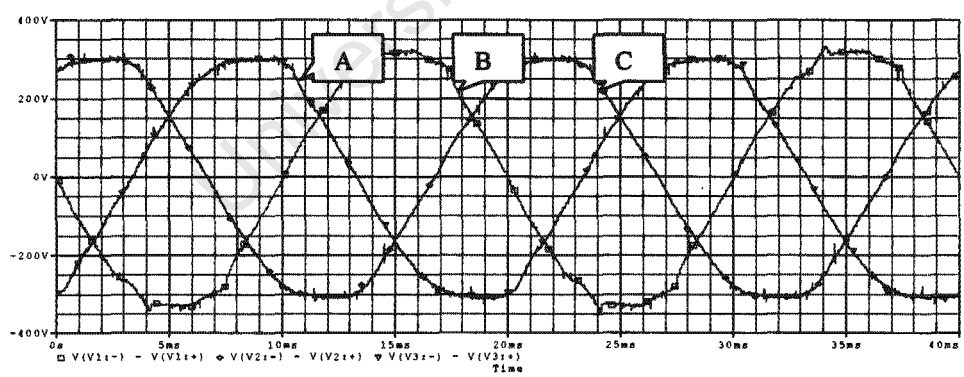

Figure 3.12: Mains three-phase voltage supply with unbalance

Table 3.9: Unbalance line-to-neutral voltages

	V_{an}	V_{bn}	V_{cn}
V_m [V]	331	315.5	309.3
V_{RMS} [V]	236.7	223	223.8
Phase	0°	120°	240°

Since these voltages were set arbitrarily, the percentage unbalance according to the NEMA definition can be calculated. The corresponding line-to-line voltages are:

$$V_{ab} = 397.84V$$

$$V_{bc} = 384.92V$$

$$V_{ca} = 400.2V$$

And the average line-to-line voltage is:

$$V_{ave} = 394.32V$$

The fact that the average voltage is greater than 380V, which is the nominal voltage magnitude, means that there is an overvoltage. The overvoltage is 14.32V on average, correspond to 3.8% of 380V. The maximum deviation from the average is;

$$\Delta V_{\max} = \|394.32 - 384.92\| = 9.4V$$

$$\therefore \%LUVR = 100 * \frac{9.4}{394.32} = 2.4$$

3.7.1 Impact of voltage unbalance on rectifier current

Figure 3.13 and 3.14 shows the rectifier current waveform for one cycle and phase measured for the unbalanced calculated above. The effects of unbalanced voltage supply are evident from the unequal current pulses. Table 3.10 tabulates the comparison of the measured and simulated current magnitudes.

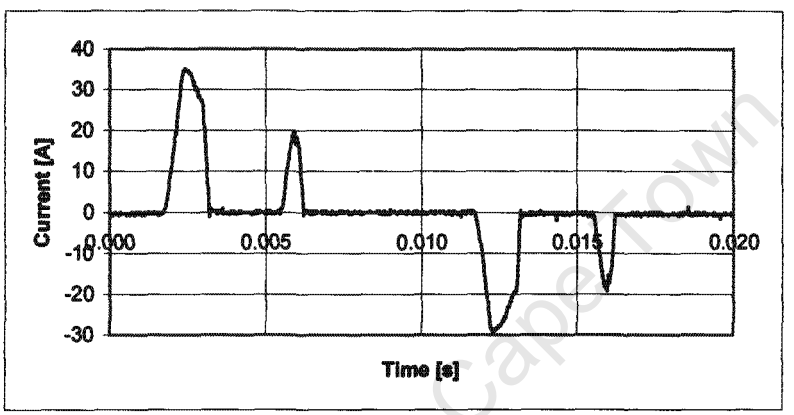

Figure 3.13: Measured rectifier current

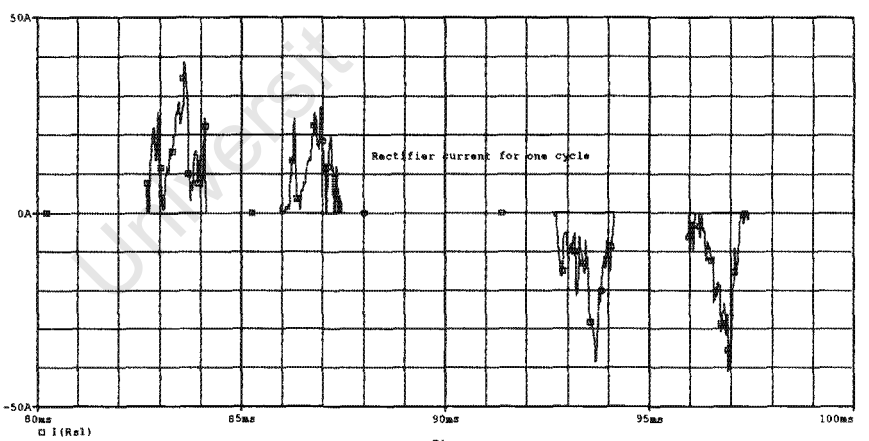

Figure 3.14: Simulated rectifier current

Table 3.10: Rectifier line currents showing the effect of unbalance

	Line a		Line b		Line c	
	I_m	I_{RMS}	I_m	I_{RMS}	I_m	I_{RMS}
Simulated	37	8.8	39.1	7	42	6.2
Measured	35.5	8.3	34.4	6.7	33.3	6.9
% Error	4.2	5.9	13.7	3.4	26	10.3

Therefore, unbalanced voltage with an overvoltage increases the peak rectifier currents and causes an uneven distribution of load amongst the three rectifier lines. This is undesirable because the peak rating of power handling semiconductors may be exceeded, resulting in equipment failure. Moreover, other sensitive loads connected at the same coupling point may be affected due to the uneven current drawn by the drive.

3.7.2 Impact of voltage unbalance on DC-link voltage

The average dc-link voltage at nominal balanced voltage supply of 380V line-to-line is 555V. Under unbalance conditions with overvoltage, the dc-link voltage is predicted to be 564.4V and the actual is 570.3V as shown in Table 3.11. The measured and simulated waveforms are displayed in Figure 3.15 and 3.16.

Table 3.11: DC-Link voltage showing the effect of voltage unbalance

	V_{ave}	V_{pp}	% Ripple
Simulated	564.4	19.77	3.5
Measured	570.3	14.7	2.6
% Error	1	34	35

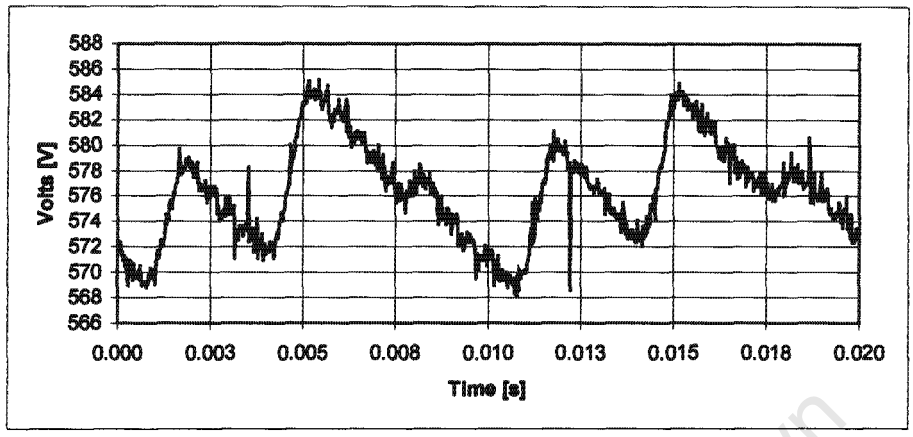

Figure 3.15: Measured dc-link voltage showing effects of unbalance

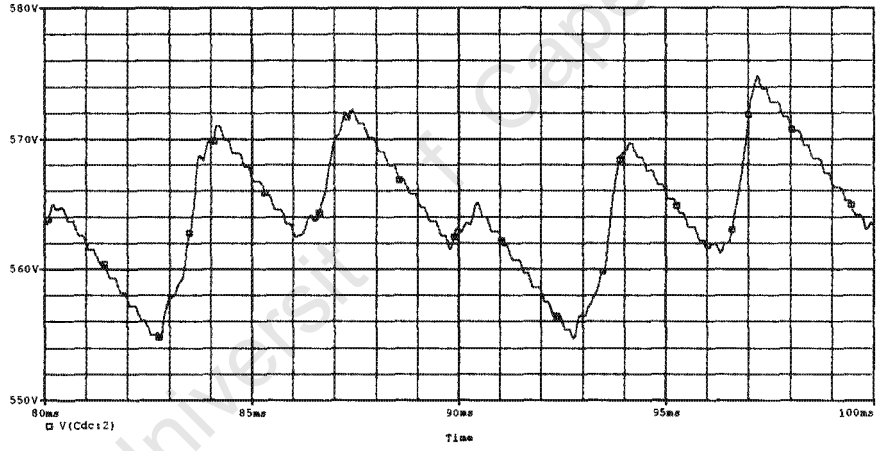

Figure 3.16 Simulated dc-link voltage showing effects of unbalance

The simulation overestimates the dc-link ripple by 0.9%. The test bed exhibits a peak-to-peak voltage of 14.7V and the simulation, 19.8V, an over estimate by 5.1V. Voltage unbalance increases the DC-Link voltage above the nominal voltage and the percentage ripple. The simulation correlates with the measured magnitude. An error of 1% on the average dc-link voltage is recorded. There are larger with ripple voltage.

3.7.3 Impact of voltage unbalance on inverter output voltage

The inverter voltage is balanced for all three phases. It is observed that the inverter draws power from the dc-bus, hence the peaks correlate with the dc-link peak voltage magnitude. Therefore, the induction machine "sees" balanced three-phase voltages with increased peaks due to the unbalances on the supply side. Therefore, the effect is only on the voltage peak magnitude. These voltage magnitudes are tabulated in Table 3.12. The measured and simulated inverter output waveforms are displayed in Figure 3.15 and 3.16.

Table 3.12: Inverter output line-to-line voltage

	Line a		Line b		Line c	
	V_m	V_{RMS}	V_m	V_{RMS}	V_m	V_{RMS}
Simulated	570	317	565	317	574	317
Measured	570	314	575	321	575	315
% Error	0	1	1.7	1.2	0.2	0.6

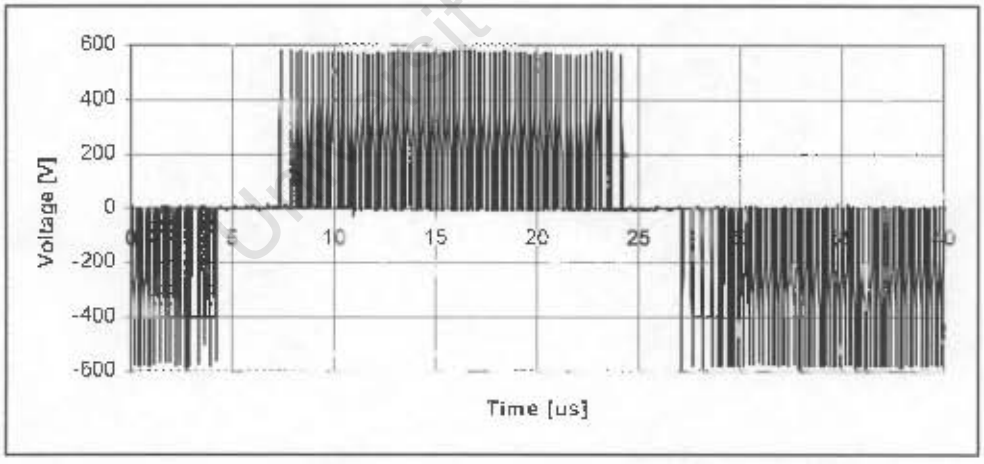

Figure 3.18: Measured inverter output voltage waveform

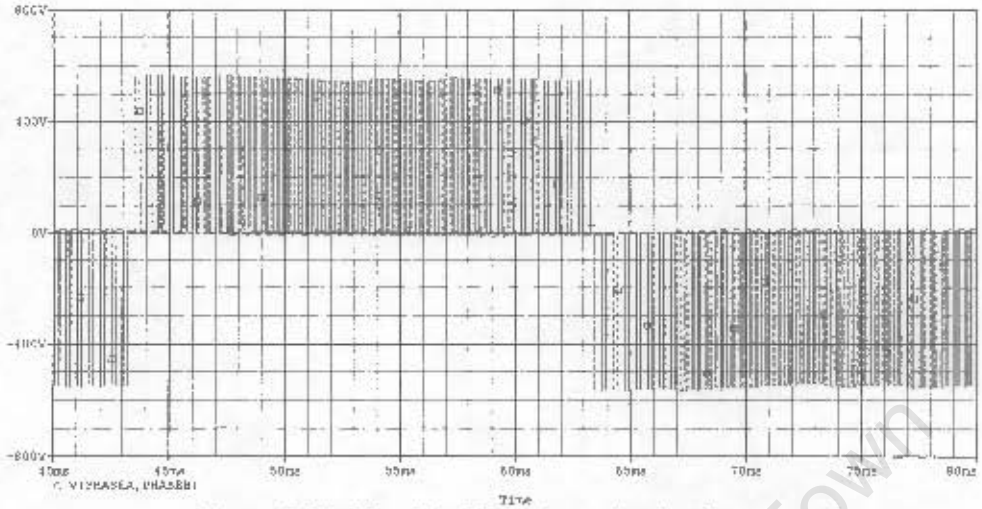

Figure 3.19: Simulated inverter output voltage waveform

3.7.4 Impact of voltage unbalance on inverter output current

The corresponding currents are also balanced. This is in agreement with the fact that the load is balanced. The induction motor "load" is rated at 6.5A in star connection. The simulation and test show that the motor is drawing over-currents of, 7.47A and 7.2A. The additional current will increase the operating temperature of the motor. Moreover, the copper losses will increase and the life of the machine will be degraded. The line current magnitudes are tabulated in Table 3.13 and the measured and simulated waveforms are displayed in Figure 3.20.

Table 3.13: Inverter output line currents

	Line a		Line b		Line c	
	I_m	I_{RMS}	I_m	I_{RMS}	I_m	I_{RMS}
Simulated	10.76	7.47	10.85	7.47	10.84	7.47
Measured	10.76	7.2	10.76	7.27	10.72	7.2
% Error	0	3.8	0.8	2.8	1.1	3.8

It can therefore be stated from the above results that the developed drive model can be used to predict the impact of voltage unbalance on induction machines.

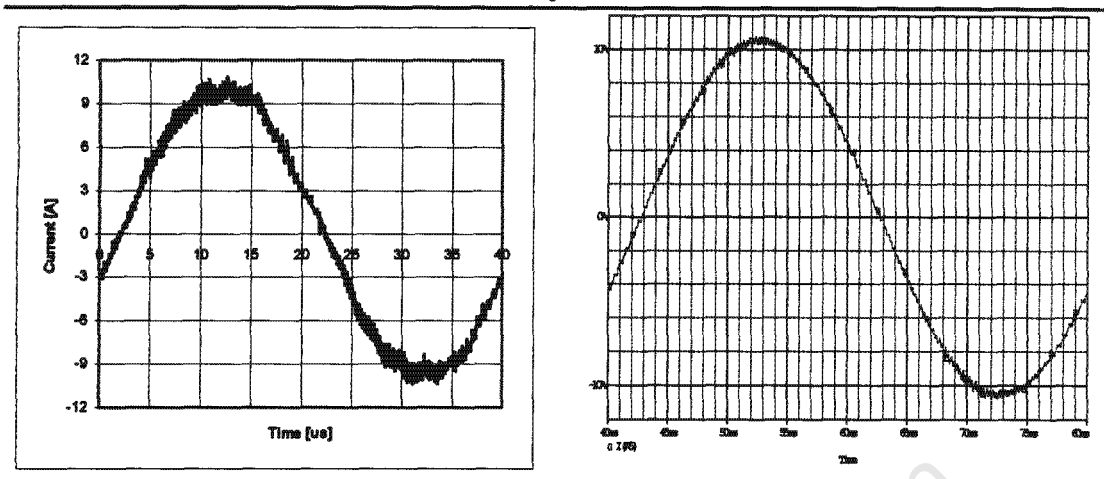

Figure 3.20: Rectifier currents, measured & simulated, respectively

3.8 VOLTAGE UNBALANCE SIMULATION OF IM VSD

The developed PSpice model has proved the capability of modeling induction motor variable speed drives within acceptable accuracy. Furthermore, the model works for unbalanced voltage conditions. The only critical requirement is knowledge of system parameters. This section is a parametric study of the impact of increasing unbalance on the induction motor variable speed drives.

3.8.1 Three-phase voltage supply

Three-phase voltages with 1%, 2%, 3%, 4% and 5% unbalance are generated using the true definition of voltage unbalance. These voltages are generated such that the NEMA definition of voltage unbalance is also valid. Figure 3.21 displays the three-phase line-to-line voltages, starting with balanced voltage supply and with 1%, 3% and 5% voltage unbalance.

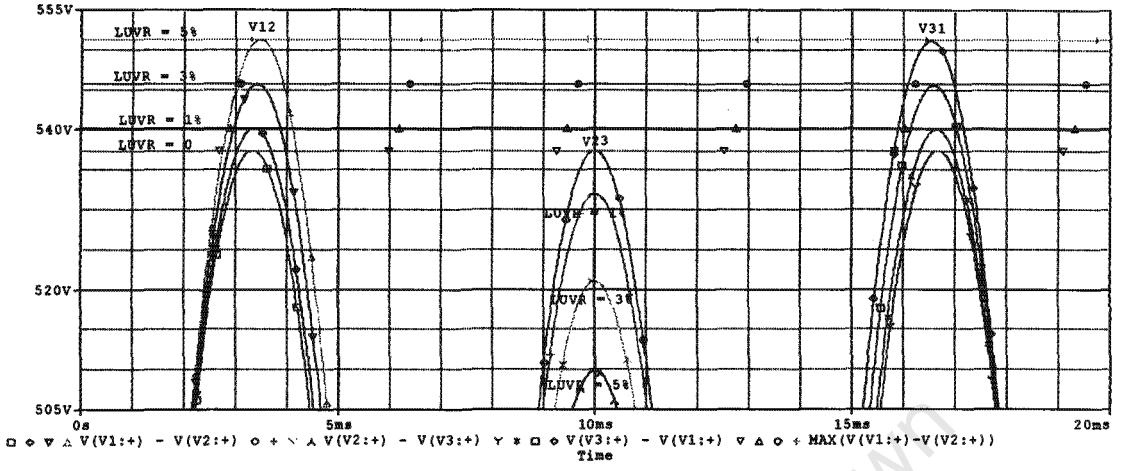

Figure 3.21: Supply voltage peaks for zero, 1%, 3% and 5% voltage unbalance

A closer look at Figure 3.21 shows that V_{12} and V_{31} increase in magnitude, while V_{23} decreases. Moreover, V_{23} serves as the reference voltage for the other two, with phase angle at zero degrees. Table A3.3 in Appendix A3.2 tabulates the selected voltage magnitudes and phase angles as a function of voltage unbalance for simulation purposes.

3.8.2 Dc-link voltage

The average dc-link voltage increases with an increase in voltage unbalance for a constant average voltage. For balanced conditions the dc-link voltage has six-pulses, due to the six line-to-line charging voltages. This is the characteristic of the dc-link voltage. In the presence of voltage unbalance this characteristic is degraded resulting in only four pulses per cycle, for a 2% voltage unbalance indicating that not all phases are conducting. Figure 3.22 shows the dc-link voltage for one cycle of the supply voltage (50Hz) starting at balanced conditions up-to 5% voltage unbalance. It is observed that unbalance changes the frequency of the dc link voltage.

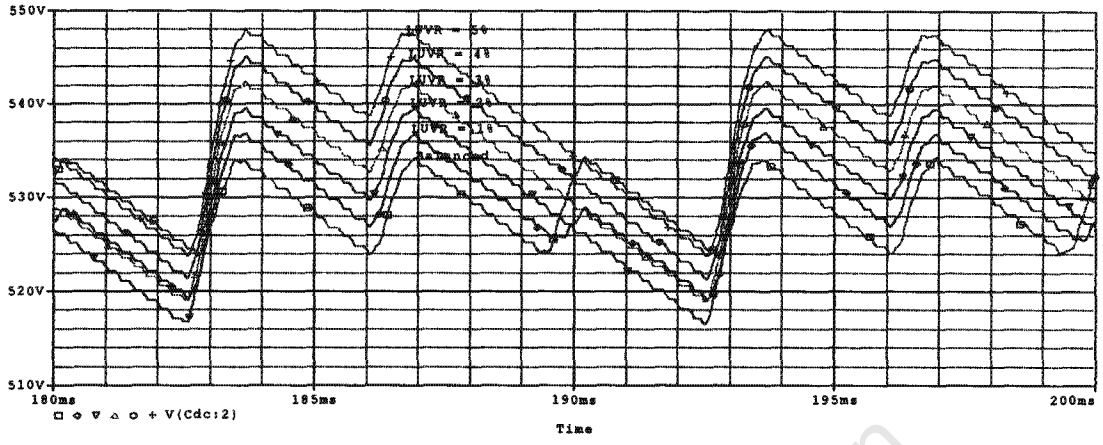

Figure 3.22: DC-Link voltage for balanced voltage supply up-to 5% voltage unbalance

The average dc-link voltage increases from 529.14V under balanced conditions to 538.3V at 5% voltage unbalance for a constant average unbalance supply voltage. The peak-to-peak ripple shows distortion due to the unbalanced voltage supply, with a ripple of 10.44V (1.97%) under balanced conditions. This ripple increases to 24.6V (4.57%) at 5% supply voltage unbalance, as tabulated in Table 3.14. Furthermore, the ripple frequency is reduced from 300Hz at balanced conditions to 100Hz for unbalanced conditions.

Table 3.14: Average dc-link voltage

	DC-Link voltage [V]		
%LUVR	Vdc	Vp-p	%Ripple
0	529.14	10.44	1.97
1	529.3	17.8	3.36
2	530.4	23.15	4.36
3	533	23.75	4.46
4	535.6	23.95	4.47
5	538.3	24.6	4.57

3.9 RECTIFIER CURRENT EVALUATION

The current drawn by the rectifier and associated harmonics affect the drive and other loads connected at the same point of coupling.

3.9.1 Peak to peak rectifier current

At steady state, the dc-link capacitor is fully charged with the characteristic voltage ripple. Consider the top-three diodes, D1, D3 and D5 in Figure 3.23. Current only flows when the voltage supply to the diode rectifier is greater than that of the dc-link capacitor. This happens at the voltage peaks when the diodes are forward biased, as shown in Figure 3.24.

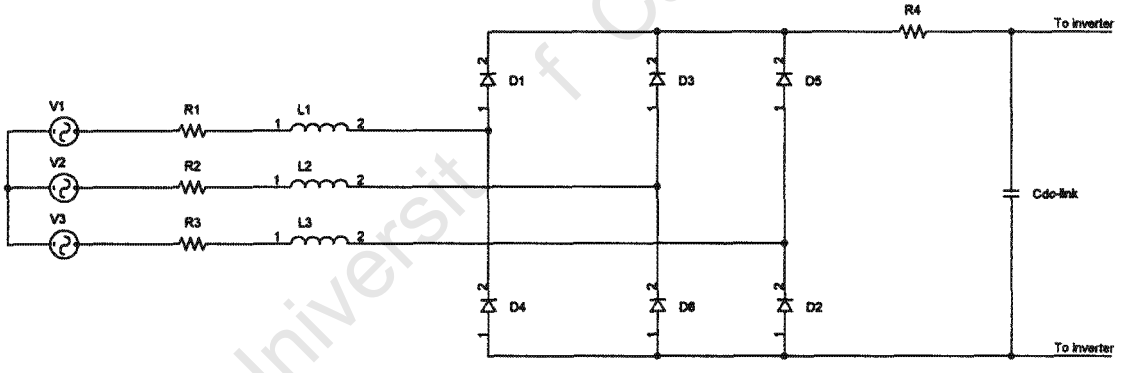

Figure 3.23: Three-phase diode rectifier

$\upsilon_{1,2,3} > \upsilon_p$ For the positive peaks

$\upsilon_{1,2,3} < \upsilon_n$ For the negative peaks

Where, υ_p and υ_n, are the positive and negative bus voltages respectively.

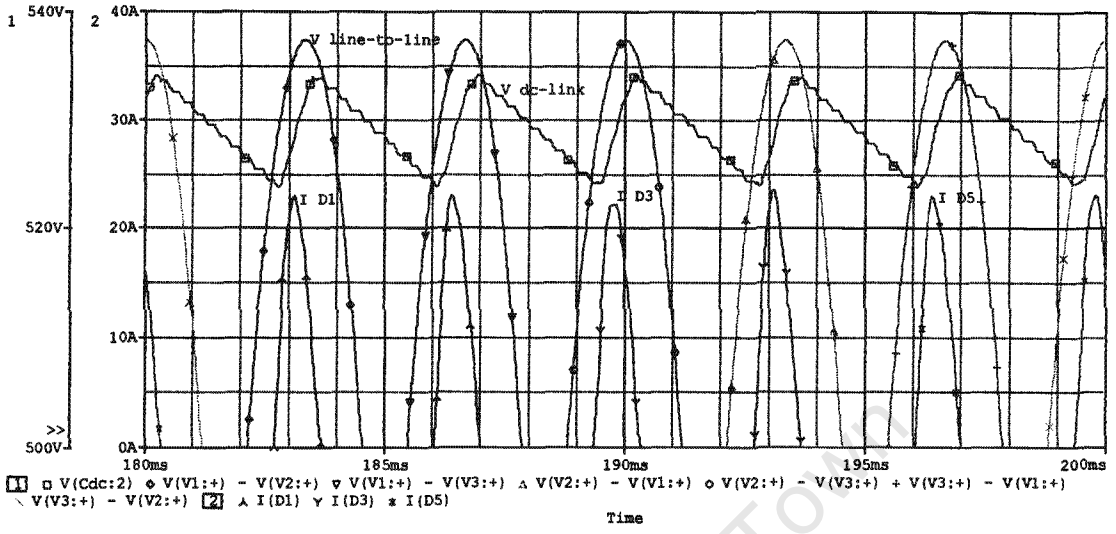

Figure 3.24: Forward biased rectifier diodes conducting

The dc-link voltage in Figure 3.25 is compared to the six line-to-line voltages for the balanced simulated voltage scenario. The diode current can be seen only during the periods where the supply voltage is greater than the dc-link voltage. Current flows for approximately 1ms per current pulse. This is equivalent to 18°

of the 360°,supply voltage cycle. There are two pulses per diode, therefore, current only flows for 2ms (36°), and not 6.67ms (120°), which occurs with an inductive dc link. During this period the current peak rises from zero to 23.6A, with an RMS value of 6.9A for balanced voltage supply. It is noted that during the 2ms, the diode current is discontinuous, with two equal pulses. There are six line-to-line voltages charging the dc-link capacitor. Let the three phase voltages be 1, 2 and 3. Therefore the six line-to-line voltages are,

$$V_{12}, V_{13}, V_{21}, V_{23}, V_{31} and V_{32}$$

Hence the three-phase diode rectifier is also known as a six-pulse diode rectifier. In the presence of voltage unbalance the six line-to-line voltages are unequal.

Therefore the dc-link capacitor charges to three different voltage levels. Figure 3.11 shows the dc-link voltage for one cycle at steady state for two scenarios.

The pulses are all identical to the balanced voltage supply case. Superimposed on Figure 3.11 is the dc-link voltage with 1% voltage unbalance.

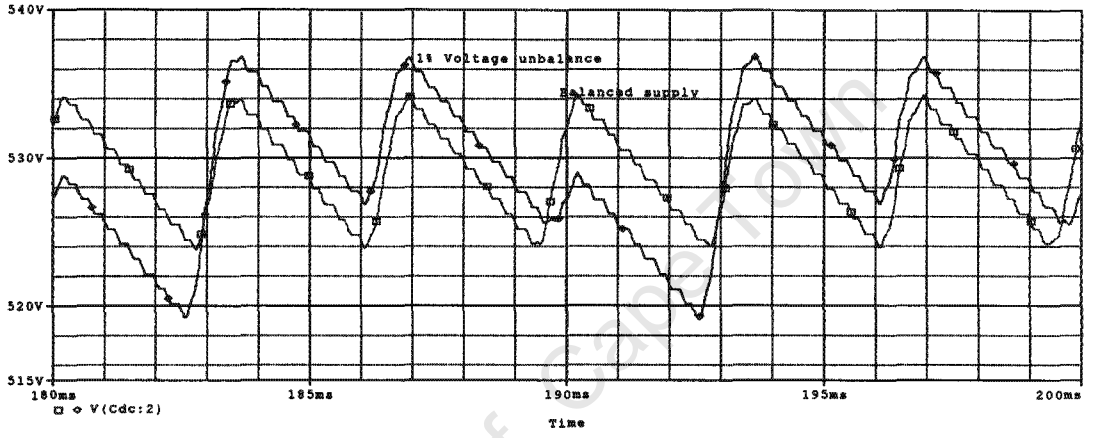

Figure 3.25: DC-link voltage for balanced and 1% unbalance voltage supply

In Figure 3.26 the current through D1, D3 and D5 show the result for 1% voltage unbalance, which is evident through the unequal peaks of the double-pulse rectifier current characteristic. Consider the current through D1, the 1st pulse from the left in Figure 3.26, peaks at 31.27A. The conduction lasts for 1.2ms (21.6°). The diode conducts for a longer period than for balanced conditions, for the first pulse. Hence, the peak is greater than for balanced conditions. The second pulse, diode D1 conducts for only 0.928ms (16.704°), resulting in a peak of 22.8A. This peak is less than at balanced conditions.

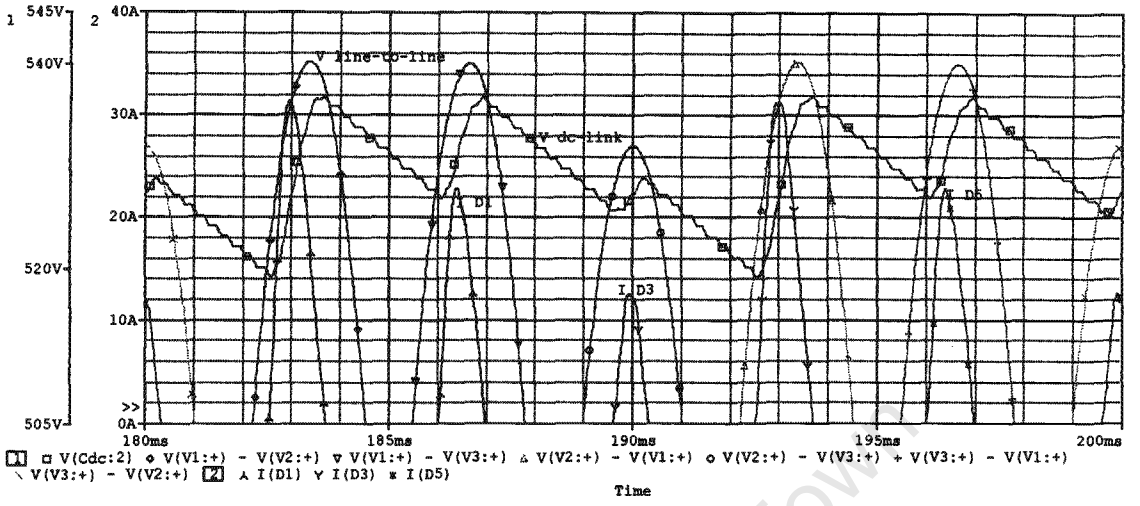

Figure 3.26: Diode currents for 1% unbalanced voltage supply

The 3rd current pulse flowing through D5, on Figure 3.26 peaks at 12.5A. D5 conducts for 0.79ms (14.22°). At 2% voltage unbalance the 1st current pulse-peak through D1 is 37.27A. D1 conducts for 1.322ms (23.796°), while the 2nd pulse, peaks at 23A and conducts for 1ms (18°) as shown in Figure 3.27.

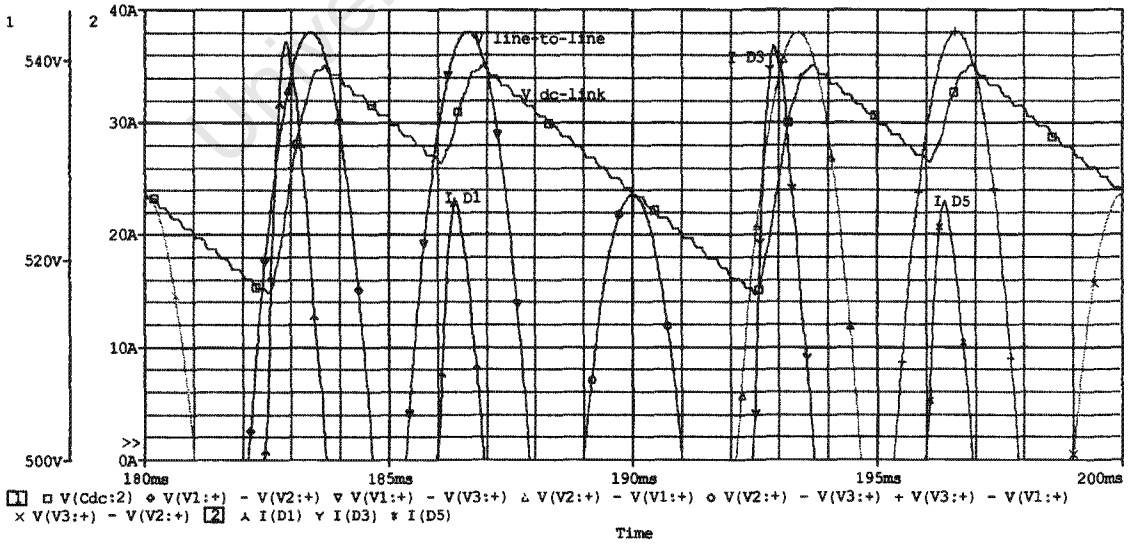

Figure 3.27: 2% Voltage unbalance, resultant dc-link voltage and currents

A closer look at Figure 3.27 shows that at 2% voltage unbalance two of the six supply voltage peaks have decreased to such an extent that two diodes cannot be forward biased (see Figure 3.23 at 190ms). Diode D1 conducts for both instants, with two unequal current pulses. Diode D3 only has the 2nd of the two current pulses. This is because the line-to-line voltage supply does not exceed the dc-link voltage, hence the diode is not forward biased. This is also evident through the continuous decay of the dc-link voltage to 190ms in Figure 3.23. That is, the dc-link capacitor is not charged at this instant and the inverter continues to draw power as the dc-bus voltage is degraded. In the cases of 3%, 4% and 5% voltage unbalance, the response to voltage unbalance is similar.

3.9.2 Impact of unbalance voltage on rectifier current waveform

The effect of unbalanced voltage on the rectifier current depends on a comparison of the supply line-to-line voltage with the dc-link voltage at steady state. The current in each line follows the voltage trend, that is, two line currents tend to increase with an increase in voltage unbalance. The third line current decreases with an increase in voltage unbalance. In Table 3.15, the RMS line current as a function of percentage voltage unbalance ratio and corresponding peaks are listed.

Table 3.15: Rectifier line currents as a function of LUVR

%LUVR	Rectier line Currnt [A]					
	Phase A		Phase B		Phase C	
	I_{peak}	I_{RMS}	I_{peak}	I_{RMS}	I_{peak}	I_{RMS}
0	23.6	6.9	23.1	6.9	23.6	6.9
1	31.27	8.66	31.27	7.6	22.8	5.31
2	37.27	10	37.27	8.8	23	4.8
3	37.5	10.05	37.5	8.85	22.8	4.9
4	37.5	10.05	37.5	9.0	23	4.7
5	37.8	10.2	37.5	9.1	22.6	4.6

Figure 3.248 displays the current for the three top diodes of the rectifier, from balanced conditions to 5% voltage unbalance, Appendix A3.3 displays the current waveforms through each diode.

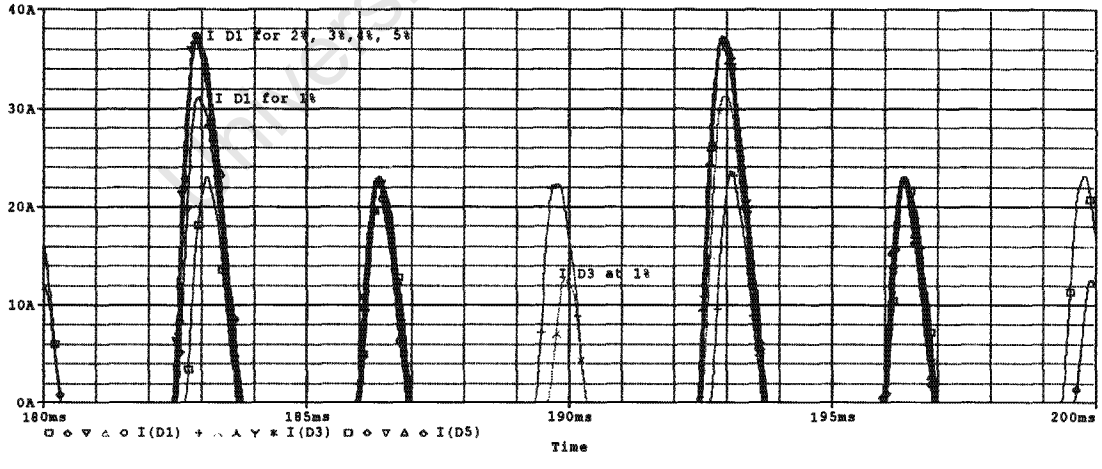

Figure 3.28: Current through Diode 1, 3 and 5

The first current peak through D1 reaches a maximum value at 2% LUVR. After this, any increase in LUVR causes an insignificant increase in the current peak.

The second peak remains almost constant at 23A. In D3 the first peak and in D5 the second peak reduces to zero at 2% LUVR.

3.10 INVERTER OUTPUT VOLTAGE AND CURRENT (Induction motor input)

The output voltage and current of the inverter become the input to the motor.

3.10.1 Inverter line-to-line output voltage

The dc-link voltage increases with increase in voltage unbalance, which is in turn pulsed through the switches (PWM) on to the inverter output voltage. Hence the inverter output voltage has peaks equal to the dc-link voltage peaks. This is extracted from the result tabulated in Table 3.16, whereby the voltage peaks increase with an increase in percentage unbalance. Figure 3.29 is a plot of percentage unbalance and the peak inverter voltage.

Table 3.16: Inverter line-to-line voltage

%LUVR	V_{peak}	V_{RMS}
0	534	300
1	537	300
2	540	300
3	543	300
4	546	300
5	550	300

In ideal terms the line-to-line RMS voltage at the fundamental frequency is given by:

$$V_{LL1(line-to-line)} = \frac{\sqrt{3}}{2\sqrt{2}} m_a V_{dc} \qquad (3.9)$$

Where, m_a is the amplitude modulation ratio and

V_{dc} is the average dc-link voltage.

Consider a case where m_a is constant, such as in the drive model simulated in this report ($m_a = 0.6$). Therefore Equation (3.9) would be,

$$V_{LL1(line-to-line)} = k_1 V_{dc} \qquad (3.10)$$

Where k_1 is the constant of proportionality.

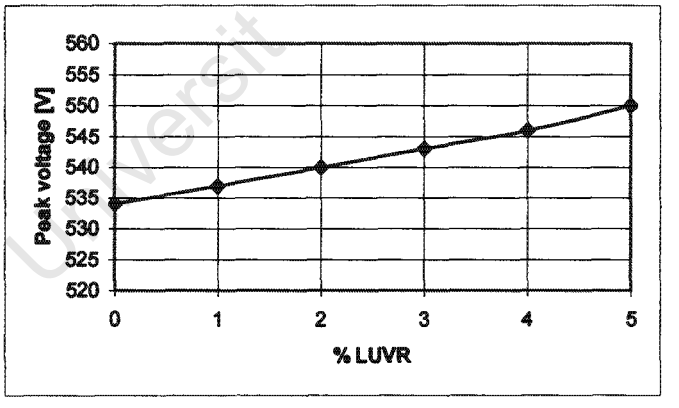

Figure 3.29: Inverter output peak voltage

It can be observed from Equation (3.10) that the fundamental line-to-line inverter output voltage should increase linearly with an increase in the dc-link voltage. The RMS voltages remain constant; this is because the modulation ratio (m_a = 0.6) and the switching frequency (f_s = 2kHz) are constant. But in Table 3.17 it's

not the case. The RMS voltage in Table 3.17 is the RMS voltage of the whole waveform, not the fundamental component only as in Equation (3.10).

3.10.2 Inverter line current

Noting that the modulation ratio and switching frequency are constant at,

$$m_a = 0.6$$

$$f_{ss} = 2kHz$$

Table 3.17: Induction motor line currents

%LUVR	I_{peak}	IRMS
0	10	7
1	10	7
2	10	7
3	10.1	7.05
4	10.1	7.05
5	10.1	7.1

The motor will draw a current to match the required torque. Table 3.17 shows that the motor draws balanced constant three-phase currents, because the load torque is constant.

3.11 CONCLUSIONS

The three-phase mains supply at the University of Cape Town Machine's Laboratory is distorted and unbalanced. This introduces undesirable inaccuracies in the tests results. However, this does represent the practical scenario, where an acceptable unbalance is always present in a distribution network.

CHAPTER THREE

Drive Model Development and Simulation

A PSpice Supply-Drive-IM model has been successfully developed and correlated with test measurements for balanced voltage supplies. Furthermore, the model was also tested for simulating the impact of voltage unbalance on IM drives. The results were compared and verified with test measurements.

Percentage unbalance as low as 2% can cause considerable increase in the rectifier input peak currents. The rectifier current peak at balanced conditions was measured to be 23.6A. It increased to 37.3A at 2% voltage unbalance. This is an increase of 58%. The voltage unbalance may seem small, but the effect it has on current is considerable. At 3%, 4% and 5% voltage unbalance, the increase in the rectifier current peak is not as large as the initial increase with the 2% unbalance.

The dc-link voltage characteristic six-pulse is distorted in the presence of voltage unbalance, resulting in an increase in the average dc-link voltage. Ultimately the IM draws 0.5A more current than the rated 6.5A RMS.

The output voltage of the inverter is balanced, despite the presence of voltage unbalance on the supply. As a result the line currents drawn by the motor are also balanced.

A baseline for future reference has been documented at balanced voltage supply conditions. Furthermore, unbalance voltage does not exist in isolation, it is normally coupled with under or overvoltage supply, which the developed PSpice program is able to simulate.

CHAPTER FOUR

Impact of Cables in PWM VSDs

4.1 INTRODUCTION

The effective application of VSDs requires a detailed understanding of VSD operation, motor performance, load characteristics and installation problems. The use of IGBTs switches has not only improved the performance of VSDs, but also introduced new issues with regard to motor overvoltages [17].

An inverter duty motor is interpreted differently by different motor manufactures. It may not imply the ability to handle the increased reflected wave voltage stress resulting from IGBT drive applications [17]. This chapter uses an existing cable model for simulating the 2pu or greater (1pu = dc bus voltage) reflected voltage wave phenomenon for both the cable and induction motor. The system is analyzed for a balanced voltage supply initially. Unbalanced voltage supplies are then applied to the model and the results discussed. It is discovered that the initial model employed is insufficient because there are two frequency bands, the normal power frequency waveform and the reflected high frequency waves. This necessitates a modification to the existing cable model.

4.2 REFLECTED WAVE PHENOMENON (RWP)

4.2.1 RWP analysis

The inverter of a PWM drive does not produce a sinusoidal output voltage but generates a continuous string of pulses as shown in Figure 4.1. These pulses propagate through the cable from the inverter output to the motor terminals. The peak of the inverter output voltage is equal to the dc bus peak voltage. However, the voltage peaks at the motor terminals are not necessarily equal to the dc bus voltage peaks, but depend on the dynamics of the drive-cable-motor circuit [17].

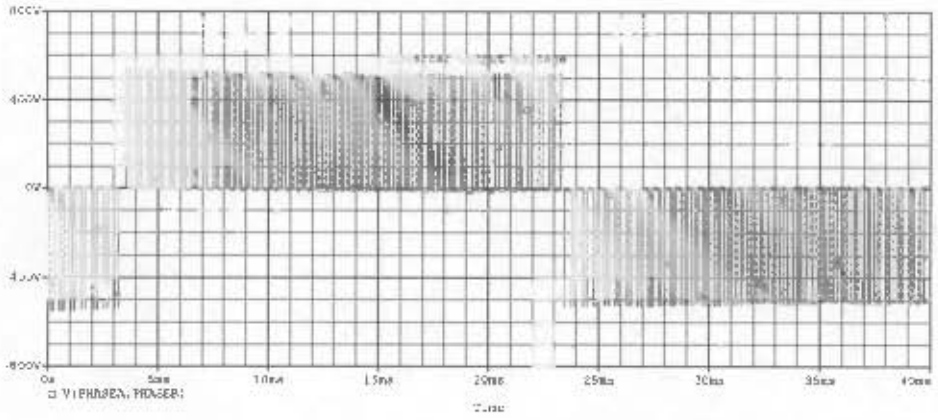

Figure 4.1: Inverter output voltage "Train of pulses"

The drive-cable-motor circuit dynamics depend on:-

- *Inverter output voltage rise time, $\frac{dv}{dt}$,*
- *Cable length,*
- *Cable transmission line characteristic and*
- *Motor impedance.*

Transient overvoltages at every switching point are evident at the motor's terminals, and are illustrated in Figure 4.2 for one pulse. The overvoltages can exert destructive stresses on the motor insulation, thereby reducing motor life.

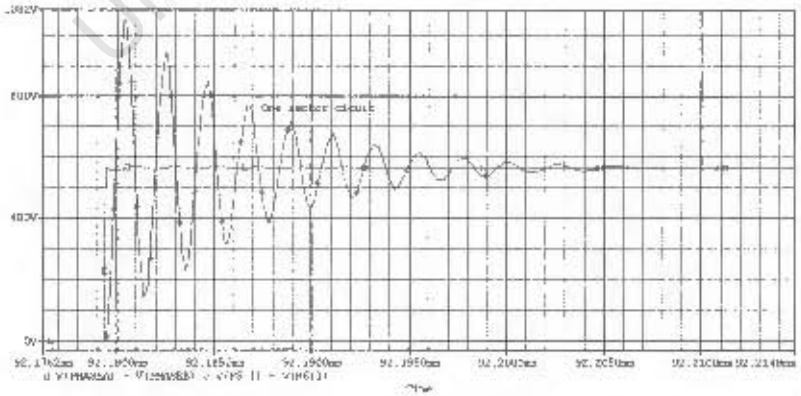

Figure 4.2: Transient overvoltage at switching for one phase

A space-time ladder diagram, as shown in Figure 4.3, is a technique of tracing the various reflections and their resultants. The horizontal axis is the distance along the cable length, and time is plotted on the vertical axis. Distance is from left to right, while time is from the top to bottom. The zigzag lines represent the wave fronts of the various reflections and the numbers attached to the lines indicate the magnitudes of the individual waves. The magnitude of each reflection is obtained by multiplying the magnitude of the incident wave by the reflection coefficient at the point where the reflection takes place. The number shown in each intervening space is the sum of the individual waves above that point, and represents the net voltage in that region of the diagram. The voltage at any time can be obtained from the diagram.

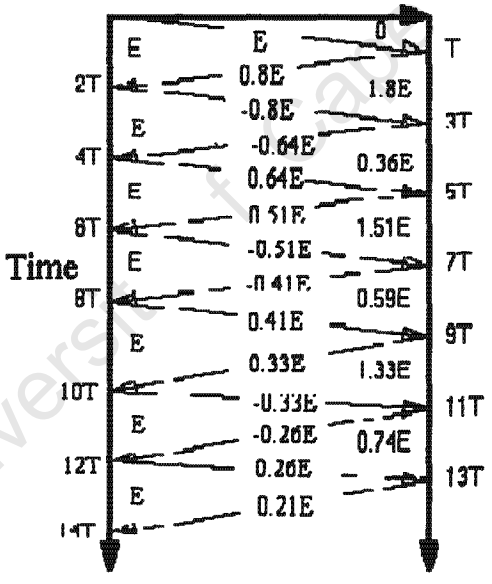

Figure 4.3: Voltage reflection diagram

With time, the reflected voltage will decay to 0 and the voltage at the load will converge to E. However, at the next PWM switching point, the process will be repeated. The voltage at the source will remain at E for all times for zero source impedance. The waveform of the voltage at the load end is shown in Figure 4.4, for a terminal reflection coefficient of 0.87.

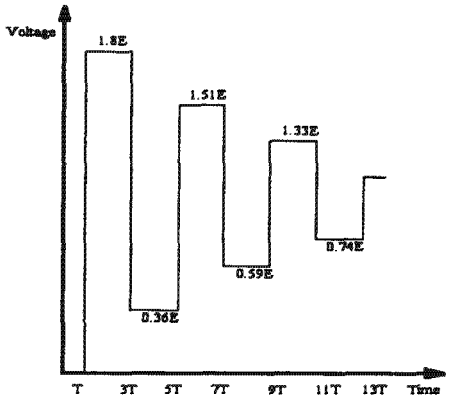

Figure 4.4: Voltage at induction motor terminals

4.2.2 Causes of reflected waves in long cable leads

The reflected wave phenomenon in long cables can be explained using transmission line theory. The inverter output voltage is equal to the dc bus voltage. However at the receiving end, at the IM terminals, the voltage peak depends on a voltage ring-up factor Γ [17].

Where,

$$0 \leq \Gamma \leq 1$$

It is also referred to as the 'Reflection coefficient' and is a function of source impedance (Z_s), cable surge impedance (Z_0) and load surge impedance (Z_{load}). The relation between these parameters is expressed in Equation (4.1) and (4.2).

$$\frac{E_t^-}{E_t^+} = \frac{Z_t - Z_0}{Z_t + Z_0} = \Gamma_t \qquad (4.1)$$

Where: E_t^- is the incident voltage wave at the load end,

E_t^+ is the reflected wave at the load.

$$\frac{E_s^-}{E_s^+} = \frac{Z_{load} - Z_0}{Z_{load} + Z_0} = \Gamma_t \qquad (4.2)$$

Similarly: E_s^- is the incident voltage wave at the source and,

E_s^+ is the reflected wave at the source.

$$\therefore V_{IM} = (1 + \Gamma_t) * V_{inverter} \qquad (4.3)$$

In long cables the voltage propagates in waves. Whenever the cable surge impedance does not match that of the motor, the voltage wave will be reflected at the motor terminals. It can be shown that the peak of the reflected wave can exceed 2pu of the sending end voltage [18].

4.2.3 Variables affecting reflected wave magnitude

Factors affecting motor overvoltage magnitude can be summarized as [17]:

- Motor and cable surge impedance
- Motor load
- Cable length
- Magnitude of drive pulse
- Rise time of drive pulse
- Spacing of PWM pulses

The cable and motor surge impedance mismatch are the primary causes of the motor terminal overvoltage problem.

4.3 CABLE CHARACTERISTIC IMPEDANCE

Long cables are inevitable because the converter is often housed in a clean positive pressure environment, to prevent problems associated with dust and for cooling purposes. The induction motor would be where the process takes

place several tens or hundreds of meters from the drive as shown in Figure 4.5.

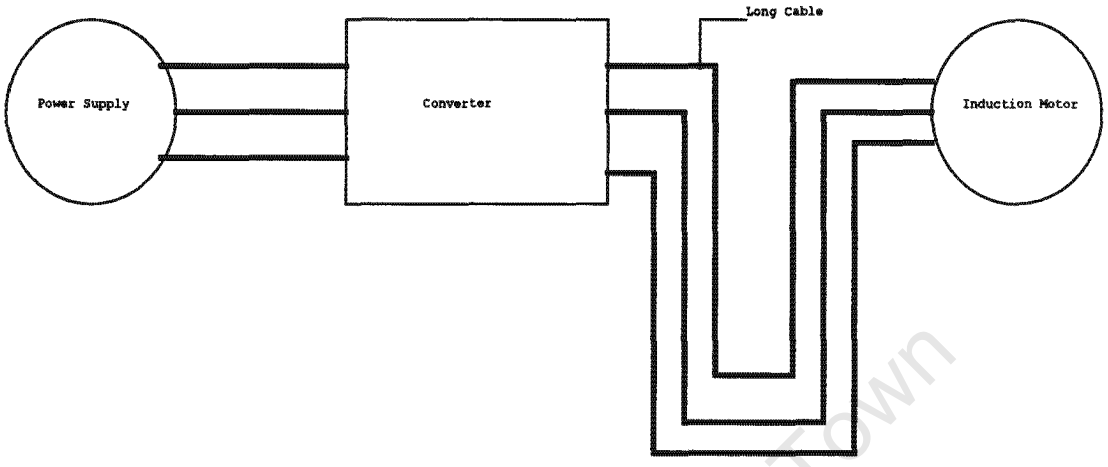

Figure 4.5: General supply-drive-motor layout

Lumped RLC circuits can model long cables. Due to the high ringing frequencies of the reflected voltage wave, the motor model needs modification for simulation purposes. This is to allow it to cater for the high overvoltage frequency and low power frequencies simultaneously.

4.3.1 Cable parameters

The cable used in this study, is a four-core PVC insulated copper cable of length 36m, manufactured according to SABS 1507-1990 standard. The cable is connected between the inverter output and the induction motor terminals with specifications in Table 4.1.

Table 4.1: Cable Specifications

Parameter	Units	Value
Surface Area	mm^2	2.5
Diameter	mm	1.25
Number of Cores		4
Insulation		PVC
Length (for test)	m	36
Nominal current	A	20
Voltage rating	V	600/ 1000

In general, the model adopted for the cable is a RLC circuit. It is found that for this particular cable type, one RLC branch is sufficient and accurate enough for simulation. Figure 4.6 is the per phase cable model adopted for simulation that is generally used for power frequency modeling [19].

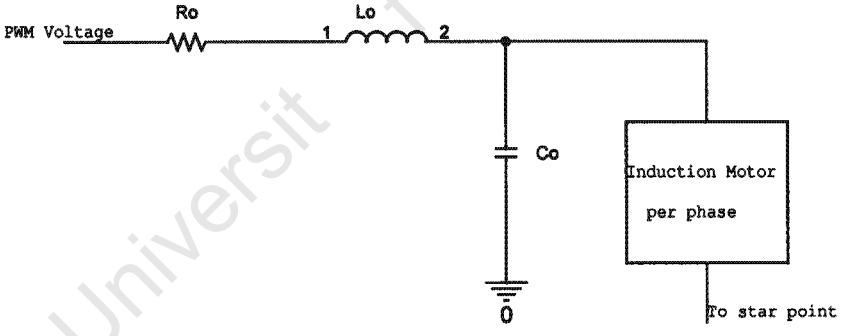

Figure 4.6: Per phase cable parameter model

A challenge is faced in determining the value of R_o, L_o and C_o of the cable model. Initially a step response test for an uncharged cable is undertaken to determine the propagation delay of the voltage waveform, to travel from one end to the other as illustrated in Appendix A4.1. That is, two phases of the four-core copper cable are used. One end of one phase is connected to a dc-supply of 250V and a voltmeter. The other end is connected to a voltmeter. The switch is closed and the step voltages at each end are captured in an

oscilloscope. Figure 4.7 shows the step response of the cable specified in Table 4.1.

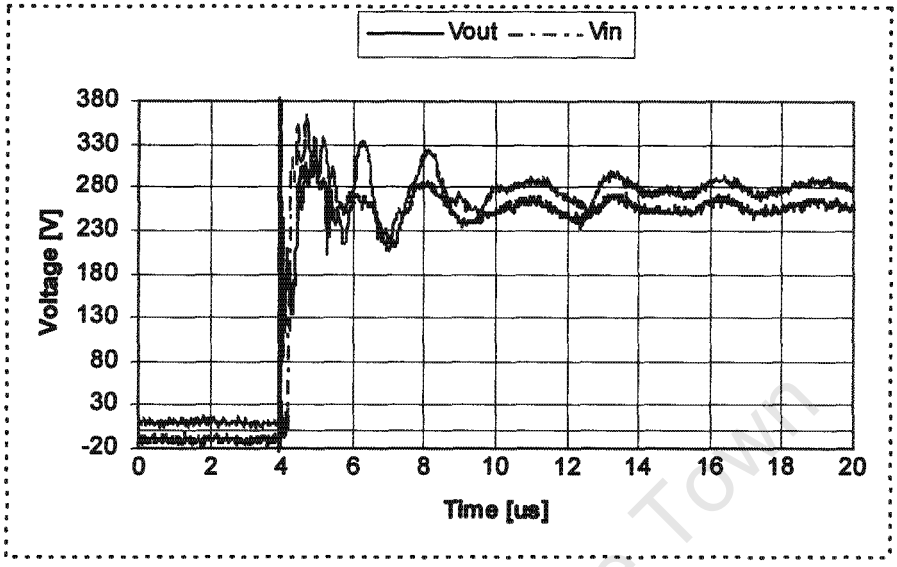

Figure 4.7: Dc-voltage step response waveforms

The propagation delay is determined to be,

$$t_p = 220ns$$

A reflected wave is required to traverse the cable length, a (a is the symbol for cable length) four times to complete one oscillation cycle. Therefore, the period of oscillation is given by;

$$T_{cycle} = 4t_p \qquad (4.4)$$

Oscillation frequency (ringing) is inversely proportional to the cable length (4.5). Therefore, high oscillation frequencies occur for short cable lengths [18]. The ringing frequency for the 36m long cable is given by;

$$f_0 = \frac{1}{T_{cycle}} = \frac{1}{4t_p} \qquad (4.5)$$

$$f_0 = \frac{1}{4*220ns} = 1.136MHz$$

The ac resistance R_s(Ω/m/conductor) of the cable is a function of cable oscillation frequency and is higher than the dc resistance due to skin and proximity effects. The skin effect is attributed to high internal inductance at the center of the conductor. The proximity effect is due to adjacent conductors distorting and effectively reducing current flow in the primary conductor and is dependent on the cable design. Therefore, high frequency f_o, currents turn to crowd on the conductor surface, this effectively decreases the conductor area and increases the ac resistance. The effective ac resistance is then given by;

$$R_{ac} = K_p K_{skin(f_0)} R_{dc} \qquad (4.6)$$

Where, $$K_{skin(f_0)} = \frac{d_o\sqrt{f_0}}{2(0.0661)} \qquad (4.7)$$

Therefore, $$R_a = \frac{K_p 16.61*10^{-8}\sqrt{f_o}}{d_o} \qquad (4.8)$$

The proximity effect increases the ac resistance by a factor of two ($K_p = 2$) for tightly bundled round conductor cables [18]. Using the cable oscillation frequency calculated above in Equation (4.6) the ac resistance is found to be,

$$R_{ac} = 5.7\Omega,$$

The cable parameters, L_o and C_o, are very difficult to measure experimentally and the machine's laboratory is not well-equipped with the required instrumentation. Therefore, an ESCORT ELC-2260 RLC Meter is used to measure the capacitance and inductance and to confirm the ac resistance magnitude. These quantities are compared to a 3mm square cable parameter and are found to be within acceptable limits [18].

Table 4.2: Cable parameters

	Units	Cable Used
Area	mm^2	2.5
Rdc	mΩ	282.5
Rac	Ω	5.695
Lo	uH	25
Co	nF	3.915

4.4. MOTOR MODEL

The inverter output voltage has two frequency components of interest produced by the presence of long cables in PWM drives. The first one is the desired power frequency, which sets the IM speed. The second frequency is the undesirable cable oscillation (ringing) frequency in the order of MHz. A model robust enough to handle steep voltage wavefronts at high frequencies is desirable for accurate simulation. The high frequencies are a transient effect that takes place at every switching point of the PWM voltage. The extreme stress on the IM winding is primarily due to IGBT's with small rise time. Thus, the IM model must be able to simulate high frequency effects and the normal operating frequency effects.

A motor model suitable for predicting the surge performance is shown in Figure 4.8 [23].

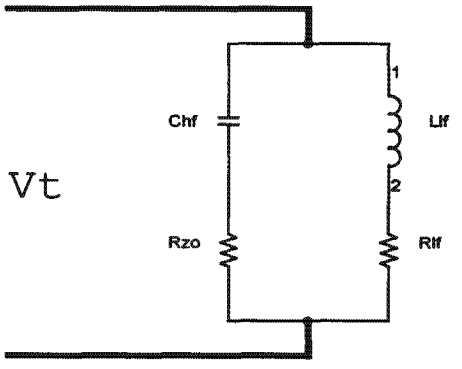

Figure 4.8: Differential mode motor model

At low frequencies, the motor behaves as an inductive series impedance $(R + j\omega L)$ just like a standard IM. At high frequencies, the motor behaves as a capacitive series impedance $\left(R + \frac{1}{j\omega C}\right)$ to allow the passage of surges. In Figure 4.8, the low frequency inductance L_{lf} and low frequency resistance R_{lf} are consistent with the parameters determined in Chapter Two for the power frequencies. The high frequency resistance, R_{hf}, corresponds to the surge impedance of the IM and establishes the reflection coefficient, Γ_t [23]. The high frequency capacitance, C_{hf}, allows the surge to pass through, while blocking the power frequency.

4.5 MOTOR PARAMETERS

The load impedance as seen by the cable at the termination point is dependent on the reflection coefficient and is given by Equation (4.7).

$$\frac{E_t^-}{E_t^+} = \frac{Z_t - Z_0}{Z_t + Z_0} = \Gamma_t \qquad \text{From (4.1)}$$

And

$$\therefore V_{IM} = (1 + \Gamma_t) * V_{inverter} \qquad \text{From (4.3)}$$

The low voltage test bed is run with a balanced supply voltage, 380V line-to-line. The 36m long-cable as specified in Table 4.1, connects the inverter output to the IM terminals. The inverter is set at 25Hz output frequency, and the IM is fully loaded with 20Nm on the output shaft. The switch is closed and the motor allowed to reach the steady state operating conditions. Figure 4.9 is captured and the reflection coefficients at the termination point is calculated as follows:

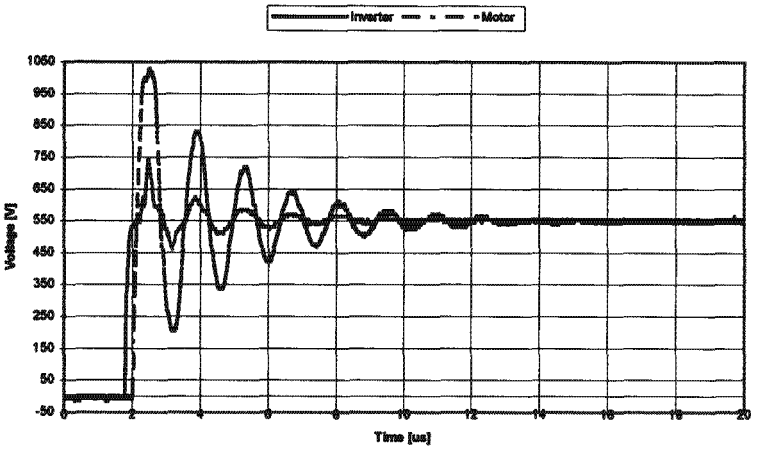

Figure 4.9: Measured inverter output and IM terminal voltage

The measured incident voltage at the termination point is,

$$E_t^- = 555V$$

And the reflected voltage is measured to be,

$E_t^+ = 1030$, But

$$E_t^+ = (1+\Gamma_t)E_t^-$$

Therefore, $\Gamma_t = 0.856$

The motor illustrated in Figure 4.8, has the following parameter values, which are computed and tabulated in Table 4.3.

The magnitudes of R_{lf} and L_{lf} remain unchanged as determined in Chapter Two for an operation frequency of 25Hz.

Where $R_{lf} = 13.74\Omega$, and

$$L_{lf} = 42.37mH$$

The magnitude of R_{zo} is computed as follows:

$$Z_o = \sqrt{\frac{L_o}{C_o}\left(1 - j\frac{R_o}{2\omega L_o}\right)} \qquad (4.9)$$

As $\omega \to \infty$, $\quad Z_o = \sqrt{\frac{L_o}{C_o}}$ (4.10)

Substituting the reflection coefficient at the motor terminals, $\Gamma_t = 0.856$, in Equation (4.1) results in:

$$Z_t = (R_{zo}) = 12.889 * Z_0 \qquad (4.11)$$

Therefore, $\quad R_{zo} = 12.889\sqrt{\frac{L_o}{C_o}}$ (4.12)

Substituting, $L_o = 25\mu H$ and $C_o = 3.92nF$ from Table 4.2, in Equation (4.12) results in :

$$R_{zo} = 1030\Omega$$

The high frequency branch, R_{zo} in series with C_{hf}, is to due to the reflected wave oscillation. Therefore, the high oscillation frequency capacitance of the motor is estimated as follows:

$$f_o = \frac{1}{2\pi * Z_o C_{hf}} \qquad (4.13)$$

Solving for C_{hf} and substituting for the known magnitudes,

f_o, the oscillation frequency was computed to be 1.136MHz from the step response test. $Z_o = 79.86\Omega$, from Equation (4.10).

$$\therefore C_{hf} = 1.77pF$$, for the 36m cable.

The motor parameter magnitudes are summarized in Table 4.3 below.

Table 4.3: Motor model parameters

	Units	Magnitude
R_{lf}	Ω	13.74
L_{lf}	mH	42.37
R_{zo}	Ω	1030
C_{hf}	pF	1.77

4.6 SIMULATED AND MEASURED TEST RESULTS

The measured and simulated reflected wave peaks and IM line currents are compared for the balanced voltage supply to validate the cable model.

4.6.1 Cable voltage drop and IM line currents comparison

Table 4.4 summarizes the validation of the model capability to model reflected waveforms. However, the large volt-drop predicted by the cable model employed is unacceptable. A percentage error of 1400 on the cable volt-drop, based on 5V, measured volt-drop is computed.

Table 4.4: Balanced voltage supply reflected voltage

	Vp1	pu	Volt drop [V]
Test	1030	1.94	5
Simulation	1060	1.91	75
% Error	2.9		1400

Figure 4.10 is the measured inverter output and IM terminal voltages; a closer view is displayed in Figure 4.11. By averaging the two voltages for the case in Figure 4.11 a volt-drop of 5V is realized. This is compared to simulated volt-drop displayed in Figure 4.12, whereby a volt-drop of 75V is predicted.

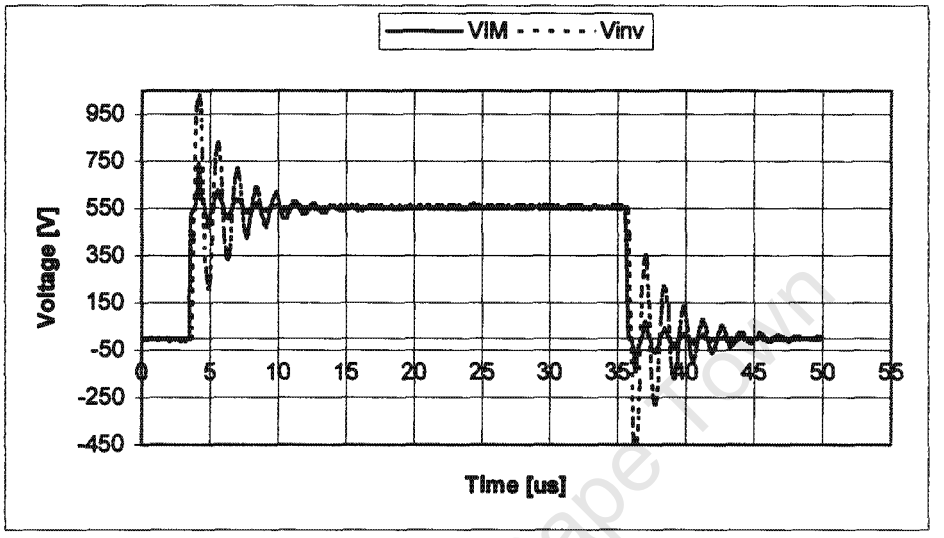

Figure 4.10: Measured inverter output and IM terminal line-to-line voltages

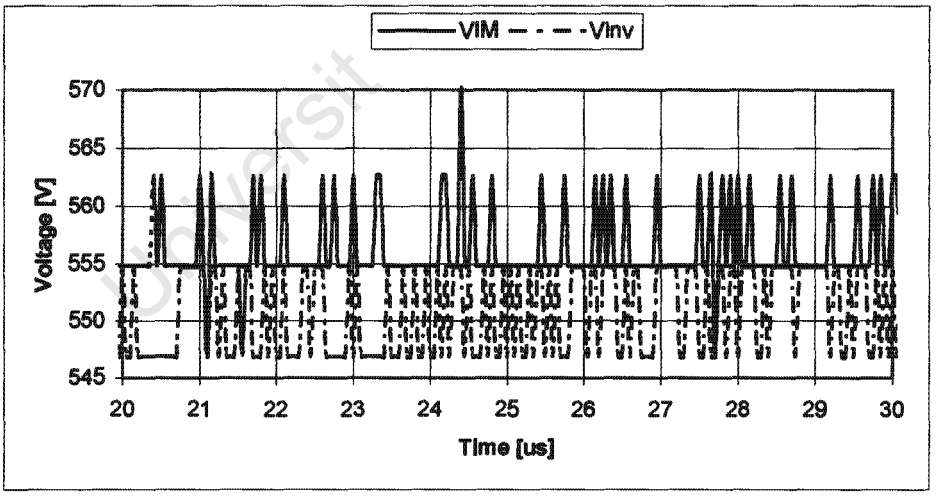

Figure 4.11: A closer view of Figure 4.10

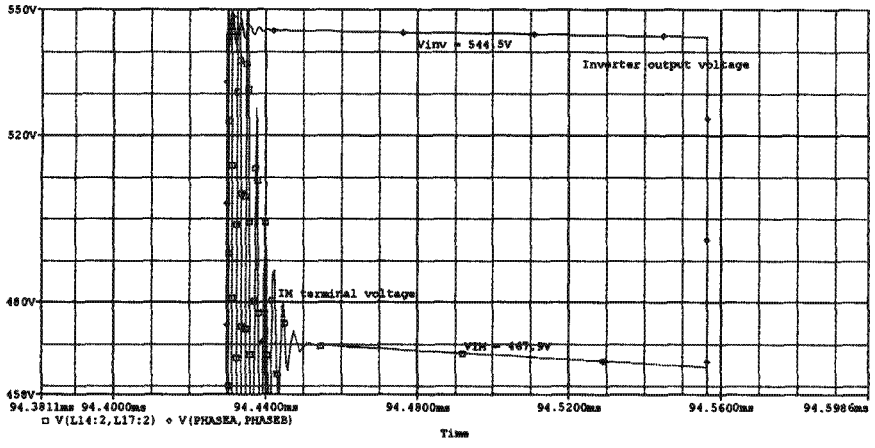

Figure 4.12: Simulated inverter output and IM terminal line-to-line voltages

Furthermore, another discrepancy observed is in the IM line currents. The measured RMS current is 7.2A and the predicted is 5.5A. In both current magnitudes, amplitude and RMS percentage errors of 29.8% and 23.6% occur. Table 4.5 and Figures 4.13 and 4.14 summarizes the results.

Table 4.5: Balanced supply IM line currents

	Cable Length [m]	IM line current [A]	
	a	I_{RMS}	I_m
Test	36	7.2	11.4
Simulation	36	5.5	8
% Error		23.6	29.8

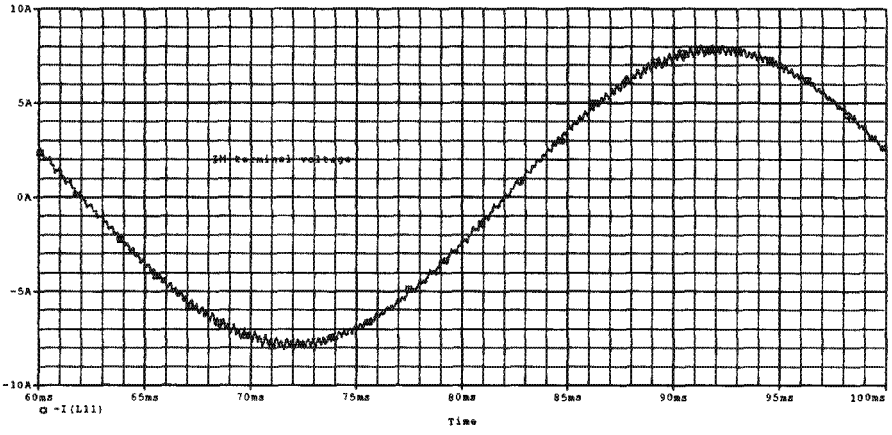

Figure 4.13: Simulated IM line current

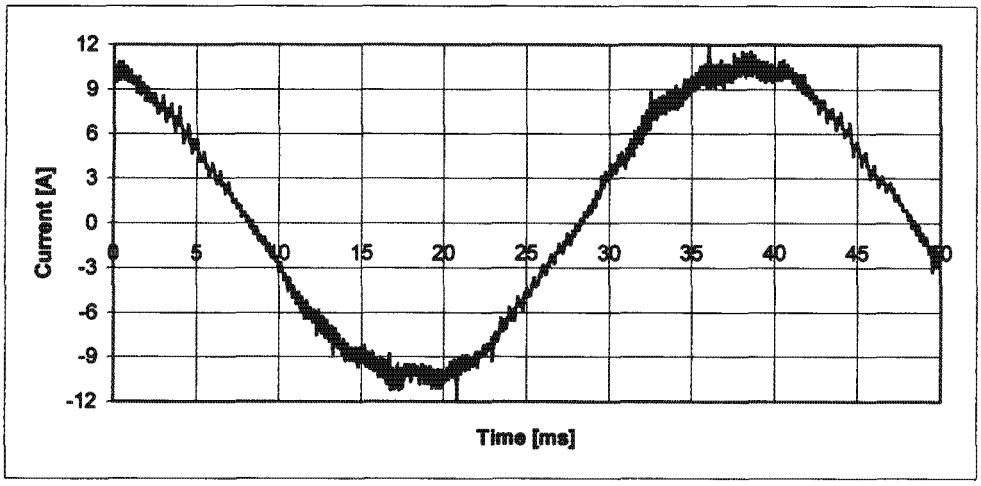

Figure 4.14: Measured IM line current

4.6.2 Discussion

The simulation accurately predicts the shape, magnitude and damping of the drive-cable-motor system and has been verified experimentally. However, the cable model in sections 4.3 is inadequate.

- The voltage drop between the inverter output voltage and motor terminal voltage predicted when skin and proximity effects are considered is 75V. This is much larger than the measured value of 5V.
- Moreover, there are two categories of waveforms from the inverter to the motor, the 'normal' pulse-train characteristic of the PWM drive at the power frequency range and the high oscillation frequency of the reflected waveforms. These waveforms, effectively 'see' a different cable impedance.

4.7 CABLE MODEL REVISION/ MODIFICATION

The lumped RLC cable model in Figure 4.6 is found to be insufficient to accurately predict the cable behaviour at high ringing frequencies. The PWM inverter output voltage waveform produces several frequencies in the cable. The cable/ motor impedance mismatch creates voltage reflections, which oscillate in the MHz, while the fundamental frequency is in the 10's of Hz and

the PWM frequency is in the kHz range. Attention here is directed at modeling the voltage reflection problem, while at the same time maintaining the correct power flow through the cable. Hence, the model here is suitable for the voltage reflection problem and fundamental frequency power flow operation. The skin effect is not significant at power frequency, but the high oscillation (ringing) voltage waves do experience high ac resistance due to proximity and skin effects.

Therefore, as in the resonant tank motor model adopted from [23] the cable model is modified such that it is capable of handling both low and high frequency voltage waves. The modified cable model is shown in Figure 4.15. The assumptions and calculations made are as follows:

- At least two RLC branches are required, one for the fundamental and PWM frequencies,
- The second for the high frequency oscillation of the reflected voltage waves,
- A cut off frequency of 6kHz is used for the power and PWM RLC branch.

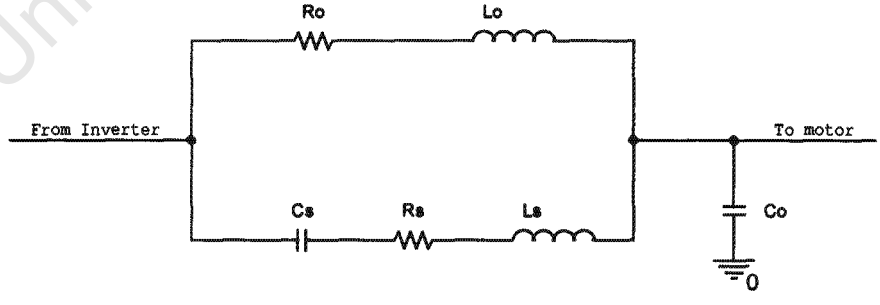

Figure 4.15: Modified cable model

The magnitudes of, R_o, L_o and C_o are the cable parameters for the power and PWM frequency range and are the same as in the model in Figure 4.6. Furthermore, R_s is R_o adjusted for skin and proximity effects as described by Equations (4.6 And 4.7). The inductance L_s, remains unchanged, and is therefore equal to L_o. The magnitude of C_s, for the cable model specified in Table 4.1, is calculated using filter circuit theory, as follows:

Consider Figure 4.16 below,

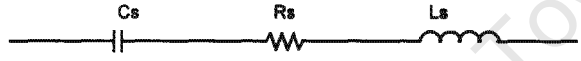

Figure 4.16: RLC high frequency branch

$$Z = sL + R + \frac{1}{sC} \qquad (4.14)$$

At resonance, the imaginary part of Equation (4.9) is zero

$$\therefore sL + \frac{1}{sC} = 0$$

$$\Rightarrow j\omega L = \frac{1}{j\omega C}$$

$$f = \frac{1}{2\pi\sqrt{LC}}$$

Therefore, for the 36m cable length Cs is,

Rs = 5.69Ω

Lo = 25μH

f = 6kHz

∴ Cs = 28.14μF

4.8 ANALYSIS OF THE REVISED CABLE MODEL FOR A BALANCED VOLTAGE SUPPLY

The predicted volt-drop across the cable agrees with the measured value of 5V as tabulated in Table 4.6. Figures 4.17 and 4.18 are the simulated and measured inverter output and IM terminal voltages.

Table 4.6: Balanced voltage supply reflected voltage

	Vp1	pu	Volt drop [V]
Test	1030	1.94	5
Simulation	1054	1.91	5
% Error	2.3		0

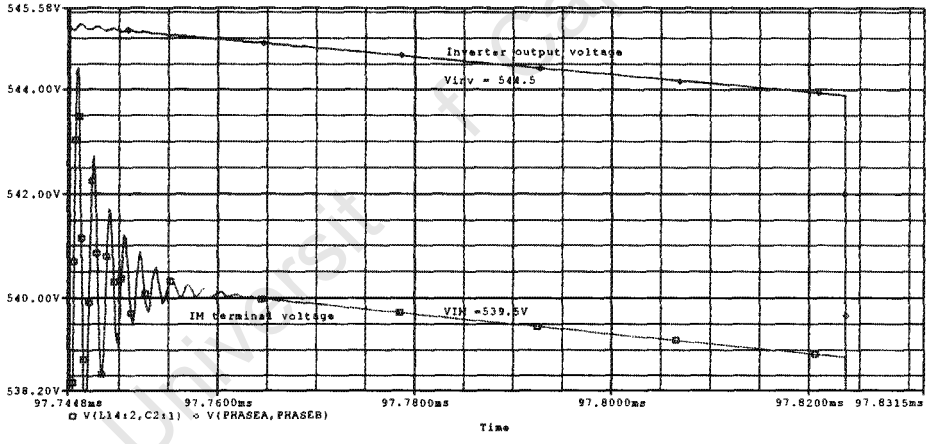

Figure 4.17: Simulated volt-drop across the cable

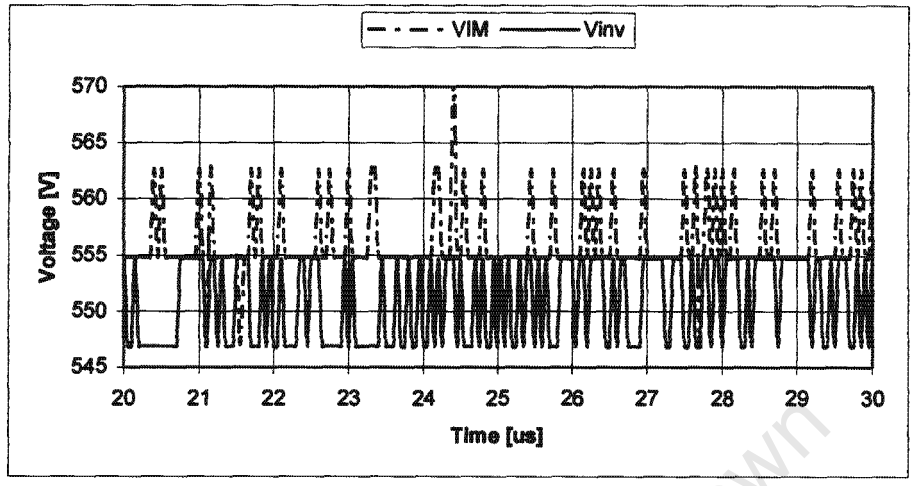

Figure 4.18: Measured volt-drop across the cable

The modified cable model has reduced the percentage error for the RMS current from over 20% to 1.4%. Also, the amplitude of current error has decreased to 6.9%. The results are summarized in Table 4.7. Moreover, Figures 4.19 and 4.20 are the simulated and measured current waveforms, validating the modified cable model.

Table 4.7: IM terminal current

	Cable Length [m]	IM line current [A]	
	a	I_{RMS}	I_m
Test	36	7.2	11.4
Simulation	36	7.3	10.6
% Error		1.4	6.9

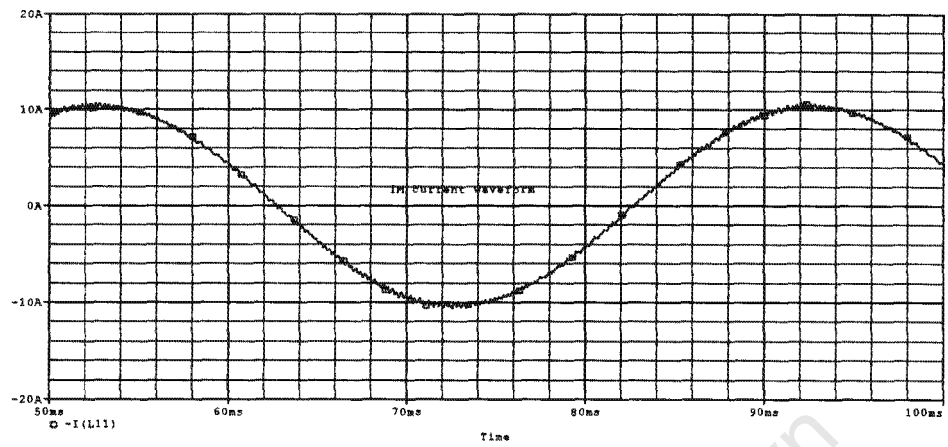

Figure 4.19: Simulated IM line current

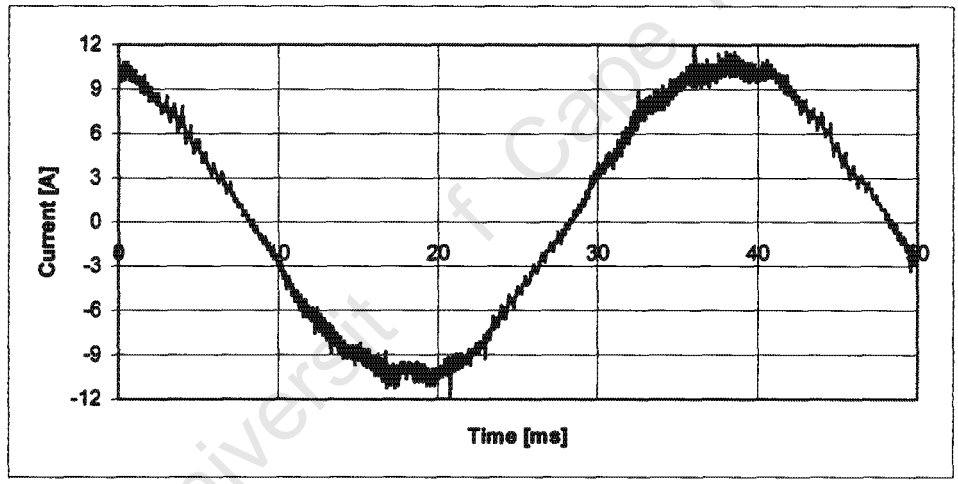

Figure 4.20: Measured IM current

Therefore, from the above results it is concluded that the modified cable model produces acceptable results, when compared to the previous model.

4.9 PARAMETRIC STUDY BASED ON THE MODIFIED CABLE MODEL

The cable model is modified for the reasons discussed in section 4.6 and simulations undertaken, for increasing cable length. The peak reflected voltage at the motor terminals decreases with increasing cable length. The voltage drop across the cable length follows the same trend. It is observed that the voltage drop varies from pulse to pulse, therefore, during the analysis of results, the

worst voltage drop was recorded. The variation in the voltage drop across the cable is due to pulse width period difference.

4.9.1Analysis of the 36m-cable test and simulation result

The reflected voltage is found to be 1.9pu and correlates with the measured result. The test undertaken with a 36m long cable correlates with the simulation. The measured and simulated results are summarized in Table 4.8, for constant switch rise time.

Table4.8: Improved cable model reflected voltage summary

Result Origin	Cable Length	Peak Voltages [V] V_{p1}	Inverter output V_{inv}	Voltage Drop	pu
Test	36	1054	554	5	1.9
Simulation	25	1069	569	6	1.9
Simulation	36	1064	569	5	1.9
Simulation	50	1062	569	4.5	1.9
Simulation	100	1054	569	3.5	1.9
% Error	36	0.9%	2.7%	0	0

The average dc-link voltage and ripple are not affected by the presence of a long cable. The results summarized in Table 4.9, show that 581V were measured while the simulation predicts 564.5V, an under-estimate by 2.8%. If the drive were operating in regenerative braking mode, then it would be expected that the dc-link voltage be affected by the reflected voltage waves. However, regenerative braking is beyond the scope of this project.

Table 4.9: Dc-link voltage with modified model

Result Origin	Cable Length	DC-Link Voltage V_{ave} [V]	V_{pp}	% Ripple
Test	36	581	20	3.44
Simulation	25	564.5	20	3.54
Simulation	36	564.5	20	3.54
Simulation	50	564.5	20	3.54
Simulation	100	564.5	20	3.54
% Error	36	2.8	0	

The only impact observed is on the inverter output current amplitude, which has increased from 10.2A as measured, for no cable, to about 15A for long cable conditions. This is due to current harmonics generated by the reflected waves. The cable impedance filters out these current harmonics, which are embedded on the inverter output current, by the time the current reaches the motor terminals. Table 4.10 shows that the cable length does not affect the motor RMS current. It was established in Chapter Three, that voltage unbalance does not affect the voltage balance of the inverter output.

Table 4.10: Revised cable inverter and IM currents [A]

Result Origin	Cable Length [m] a [m]	Inverter output current I_{RMS}	I_m	IM line current I_{RMS}	I_m
Test	36	7.3	15.8	7.3	10.2
Simulation	25	7.3	14.8	7.3	10.6
Simulation	36	7.4	15	7.4	10.6
Simulation	50	7.4	15	7.4	10.6
Simulation	100	7.4	15	7.4	10.6
% Error	36	1.4	5.1	1.4	3.9

4.10 IMPACT OF CABLE LENGTH UNDER UNBALANCED SUPPLIES

An arbitrary voltage unbalance setting is chosen for both the test and simulation, similar to the case discussed in Chapter Three. The percentage unbalance of 2.4% and overvoltage of 3.8% were determined from the arbitrary voltage setting.

The supply voltage waveforms are displayed in Appendix A4.2. The purpose of the work in this section is to prove that the developed model is capable of predicting the impact of long cables in the presence of unbalanced voltage supplies. The test is undertaken and the relevant quantities measured. The same voltage supply is captured and applied to the PSpice model. The results are analyzed and correlated.

4.10.1 Rectifier current

The rectifier line currents show unbalance in both their peaks and RMS values. The peak and RMS currents are tabulated in Table 4.11, Figure 4.21 and 4.22 are the rectifier current waveforms for line A. The rectifier currents are in line with the findings in Chapter Three, that is, each line current peak is dependent on the length of the diode conduction period. This is purely a function of the three-phase unbalanced voltage supply arrangement. Therefore, the same voltage unbalance can give different current unbalance results, depending on the phase sequence, employed.

Table 4.11: Rectifier line currents

	Phase A		Phase B		Phase C	
	I_{peak}-A	I_{RMS}[A]	I_{peak}-B	I_{RMS}[B]	I_{peak}-C	I_{RMS}[C]
Test	35.2	7.9	33.1	6.3	35	6.4
Simulation	38.7	8.7	38.4	6.9	41	6.1
% Error	9.9	10.1	16	9.5	17	4.7

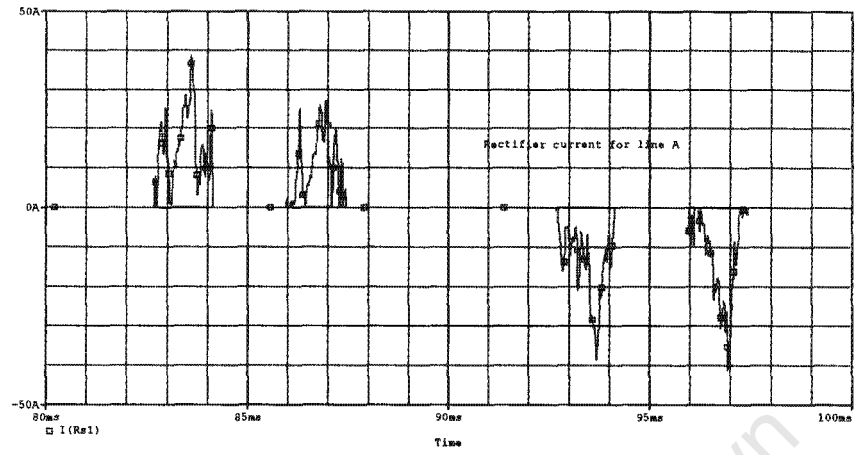

Figure 4.21: Simulated rectifier current for line A

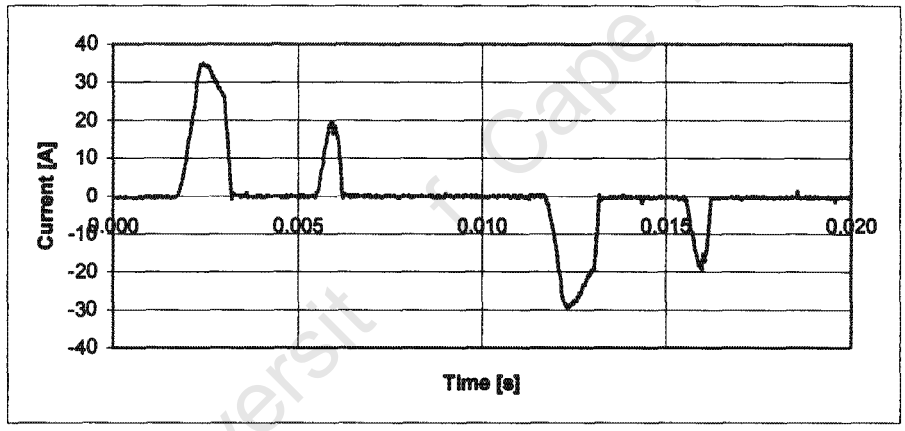

Figure 4.22: Measured rectifier current for line A

4.10.2 Dc-link voltage

The average dc-link voltage from the test result is 2.2% greater than that predicted by the simulated model. A percentage ripple of 3.54% is predicted, while an actual ripple of 2.84% is computed from the measured parameters. Table 4.12 tabulates the dc-link voltage comparison between the measured and simulated values, and Figure 4.23 and 4.24 are the dc-link voltage waveforms.

Table 4.12: Dc-link voltage analysis

	V_{ave} [V]	V_{pp} [V]	% Ripple
Test	577.3	16.41	2.84
Simulation	564.5	19.99	3.54
% Error	2.2	21.8	
% Ripple	2.2	21.8	24.4

Where, V_{ave} is the average voltage,

V_{pp} is the peak-to-peak voltage.

Figures 4.23 and 4.24 are the measured and simulated dc-link voltage waveforms, respectively. The two waveforms are comparable, indicating validity of the model.

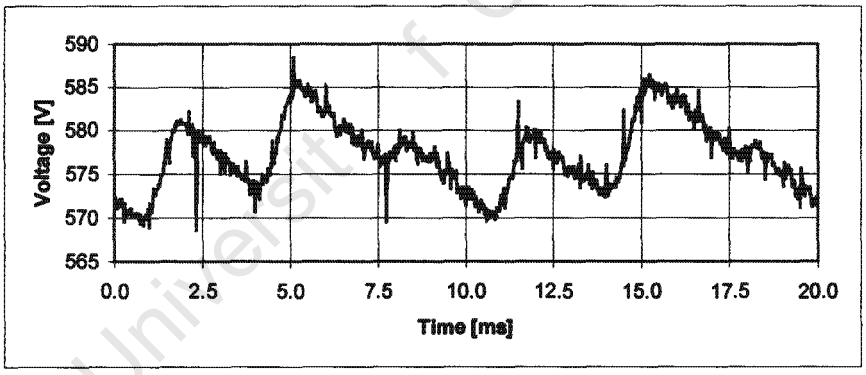

Figure 4.23: Measured dc-link voltage waveform

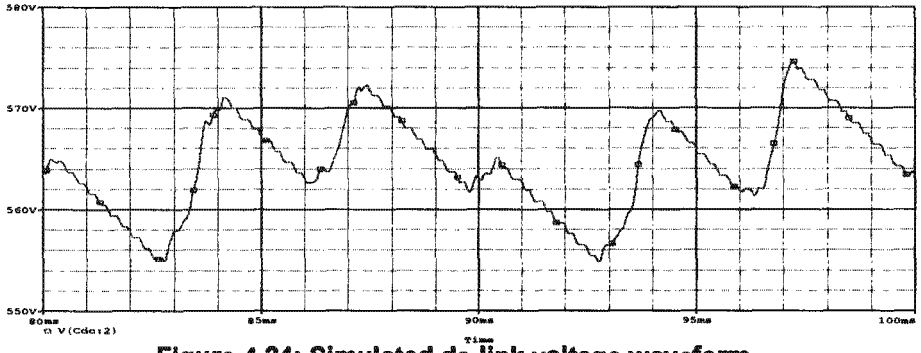

Figure 4.24: Simulated dc-link voltage waveform

4.10.3 Inverter output and IM currents

The inverter output and IM line currents also correlate well with measured values. The filtering effect of the cable is evident from the measurement of the inverter output current amplitude of 17A and 11A at the motor terminals. The RMS values are not affected by the presence of a long cable, as displayed in Table 4.13. Figure 4.25 and 4.26 are the simulated and measured inverter current waveforms. Figures 4.27 and 4.28 are the simulated and measured IM terminal currents waveforms.

Table 4.13: Inverter and IM currents

	Cable Length [m]	Inverter output current [A]		IM line current [A]	
	a	I_{RMS}	I_m	I_{RMS}	I_m
Test	36	7.14	17.83	7.23	11.35
Simulation	36	7.4	15	7.35	10.6
% Error		3.6	15.9	1.7	6.6

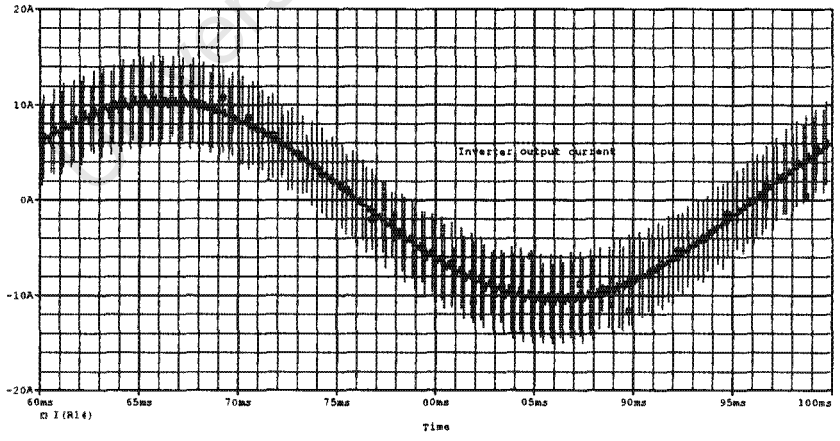

Figure 4.25: Simulated inverter output current

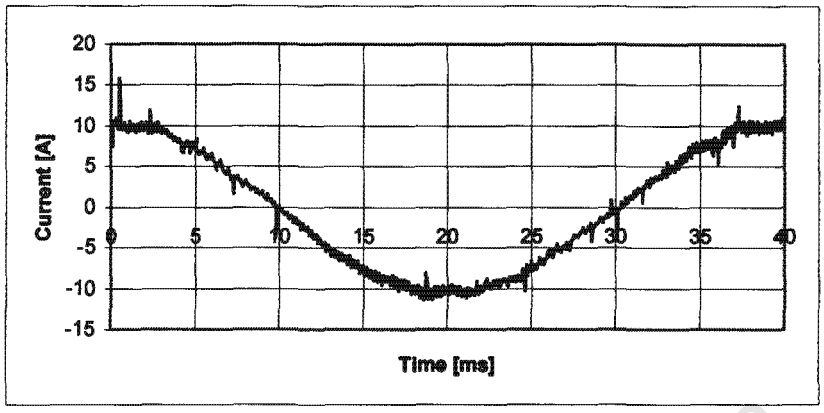

Figure 4.26: Measured inverter output current

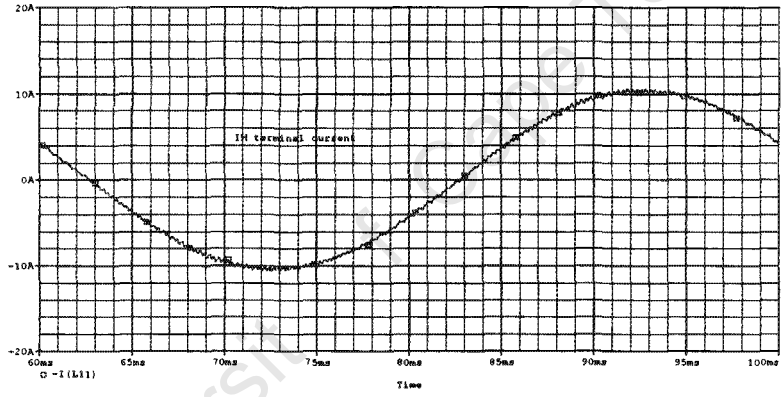

Figure 4.27: Simulated IM terminal current

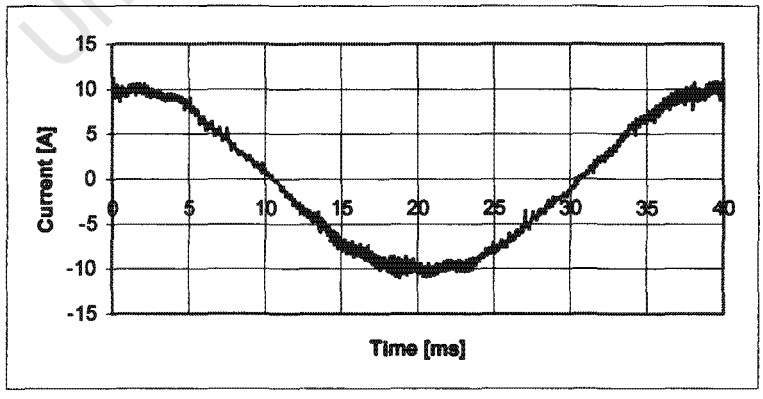

Figure 4.28: Measured IM terminal current

4.11 PARAMETRIC STUDY FOR INCREASING %LUVR

Four cable lengths, of 25m, 36m, 50m and 100m are simulated for increasing percentage unbalance, from 1% up-to 5%. The reflected peak voltage, dc-link voltage, cable volt-drop and inverter output voltages are monitored.

Table 4.14 and Figure 4.29 illustrate the reflected voltage peak voltage as a function of percentage unbalance. The voltage peak increases almost linearly with increasing voltage supply unbalance. On average, the voltage increases by 6% at 5% unbalance conditions from the nominal reflected peak voltage. The nominal voltage peak is measured at balanced conditions.

Table 4.14: Reflected peak voltages

%LUVR	Reflected peak voltage 25m	36m	50m	100m
1	1003	1000	1001	986
2	1004	1007	1002	990
3	1005	1013	1003	998
4	1021	1019	1011	1000
5	1026	1020	1020	1008

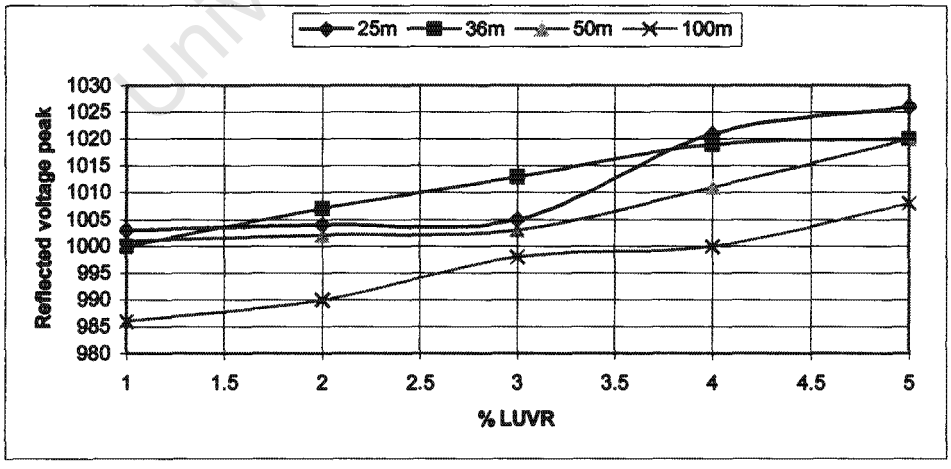

Figure 4.29: Reflected voltage peak

The dc-link voltage is found to be as simulated in Chapter Three, that is, only the effect of voltage unbalance was observed. This effect is illustrated in Figure 4.30, where the average dc-link voltage and the ripple are plotted. Therefore, the presence of long cables between the inverter and induction motor does not affect the dc-link voltage under the conditions simulated.

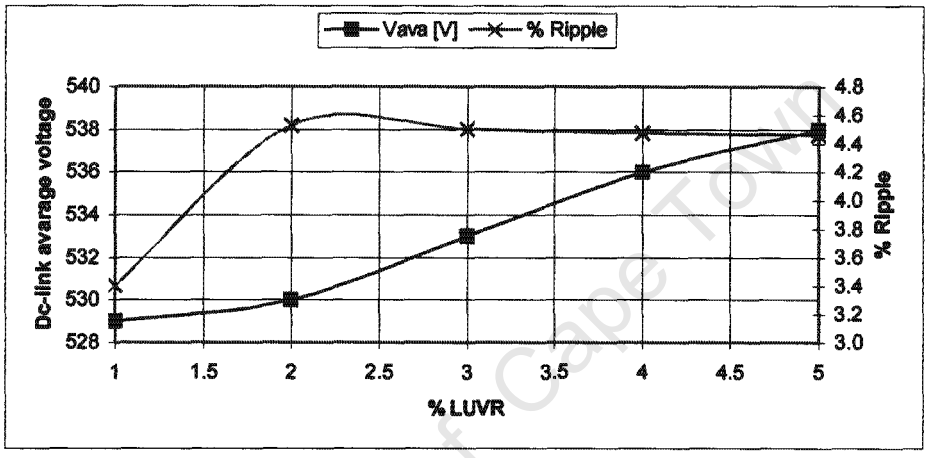

Figure 4.30: Average dc-link voltage and ripple

Table 4.15 tabulates the dc-link voltage ripple; with all the cable lengths exhibiting the same percentage ripple. The ripple is 4.5% on average, except 3.4% at 1% unbalance is predicted from the simulations. The measured dc-link voltage ripple was 3.44% for the 36m long cable at 2.4% unbalance with 3.8% overvoltage on the three-phase supply voltage.

Table 4.15: Percentage ripple with increasing %LUVR

%LUVR	% Ripple
1	3.40
2	4.53
3	4.50
4	4.48
5	4.46

Another parameter monitored during the parametric study, was the volt-drop across the cable. The volt-drop measured for the 36m long cables under balanced voltage supply conditions is 0.9% of the peak inverter output voltage across the cable. Figure 4.31, is a plot of the volt-drop per cable length for increasing percentage unbalance. The volt-drop is inversely proportional to cable length. This is because, at 25m and 36m, the oscillation frequency is in the MHz range, and hence the skin effect is stronger than at 50m and 100m, where the oscillation frequency is in the kHz range. As a result, a larger volt-drop exists in the 36m long cables than at 100m.

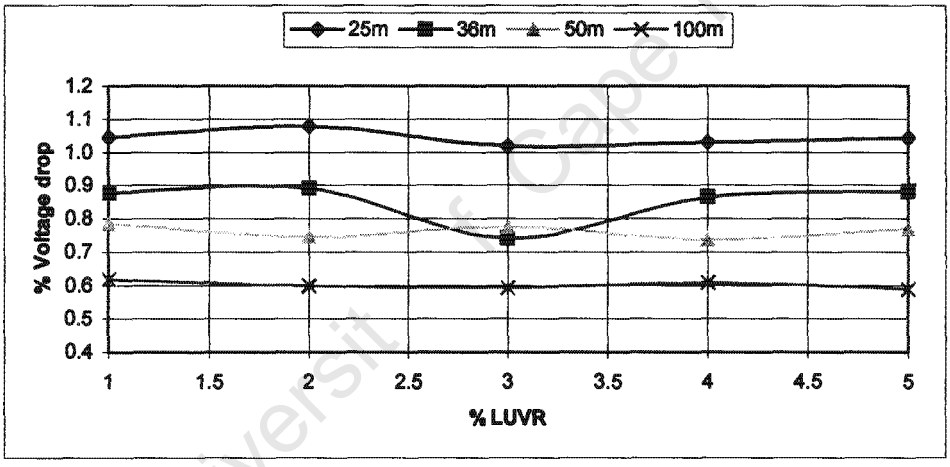

Figure 4.31: Percentage voltage drop along the cable

4.12 WORST CASE CONSIDERATIONS

Two worst voltage supply cases are simulated,

- 10% overvoltage with 5% unbalance on the supply voltage
- 10% undervoltage with 5% unbalance on the supply voltage

The actual numerical values of the worst-case scenario voltage supplies are tabulated in Table 4.16 and 4.17.

Table 4.16: Supply voltage with 5% LUVR and 10% overvoltage

	RMS	V_m	Phase Angle
V_{ab}	428.8741	606.304	0
V_{bc}	396.0531	560.7212	118.0522
V_{ca}	428.3894	606.335	232.88

Table 4.17: Supply voltage with 5% LUVR and 10% undervoltage

	RMS	V_m	Phase Angle
V_{ab}	351.042	496..0753	0
V_{bc}	324.4488	458.8399	117.556
V_{ca}	350.7327	496.011	235.097

Applying the same drive-motor model developed in Chapter Three, a 5% voltage unbalance and a 10% over or undervoltage are added to the three-phase supply voltage and the results analyzed. NEMA[ξ] standards state that induction machines can be operated under unbalanced voltage supplies up to 5% provided that the recommended derating is applied. There are no unbalanced voltage supply standards for VSDs that are known to the author at the time of writing this report. ESKOM guarantees the customer unbalanced voltage not exceeding 2% in the urban areas and 3% in the rural areas in their distribution network.

4.12.1 Reflected voltage peaks

The first three reflected voltage peaks for the three scenarios; unbalance with under or overvoltage and nominal voltage with unbalance are displayed in Figure 4.31. At nominal unbalanced voltage conditions the predicted pu reflection overvoltage is 1.87, which is the same for the undervoltage conditions. However, during overvoltages, the pu overvoltage is 1.86, see Table 4.18 below.

[ξ] NEMA: National Electrical Manufacturers Association

Table 4.18: pu reflected voltage

	Inverter output	IM Input	pu overvoltage
	V_{inv} [V]	V_{p1} [V]	
Undervoltage	492	920	1.87
Nominal voltage	545	1020	1.87
Overvoltage	602	1122	1.86

Figure 4.32 shows the simulated inverter output voltage and the reflected voltage at the IM terminals for 5% unbalance and overvoltage. The high ringing frequency is evident from the waveform in the order of MHz.

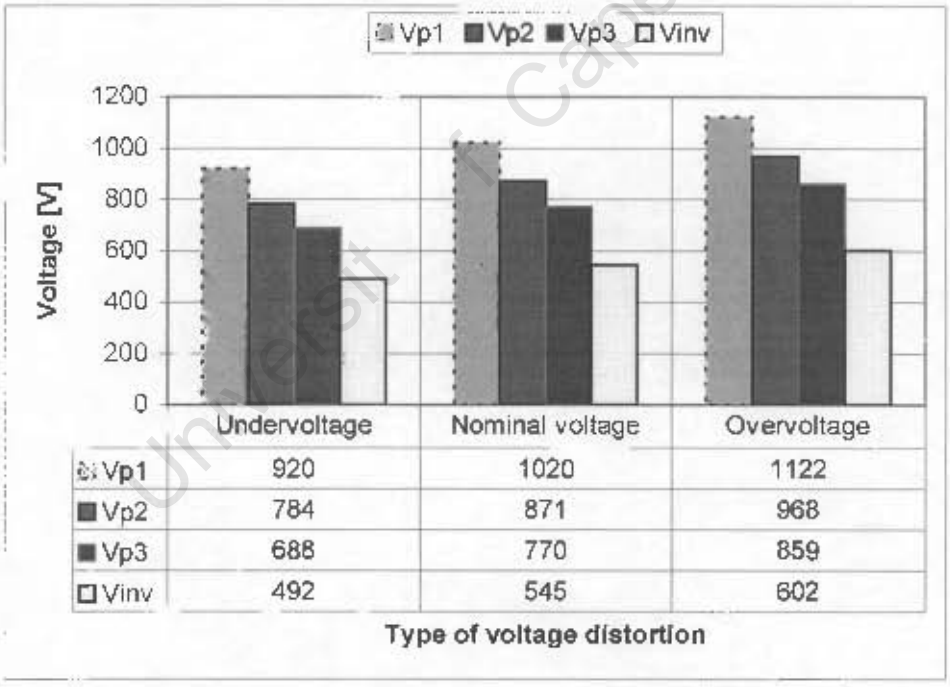

Figure 4.32: First three reflected wave peaks

4.12.2 Effect of 10% overvoltage with 5% LUVR on dc-link voltage

The results in Table 4.19 show that the presence of a long cable does not influence the magnitude of the dc-link voltage.

Table 4.19: Dc-link voltage (10% overvoltage and 5% LUVR)

	V_{ave} [V]	V_{p-p} [V]	%Ripple
No cable	592.3	26.7	4.5
36m cable	592	26	4.4
Difference	0.3	0.7	0.1

4.12.3 Effect of 10% undervoltage with 5% LUVR on dc-link voltage

Similarly, no significant impact is observed during undervoltage conditions, as shown in Table 4.20.

Table 4.20: Dc-link voltage (10% undervoltage and 5% LUVR)

	V_{ave} [V]	V_{p-p} [V]	%Ripple
No cable	484.3	21.8	4.5
36m cable	484	22	4.6
Difference	0.3	0.2	0.1

4.12.4 Inverter and IM line currents

The inverter output current has large amplitude when compared to the current at the machine's terminals. This is because the long cable has filtering effects on the current waveforms. There is no significant impact observed on the RMS current due to the presence of a long cable on both the inverter output and IM input. The only significant impact is on the inverter output current amplitude, which has increased by 42.2% at undervoltage, 40% at nominal unbalance voltage and 42.7% at overvoltage. Therefore, on average, the inverter current amplitude is increased by 41.6%, due to the cable length of 36m. (See Table 4.21)

Table 4.21: Inverter and IM currents

	Inverter output I [A]		IM terminal I [A]	
	I_m	I_{RMS}	I_m	I_{RMS}
Undervoltage	12.8	6.3	9	6.3
Nominal voltage	14	6.9	10	6.9
Overvoltage	15.7	7.7	11	7.7

4.13 CONCLUSION

The PSpice drive-cable-motor model has demonstrated through simulations, that the reflected wave phenomenon can be calculated accurately for long cables in the presence of voltage unbalance. Theoretical results were verified with measurements.

The existing lumped parameter cable model and IM motor models were inadequate because, in the presence of long cables, the inverter output voltage has two components. There is the normal pulse-train at the required modulated frequency and the high frequency component due the oscillation of the reflected voltage waves. Moreover, for every pulse there is a reflected wave. As a result, adding an RLC branch in parallel with the existing cable model branch proves to be sufficient. Similarly the standard per-phase IM model is not sufficient to correctly model an IM under long cable conditions. Therefore, a resonant tank IM model is used. The parameter determination part is challenging, however, a technique was developed, based on the measurable quantities.

The dc-link voltage is not affected by the varying cable length. Moreover similar results were found in Chapter Three. That is, the no-cable conditions rendered similar results as the long cable conditions with some exceptions. This is for motor terminal current and the dc-link voltage and ripple. The exception is with the inverter output current amplitude which increases by 40% from 10A to 14A.

It is concluded that the proposed resonant tank motor model and the modified cable model can be applied correctly to predict the reflected wave phenomenon.

CHAPTER FIVE

Energy Savings of a Pump Drive

5.1 INTRODUCTION

Variable speed drives are used in a range of applications, from small water fountains of 1 kW to boiler feed water pumps of 12 MW. Hence, it is important to understand the energy savings associated with VSDs. The capital investments in VSD equipment and peripherals could easily amount to millions of Rands. Whether energy savings are the sole or partial justification for installing VSDs, the calculation should be correct and accurate [31]. This will ensure sound and proper decision-making.

This chapter discusses and evaluates a method for determining energy savings associated with VSDs on centrifugal loads, such as pumps, fans and compressors. Relevant data is extracted from pump manufacture's performance curves and these are expressed in mathematical formulae. To illustrate this method, a practical case is undertaken from Tutuka Power Station in Standerton. A spreadsheet program for determining energy savings associated with VSDs is developed and the results presented. This is verified by comparing the results computed with an ABB spreadsheet program for energy savings.

5.2 VSD BENEFITS

Variable speed drive's benefits can far outweigh their cost, provided the application is appropriate. These benefits could be in the form of production and quality improvements or financial savings, some examples of which are as follows:

- Improved life expectancy of equipment, because it is not operated at rated load and speed unnecessarily,
- Improved process control,
- Noise reduction at reduced speeds, especially in fans.

5.3 VSD CANDIDATE IDENTIFICATION

The application engineer should appreciate the fact that not all industrial processes require the application of VSD. Therefore, feasibility studies are required before implementing such a project. Operating profile characteristics are a major factor in determining energy savings. Therefore, a thorough study and monitoring is required before a decision is made as to the applicability of a VSD in a given plant.

Contributing factors in identifying suitable VSD candidates,

- ***Variable load:*** The load is the determining factor as to what size and type of drive equipment is required, e.g. Figure 5.1 shows a variable load duty circle per annum.
- ***High annual operating hours:*** The longer the operating time, the higher the energy utilization. This creates more opportunities for energy savings.
- ***Operating at reduced loads most of the time:*** The fluctuation of the load allows the possibility of operating at different speeds.

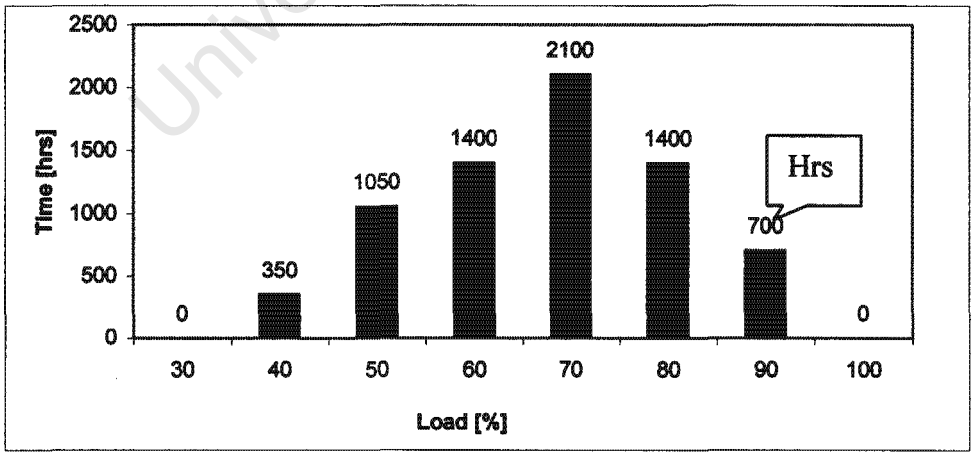

Figure 5.1: Annual duty cycle of a water pumping plant

5.4 JUSTIFICATION FOR VSD INVESTMENT

A proper and detailed evaluation of the quantities listed below is essential. These estimates can vary, because costs vary with time, for example, the price of electricity. Furthermore, in plants like power stations where there could be up to 16 identical generating units, it may take several years to completely implement a project. During such a period the cost of investment may vary considerably, especially in South Africa, where engineered equipment, such as VSDs are imported.

Factors that need consideration are:

- Plant life expectancy versus VSD equipment life expectancy,
- Present cost of VSDs and peripherals,
- Benefit per annum over the total plant life,
- Present value of benefit

A comparison between the present value benefits to the present cost can be undertaken. Assuming that the energy savings are the only determining factor, if the present benefit value is greater than the present investment value, it would mean that the VSD project is justified. Otherwise, all factors need to be considered carefully.

5.5 ENERGY UTILIZATION POINT

It is fundamental to identify exactly where energy is consumed in pumping systems. Controlling the process means varying the flow [31]. It is the technique with which variable flow is achieved that determines the amount of energy utilized. When a pump or a set of pumps operate at a fixed speed, at any given volume flow rate, the pressure developed by the pump is greater than that required by the system. Here the system refers to head required by the pumping equipment and losses due to the pipes and fittings.

The only exception is at the natural operating point, where the developed head matches the system curve. Therefore, in pump and fan type loads, there is only one natural operating point per rotational speed. At reduced loads, the pressure is dropped to match the required pressure. In doing this, control valves are normally employed to either,

- Directly drop excess pump pressure by throttling the output.
- Or indirectly drop the pump discharge pressure by recycling additional flow.

Energy is dissipated during such processes, which may amount to millions of Rands in large pumping systems and petrochemical industries.

5.6 HOW VSDs SAVE ENERGY

Figure 5.2 displays the pump performance and system curves. It can be observed that the pump characteristics are not compatible with system requirements. It can be seen that the system requires less pressure at reduced flows. The end process that requires the pumped fluid governs this. However, the pump pressure increases at reduced flows. The pressure difference between the two curves increases with flow reduction.

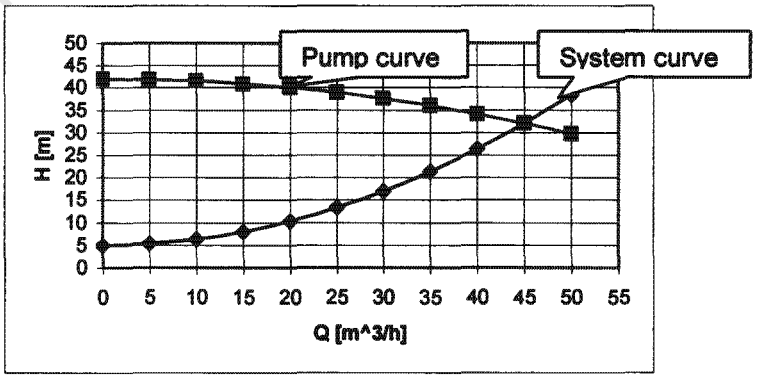

Figure 5.2: Pump curve showing operating point

CHAPTER FIVE

Energy Savings of a Pump Drive

In a fixed speed pump operation, the method of matching the required pressure to the pump output pressure dissipates electrical power. Variable Speed Drives enable flow control through shaft speed control. That is, the system and the pump pressures are matched by reducing the motor speed. Only the power required to develop the required speed and torque is used. The energy that is normally used to overcome the pressure drop across the throttling valve is now saved.

5.7 PROCESS SYSTEM MODELING

Manufacturers present pump performance data in a graphical form. As processes get more and more complicated with multiple flows and pressure settings, it becomes impractical to represent the whole process system graphically. Therefore, mathematical models need to be developed to represent these systems, so that affinity laws may be applied [31].

5.7.1 Pump performance curve

The pump curve can be represented by:

$$H_p = a + cQ^2 \qquad (5.1)$$

Where, H_p is the head developed by the pump [m]

a is the shut-in pressure, the head developed by the pump at zero flow [m]

c is a constant [hr^2/m^5] and always negative to establish the correct concavity.

Q is the volume flow rate [m^3/hr]

In computing the values of the constants a and c, the performance curves from the manufacturer are required. For this example a pump model 32-160, Rapid-Allweiler make is used (see Appendix A5.1). The shut-in pressure is read directly from the performance curves and it is found to be,

$a = 42m$, For the 170mm impeller diameter.

Before a pumping system can be designed and specifications determined, the intended design operating point must be known. This is required to calculate constant c. Therefore, consider the natural operating point from Figure 5.2 of,

N_1 operating point, [Q; H] = [45; 32,08]

Where,

N_1 is the pump impeller speed.

Therefore the pump equation becomes,

$$H_p = 42 - 4.9 * 10^{-3} Q^2 \qquad (5.2)$$

Figure 5.2 is the plot of equation (5.2) showing the pump curve at rated speed of

N_1= 2900 rpm.

5.7.2 Process lines

Process lines represent the system, the pipes and fittings losses, and the required output head. These are expressed in meters, with a parabolic shape.

$$H_s = a_s + c_s Q^2 \qquad (5.3)$$

Where,

a_s represents Net Positive Suction Pressure (NPSH) plus the pressure required before any flow can be achieved. This includes system losses due to friction.

c_s is a positive constant, since the system resistance increases with increased flow. This is analogous to electrical resistance. In practice, one computes all the system losses and adds NPSH to get the correct value of a_s.

Hence,

$$H_s = 5 + 13.37 * 10^{-3} Q^2 \qquad (5.4)$$

The system curve is superimposed on the pump curve in Figure 5.2 to establish the 'natural operating point'.

5.7.3 Affinity curve

Affinity curves are tools used to determine the correct initial conditions to be applied when the flow s

peed is varied by means of VSDs. These curves are generally represented by (5.6) below.

$$\frac{H_2}{H_1} = \frac{Q_2^2}{Q_1^2} \qquad (5.5)$$

$$H_2 = Q_2^2 \frac{H_1}{Q\frac{2}{1}}$$

$$H = cQ^2 \qquad (5.6)$$

5.7.4 Shaft power curve

The power equation is similar to the pump equation, except that Q is raised to a variable degree, d in Equation (5.6), and is determined by trial and error [31]. This gives the modeling engineer the flexibility of manipulating the flow versus power characteristics to match the manufacturers curves.

$$P_s = a + cQ^d \qquad (5.7)$$

Reading from the manufacturers pump performance curves in Appendix A5.1, the following points are noted to calculate the constants in Equation (5.7).

[Q; P_s] : [0; 1.8]; [46; 7] and [28; 5]

Solving the simultaneous equations results in Equation (5.8), which is plotted on Figure 5.3.

$$P_s = 1.8 + 113 * 10^{-3} Q \qquad (5.8)$$

Keys to the curves in Figure 5.3 are

- N_1 is the pump curve at rated pump rotational speed,
- DSC is the design system curve,
- AC_1 is the affinity curve at rated conditions and
- Ps is the shaft power curve.

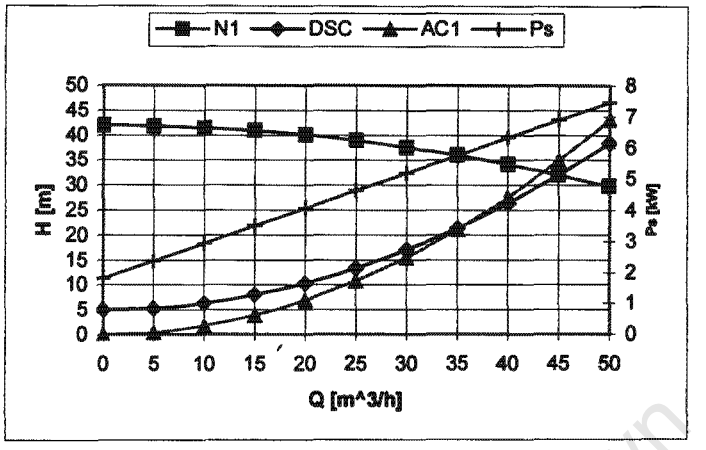

Figure 5.3: Shaft power curve superimposed on pump characteristic curves

5.8 APPLICATION OF AFFINITY LAWS

Affinity laws, in equation (5.8), (5.9) and (5.10), relates the impeller speed, head developed and the shaft power utilized by the pump.

$$\frac{Q_1}{Q_2} = \frac{N_1}{N_2} \qquad (5.9)$$

$$\frac{H_1}{H_2} = \left[\frac{N_1}{N_2}\right]^2 \qquad (5.10)$$

$$\frac{P_{s1}}{P_{s2}} = \left[\frac{N_1}{N_2}\right]^3 \qquad (5.11)$$

Where

H = pump discharge head [m]

Q = pump discharge volume flow rate [m^3/hr]

Ps = pump input shaft power [kW]

The method of controlling flow by throttling a valve, effectively forces the system curve to be compatible with the pump curve, as shown in Figure 5.4

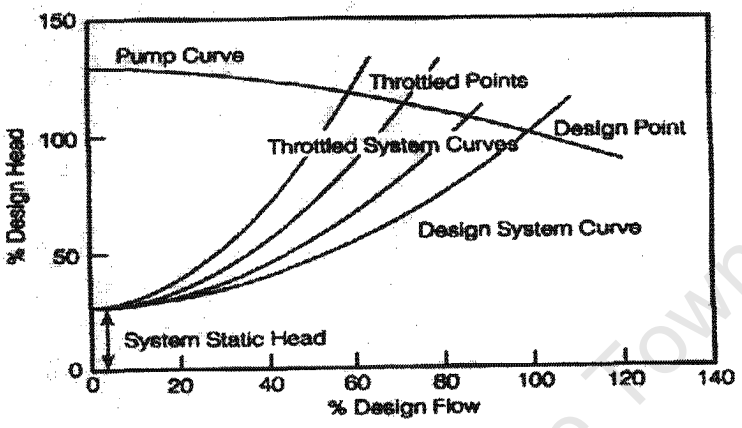

Figure 5.4: Operating points by valve flow control

Using a VSD for controlling flow by varying the shaft speed effectively displaces the pump curve to be compatible with the system as shown in Figure 5.5.

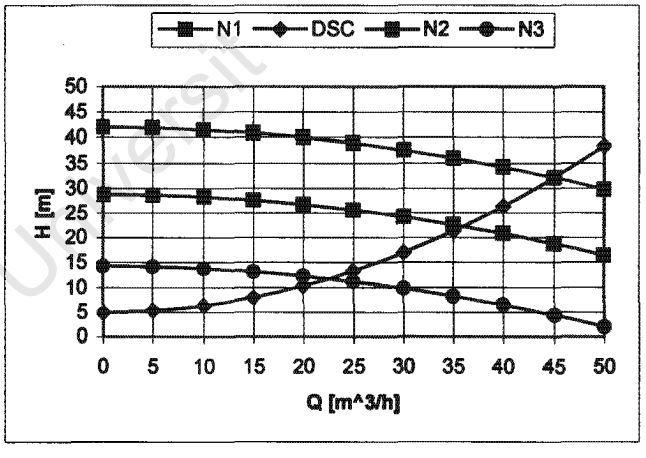

Figure 5.5: Pump curve showing three operating points

Where, N_2 and N_3 are the pump curves at reduced speeds,

The process of locating the correct shaft speed corresponding to a reduced required flow requires application of the affinity curve. Affinity curves are graphical depictions of the affinity equation derived in section 5.7.3.

If the system has no static pressure (the system curve starts at zero flow and zero head), the speed fraction equals the flow fraction using the design flow point as the initial point. However, it is most often the case that the system has static head. Therefore, the determination of the amount of speed reduction required to meet the reduced speed operating point is not obvious, and the solution requires the concept of affinity curve.

The problem of using the affinity law, which states the equivalence of flow ratios to speed ratios, is finding the full-speed initial flow rate.

$$\frac{Q_1}{Q_2} = \frac{N_1}{N_2}$$ From Equation (5.8)

Figure 5.6, below illustrates a graphical procedure for determining a flow rate for an arbitrary reduced-speed operating point. The procedure is summarized as follows:

- Construct the design system curve on the pressure/ flow performance curve.
- Substitute the desired operating point flow rate, Q_2, into the system curve equation to obtain the associated system head. This flow, Q_2, and H_2 are the coordinates of the reduced speed operating point.
- Derive the affinity curve constant using the operating point coordinates obtained above, substituting in Equation (5.6).

- Construct the operating point affinity curve on the pressure/ flow performance curve.

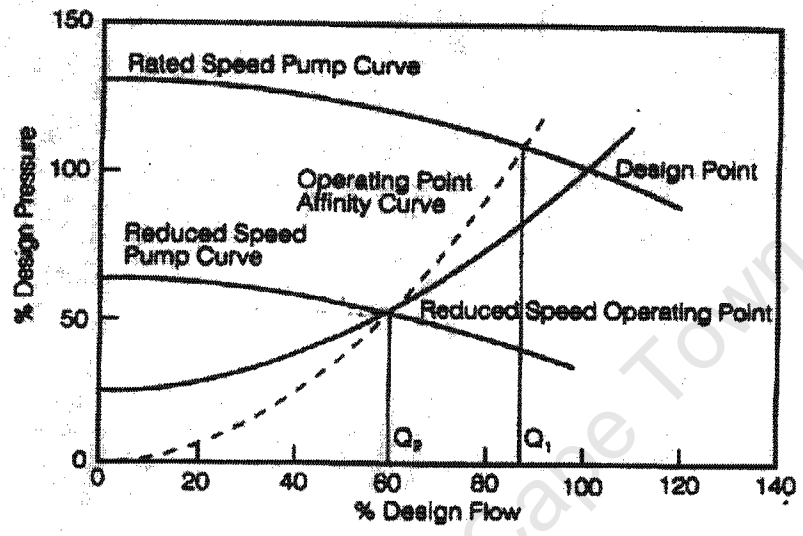

Figure 5.6: Design system curve and operating point affinity curve

The flow, Q_1, associated with the intersection of the affinity curve and the pressure/ flow performance curve is the correct full-speed initial point used in applying the affinity law. The ratio $\frac{Q_2}{Q_1}$ is equal to the required speed ratio. This procedure must be repeated for all reduced-speed operating points. There is a unique affinity curve for each point except for a system with zero static head. At zero static head conditions, all the affinity curves coincide with the design system curve.

5.9 RAND ENERGY SAVINGS

The performance curves at various operating speeds have been determined. The next step is to tabulate the electrical energy utilized and the cost of such energy. This is done for both constant speed operation and variable speed to identify the savings due to the application of a VSD.

CHAPTER FIVE

Energy Savings of a Pump Drive

Constant speed operation is the simple case, because the power drawn from the utility supply is constant. In the case of variable speed drives, the efficiencies of all interconnected power handling equipment needs to be factored in. Also the fact that these efficiencies will vary with speed should be considered. This requires experimental data, of which the manufacturer may supply some and the rest could be measured. In the absence of measured data typical values can be used. The efficiencies of the following equipment need to be considered, that is, if they form part of the system:

- Input transformers,
- Variable speed drives,
- Mechanical gears, if any,
- Electrical machines, and the
- Pump.

A spreadsheet program is developed so as to compute the energy savings in terms of Rands, associated with VSDs. Condensate extraction pumps from Tutuka Power Station are used in the case study to quantify the energy savings. The plant specifications, that is, the motor ratings, pump specifications are in Appendix A5.2.

The tariff in use has a significant impact on how much could be saved. In order to simplify the calculations, an average cost per kWh is used. This average is determined by calculating the total cost of electricity per duty cycle divided by the total kWh utilized during each period. Therefore the only input to the program is the cost per energy unit in kWh. Table 5.3 tabulates all the charges that make up the electricity total cost.

Table 5.1: Energy cost based on ESKOM's 2000 tariffs

Type of Charge	Charges	
Demand charge(R) =	40	/month
Basic charge (R) =	165	/month
Energy charge (R) =	0.35	/kWh

This tariff structure varies from distributor to distributor. The input table for the developed spreadsheet is illustrated in Appendix A5.3.

5.9.1 Cost of energy for constant speed operation

At constant speed, throttling a valve or bypassing the flow are the techniques used to control the flow. Bypassing the flow means diverting the flowing fluid back to the source. These methods are energy inefficient and present undesirable pressure on the system. The amount of energy utilized is approximately 5.8GWh amounting to R2.03 million per annum at constant speed operation in this example. The actual projected energy consumption and costs are tabulated in Table 5.2.

Table 5.2: Electrical energy cost per annum: Constant speed operation

LDC		POWER SUPPLY	ENERGY	ENERGY
Load	Hrs/yr	kW	kWh	COST
30%	0	741.81	0.00	R 0.00
40%	350	724.85	253,695.81	R 88,793.53
50%	1050	761.52	799,595.50	R 279,858.43
60%	1400	818.05	1,145,269.59	R 400,844.36
70%	2100	841.05	1,766,203.62	R 618,171.27
80%	1400	867.64	1,214,691.83	R 425,142.14
90%	700	885.95	620,162.38	R 217,056.83
100%	0	917.89	0.00	R 0.00
	7000	**6,558.75**	**5,799,618.74**	**R 2,029,866.56**

Table 5.2 is also represented by the LDC curve, Figure 5.1.

5.9.2 Cost of Energy at Variable Speed Operation

Variable speed operation matches the pump output power to system requirements by adjusting the pump impeller rotational speed. The energy utilized at variable speed operation is 2.56GWh amounting to R900 000.00 per annum. In computing these figures, consideration of VSD, motor and pump efficiencies are made. Table 5.3 tabulates the projected energy consumption and cost at variable speed operation.

Table 5.3: Electrical power cost per annum: Variable speed operation

LDC		POWER SUPPLY	ENERGY	ENERGY
Load	Hrs	kW	kWh	Cost
30%	0	72.86	0.00	R 0.00
40%	350	114.94	40,230.35	R 14,080.62
50%	1050	177.00	185,844.81	R 65,045.69
60%	1400	257.65	360,715.89	R 126,250.56
70%	2100	367.71	772,193.83	R 270,267.84
80%	1400	508.32	711,641.60	R 249,074.56
90%	700	701.84	491,290.28	R 171,951.60
100%	0	936.63	0.00	R 0.00
	7000	**3136.95**	**2,561,916.76**	**R 896,670.87**

5.9.3 Energy saved

The amount of energy and hence cost savings, is the difference between the energy utilized at constant speed and at variable speed. The developed program projects 55.8% reduction energy consumption at variable speed operation. This amounts to R1.1 million savings per annum. The projections are listed in Table 5.4.

Table 5.4: Energy and cost savings

	Energy [kWh]	Cost [R]
Throttled pump energy & cost / annum	5,799,618.74	R 2,029,866.56
Energy & cost for pump with VSD/ annum	2,561,916.76	R 896,670.87
Total energy & cost saving/ annum	3,237,701.98	R 1,133,195.69

5.10 ABB AND ESS* ENERGY SAVINGS PROGRAM COMPARISON

The same system parameters are logged into a similar program for VSD energy savings, developed by ABB. The result of the developed spreadsheet, referred to as the ESS is compared to the ABB result.

Table 5.5: ABB and ESS program result comparison

Quantity	Units	ESS Result	ABB Result
Calculated energy throttling	kWh	5,799,618.74	5,456,198.10
Throttled pump energy tolal cost /annum	Rands	R 2,029,866.56	R 1,909,669.34
Calculated energy pump with VSD	kWh	2,561,916.76	2,394,555.84
VSD energy total cost per annum	Rands	R 896,670.87	R 838,094.55
Total energy saving per annum	kWh	3,237,701.98	3,061,642.26
Total energy cost saving per annum	Rands	R 1,133,195.69	R 1,071,574.79

The total energy utilized when throttling a valve to control fluid flow is projected to be 5.8GWh by ESS and 5.5GWh by ABB. The developed program projects savings of 55.8% and ABB projects 56.1% per annum. Therefore, the two projections predict annual savings of more than 50% with an installation of variable speed drives. Observing the two right hand side columns in Table 5.5 shows that ESS values are greater than ABB's. This is attributed to slightly different assumptions that each developer used.

* ESS :- Energy Savings Spreadsheet

5.11 INVESTMENT PAYBACK PERIOD FOR TUTUKA P/S

The cost of the project consists of equipment and engineering services for system design, installation and commissioning. The investment payback calculation is based on the equipment costs quoted on the 13th November 2001 by Southern Pumps S.A. (PTY) Ltd and Siemens Automation & Drives.

The existing 1024kW induction motor is old and therefore not designed to operate through a VSD. It is therefore economically sensible to change this motor, rather than installing output filters. The recommended system equipment required, consist of an induction motor, a VSD, and a transformer. These are listed in Appendix A5.4 and their total cost is R1,186.390. Adding an estimated 20% installation and commissioning cost, the total cost projected is R1,423,668.

Depending on the project's finance method, the simple payback period could be determined as follows:

$$Y(yrs) = \frac{C(project - cost)}{S(cost - savings)} \qquad (5.12)$$

Therefore, for the project cost of R1,423,668 and annual savings of R1.1 million, the payback period is:

From Equation (5.13)

$$Y(yrs) = \frac{R1{,}423{,}668.00}{R1{,}133{,}195.69} = 1.26$$

Therefore the payback period would be 1.26 years (16 months) based on the ESS spreadsheet. The payback period based on ABB spreadsheet projections is 1.33yrs (16 months). Equation (5.13) gives a rough estimate of the payback

period. In cases where the initial project investment is a loan, which is often the case, compound interest needs to be considered. Moreover, the amount saved may decrease over the years because of factors such as equipment depreciation and an increase in energy costs.

5.12 EXAMPLE TO VERIFY THE ENERGY SAVINGS SPREADSHEET

Further verification of the developed spreadsheet's accuracy is considered. The ratings and costs of the pump, motor and selected VSDs are in Appendix A5.4, for a second case study.

5.12.1 Cost of energy for constant speed operation

The amount of energy utilized is approximately 284MWh, amounting to R99.400.00 per annum at constant speed operation. The actual projected energy consumption and costs are tabulated in Table 5.6 for the LDC in section 5.3.

Table 5.6: Electrical power cost per annum: Constant speed operation

LDC Load	Hrs	POWER SUPPLY kW	ENERGY kWh	ENERGY COST
30%	0	12.03	0.00	R 0.00
40%	350	26.62	9,315.88	R 3,260.56
50%	1050	37.24	39,105.37	R 13,686.88
60%	1400	40.57	56,791.65	R 19,877.08
70%	2100	42.44	89,114.22	R 31,189.98
80%	1400	42.54	59,552.33	R 20,843.32
90%	700	43.05	30,134.48	R 10,547.07
100%	0	50.20	0.00	R 0.00
7000		**294.67**	**284,013.94**	**R 99,404.88**

5.12.2 Cost of energy for variable speed operation

The energy utilized for variable speed operation is 130.4MWh amounting to R45 600.00 per annum. In computing these figures consideration of VSD, motor and pump efficiencies are made. Table 5.7 tabulates the projected energy consumption and cost for variable speed operation.

Table 5.7: Electrical power cost per annum: Variable speed operation

LDC Load	Hrs	SUPPLY kW	ENERGY kWh	ENERGY Cost
30%	0	0.91	0.00	R 0.00
40%	350	3.92	1,373.21	R 480.63
50%	1050	10.75	11,283.44	R 3,949.20
60%	1400	15.04	21,061.54	R 7,371.54
70%	2100	20.92	43,939.69	R 15,378.89
80%	1400	23.76	33,264.16	R 11,642.46
90%	700	27.84	19,485.19	R 6,819.82
100%	0	51.22	0.00	R 0.00
7000		**154.36**	**130,407.23**	**R 45,642.53**

5.12.3 ABB and ESS energy savings program comparison

The amount of energy and hence cost savings, is the difference between the energy utilized at constant speed and at variable speed. The developed spreadsheet, ESS, projects a 54% energy consumption reduction for variable speed operation, while the ABB program projects 52.6%, see Table 5.8.

Table 5.8: Energy and cost savings

Quantity	Units	ESS Result	ABB Result
Calculated energy throttling	kWh	284,013.94	275,583.65
Throttled pump energy tolal cost /annum	Rands	R 99,404.88	R 96,454.28
Calculated energy pump with VSD	kWh	130,407.23	130,584.44
VSD energy total cost per annum	Rands	R 45,642.53	R 45,704.55
Total energy saving per annum	kWh	153,606.71	144,999.21
Total energy cost saving per annum	Rands	R 53,762.35	R 50,749.72

5.12.4 Investment payback period for the selected example

Similarly for the selected example, 20% of the equipment cost is added for installation and commissioning. Hence the cost projected is R110.336.40. The required equipment and costs are listed in Appendix A5.4. The developed program projects a payback period of 2.07yrs (25 months) and the ABB program projects 2.19yrs (27 months).

5.13 CONCLUSIONS

A method for determining energy savings for the application of VSDs to centrifugal loads is presented. A spreadsheet program is developed to determine the energy savings. With a knowledge of equipment specifications and system requirements, payback periods are projected. A case study using condensate extraction pumps, at Tutuka power station in Standerton, is undertaken.

The projected energy savings using the developed spreadsheet are 3,237,702kWh/ yr and amount to R1.133.196.00/ yr. The results are compared and verified by using a similar package by ABB. The savings projected by ABB automation and drives spreadsheet are 3,061,642,26kWh/yr amounting to

R1.071.574.79/yr. Both projections correlate, because ESS projects 55.8% savings and ABB projects 56.1% savings.

The calculated payback period is 16 months for both the ESS and ABB spreadsheets. Furthermore, a hypothetical example using real quoted equipment costs, is presented and the results correlated between the ESS and ABB energy calculation spreadsheets.

Moreover, it is observed that the larger the VSD candidate plant, the larger the potential for energy savings. Hence, the payback period for the Tutuka condensate extraction pumps is shorter (16 months) than that of the second case study.

A spreadsheet capable of projecting energy savings and the corresponding payback period has been successfully developed and verified.
This can be used for the Demand Side Management initiatives to confirm and propose efficient use of electricity by industry. Moreover, this will result in real financial savings and optimum plant operation. Plant life will be extended due to an improved and efficient operation.

CHAPTER SIX

Conclusion and Recommendations

6.1 CONCLUSIONS

Based on the findings the following conclusions are drawn:

6.1.1 LITERATURE SEARCH

For a given voltage unbalance the corresponding current unbalance can be much higher [5]. Excessive current unbalance increases current harmonic distortion, which can overload building wiring and transformers. This can trip protection circuits, even though the average current is well below the current rating of the VSD [7]. Moreover, non-characteristic third harmonic currents and poor power factor are typical consequences of unbalanced VSD line currents [5]. Voltage unbalance causes additional loads on utilities resulting in additional charges for consumers [9]. Therefore reducing system unbalance improves the ability of the power system to meet its load.

6.1.2 TEST BED DEVELOPMENT

Two test beds were constructed and commissioned. Several operating points were analytically computed and verified by measurements. Therefore IM performance curves can be used to determine accurately, the shaft torque for a given speed with knowledge of the system curve (load curve). Moreover the system losses were measured and documented.

6.1.3 DRIVE MODEL DEVELOPMENT AND SIMULATION

The three-phase mains supply at the University of Cape Town Machine's Laboratory is distorted and unbalanced. This represents practice where an acceptable unbalance is always present in a distribution network.

A PSpice model has been successfully developed and correlated with test measurements for balanced voltage supplies. Furthermore, the model was also tested for simulating the impact of voltage unbalance on IM drives. The results were compared and verified with test measurements.

CHAPTER SIX

Conclusion and Recommendations

Percentage unbalance as low as 2% can cause considerable increase in the rectifier input peak currents. The rectifier current peak at balanced conditions can increase by 58%. The voltage unbalance may seem small, but the effect it has on current is greater. At 3%, 4% and 5% voltage unbalance, additional increase in the rectifier current occurs.

The dc-link voltage characteristic is distorted in the presence of voltage unbalance, resulting in an increase in the average dc-link voltage. The output voltage of the inverter is balanced, despite the presence of voltage unbalance on the supply. As a result the line currents drawn by the motor are also balanced.

6.1.4 IMPACT OF CABLES IN PWM VSD'S

A PSpice drive-cable-motor model that simulates the reflected wave phenomenon was developed. Furthermore, the effects of cable length on the operation of a PWM drive in the presence of voltage unbalance are simulated and verified through measurements.

Two cable models are used, a lumped RLC model and a variation to allow for modeling the standing waves. The lumped RLC model is found to be inadequate for predicting the correct volt-drop across the cable. As a result, adding an RLC branch in parallel with the existing sector branch proves to be sufficient. A resonant tank IM model is used. The parameter determination is challenging, but, assumptions were made which led to estimated parameter values, based on the measurable quantities.

The dc-link voltage is not affected by the varying cable length. That is, the no-cable condition renders similar results as the long cable conditions for the dc-link voltage, inverter current, motor terminal current and the dc-link ripple.

Furthermore, it is concluded that the proposed resonant tank motor model and the modified cable model can be adequate to correctly and accurately predict the reflected wave phenomenon and other associated effects.

6.1.5 ENERGY SAVINGS OF A PUMP DRIVE

A correct method for determining energy savings for the application of VSDs to centrifugal loads is presented. A spreadsheet is developed to determine the energy savings and payback periods. A case study using, condensate extraction pumps at Tutuka power station, Standerton, is undertaken. The results are compared and verified by using a similar package by ABB.

The calculated payback period is 16 months projected by both spreadsheets. Furthermore, a hypothetical example using actual quoted equipment costs is presented and the results correlated between the developed spreadsheet and ABB energy calculation spreadsheet. Moreover, it is observed that the larger the VSD "candidate" plant, the larger the potential for energy savings. Hence, the payback period for the Tutuka condensate extraction pumps is shorter (16 months) than that of the selected example, at (25 months).

This can be used for the Demand Side Management initiatives to confirm and propose efficient use of electricity by industry.

6.2 RECOMMENDATIONS

Based on the above conclusions the following recommendation are made:

6.2.1 LITERATURE SEARCH

Develop a table or curve that relates percentage voltage unbalance to the corresponding current unbalance for benchmarking equipment current ratings for operating under unbalance voltage conditions.

6.2.2 TEST BED DEVELOPMENT

Upgrade the test beds to impose unbalance voltage with phase unbalance capability, and also for transient testing.

6.1.3 DRIVE MODEL DEVELOPMENT AND SIMULATION

PSpice has limitations when simulating the performance of variable speed drives. Simulink will allow improved VSD performance simulation.

6.1.4 IMPACT OF CABLES IN PWM VSD'S

Investigate the causes of greater than 2pu reflected voltage wave. Consider methods of eliminating or minimizing the reflected voltage peak.

6.1.5 ENERGY SAVINGS OF A PUMP DRIVE

Use the developed program for retrofits and new energy efficiency initiatives projects in ESKOM Demand Side Management.

REFERENCES

[1] M. Mohan, "Improvement in Energy Efficiency of Induction Motors by means of Voltage Control", IEEE Transactions on Power Apparatus and Systems, vol. PAS-99, No. 4 July/ Aug. 1980, pp. 1466-71.

[2] D. A. Rendusara, A. von Jouanne, P. N. Enjeti, D. A. Paice, " Design Considerations for 12-Pulse Diode Rectifier Systems Operating under Voltage Unbalance and Pre-Existing Voltage Distortion with Some Corrective Measures", IEEE Trasaction on Industry Application, Vol. 32, No. 6, November/ December 1996.

[3] SIEMENS Power Engineering Guide, Industrial Applications

[4] V.J. Gosbell, D.L. Rose, D.R. Irvine, "Survey of Variable Speed Drive Application in Power Stations" Journal of Electrical and Electronics Engineering, Australia, Vol. 12, No. 4, December 1992, pp. 371-7.

[5] Electric Power Research Institute, "Mitigating the Effects of Line-Current Unbalance on Adjustable-Speed Drives" Power Quality Testing Network Brief, Application No. 1, September 1995.

[6] T.F. Lowery, D.W. Petro, "Application Considerations for PWM Inveter-Fed Low-Voltage Induction Motors" IEEE Transactions on Industry Applications, Vol. 30, No. 2, March/April 1994, pp. 286-93.

[7] J. Stones, A. Collinson, "Power Quality", IEE Power Engineering Journal, Vol. 15, No. 2, April 2001, pp. 58-64.

[8] Glover, Sarma, "Power System Analysis & Design" 2nd Edition, 1998, pp. 49-71

[9] Ching-Yin Lee, "Effects of Unbalance Voltage on the Operation Performance of a Three-Phase Induction Motor", IEEE Transaction on Energy Conversion, Vol. 14, No. 2, June 1999, pp. 202-8.

REFERENCES

[10] Mohan, Undeland, Robbins, "Power Electronics" 2nd Edition, 1995

[11] Wallace A.K., Rollman T.E., "High Efficiency Laboratory for Motors, Drives & Generators", Power Electronics and Variable Speed Drives, 23-25 September 1996, IEE Conference Publication No. 429, pp 220-5.

[12] Ron Carlson, "The Correct Method of Calculating Energy Savings to Justify Adjustable-Frequency Drives on Pumps", IEEE Transaction on Industry Applications, Vol. 36, No. 6, November/December 2000, pp-1725-1733.

[13] J. A. Oliver, Adjustable Speed Drives, Application Guide, Electrical Power Research Institute, "EPRI", California 1992.

[14] J.M. Bodson, J.M. De Hoe, "Energy Savings with Variable Speed Drives", Asia Beown Boveri, Belgium, pp. 5.16.1-6.

[15] G. Roger, P.E. Lawrence, "User Benefits Obtained from AC Variable Speed Drives" 29th Annual Petroleum and Chemical Industry Conference, IEEE, New York, USA, 1982, pp. 169-73.

[16] Benz J.A., Henry R.E. and Roberts D.A., "Economic and Operational Benefits for Retrofitting Variable-Speed Drives" Proceedings of the American Power Conference, Illinois Institute Technol, Chicago, USA. 1994, Vol. 2, pp. 1405-10.

[17] Saunders L.A., Skibinski G.L., Evon S.T., Kempkes D.L., " Riding Reflected Wave-IGBT Drive Technology Demands New Motor and Cable Considerations", IEEE IAS-Petroleum & Chemical Industry Conference, Philadelphia, PA., Sept. 23-25, 1996 pp. 75-84.

[18] Kerkman R., Leggate D. and Skibinski G., "Interaction of Drive Modulation & Cable Parameters on AC Motor Transients", Rockwell Automation-Allen Bradley Standard Drives Business.

[19] Ren T. and Pillay P., "Over-Voltage in High dv/ dt Inverters" Masters Dissertation Report, Department of Electrical and Computer Engineering, Clarkson University, Potsdam, New York 13699.

[20] Skibinski G., Kerkman R., Leggate D., Pankau J. and Schlegel D. " Reflected Wave Modeling Techniques for PWM AC Motor Drives" Rockwell Automation-Allen Bradley Standard Drive Division, 6400 W, Enterprise Drive PO Box 760, Mequon, WI 53092.

[21] Leggate D., Pankau J., Schlegel D., Kerkman R. and Skibinski G. "Reflected Waves and Their Associated Current" Rockwell Automation-Allen Bradley Standard Drive Division, 6400 W, Enterprise Drive PO Box 760, Mequon, WI 53092.

[22] Karakash J.J., "Transmission Lines and Filter Networks" The MacMillan Company, New York, 1950.

[23] Schlegel D., Wrate G., Kerkman R. and Skibinski G. "Resonant Tank Motor Model For Voltage Reflection Simulations With PWM Drives", IEEE IEMDC digest, 9/ 30/ 98, pp. 463-5.

APPENDIX A2

A2.1 Low power test bed equipment specifications

Table A2.1: AC circuit nameplate

AC CIRCUIT			
Induction motor		**Drive**	
		Input	**Output**
V[V] =	380	380-415	380-460
I[A] =	6.5		16
P[kW] =	3		7.5
ω [rpm] =	1415		
f [Hz] =	50/ 60	50	0-100

Table A2.2: DC circuit nameplate

DC CIRCUIT			
DC motor		**Rectfier**	
		Input	**Output**
V[V] =	220	380	400
I[A] =	15	35	40
P[kW] =	2.6		16
ω [rpm] =	1480		

Table A2.3: Load cell nameplate

Load cell	
Capacity =	50 kg
Signal =	2 mV/ V

A2.2 Medium power test bed equipment specifications

Table A2.4: IM Nameplate

P =	75kW
V =	380V
I =	144
ω =	960RPM
Insulation class	F
Poles	6
Duty	S1

Table A2.5: 75kW IM drive nameplate

	ALSTOM ALSPA MV3000	
	Input	Output
Voltage	380-440	0-380-440V
Current	145A	140A/ 105A
Frequency	45-63Hz	0-200Hz
Power		75kW

APPENDIX A3

A3.1 Load model

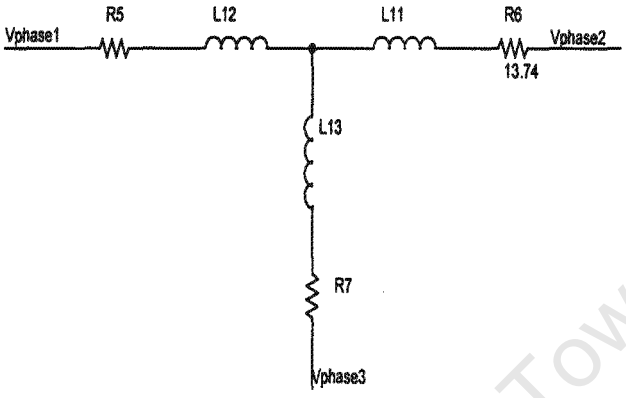

Figure A3.1: Three-Phase Induction Motor in Star Connection load model

A3.2: Unbalanced three-phase voltages used in the parametric study.

Table A3.1: Three-phase line-to-line voltages as a function of unbalance

LUVR %		RMS [V]	Angle [deg]
0	Vab =	380	0
	Vbc =	380	240
	Vca =	380	120
1	Vab =	381	0
	Vbc =	376.18	119.52
	Vca =	381.85	239.04
2	Vab =	383.83	0
	Vbc =	372.33	119.02
	Vca =	383.84	238.02
3	Vab =	385.84	0
	Vbc =	368.42	118.52
	Vca =	385.74	237.05
4	Vab =	387.76	0
	Vbc =	364.48	118.04
	Vca =	387.76	236.01
5	Vab =	389.78	0
	Vbc =	360.5	117.52
	Vca =	389.68	235.19

A3.3: Diode currents

Rectifier current waveforms through each top diode as a function of line unbalance voltage ratio.

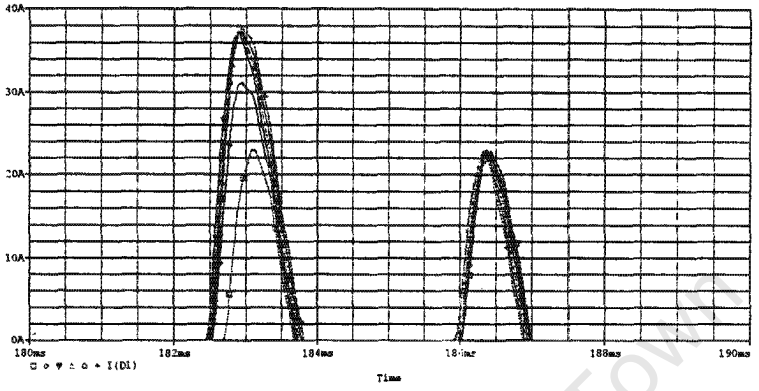

Figure A3.2: Diode D1 current from zero to 5% LVUR

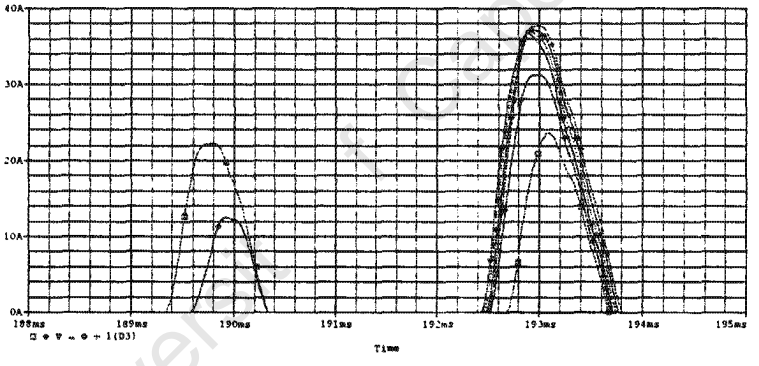

Figure A3.3: Diode D3 current from zero to 5% LVUR

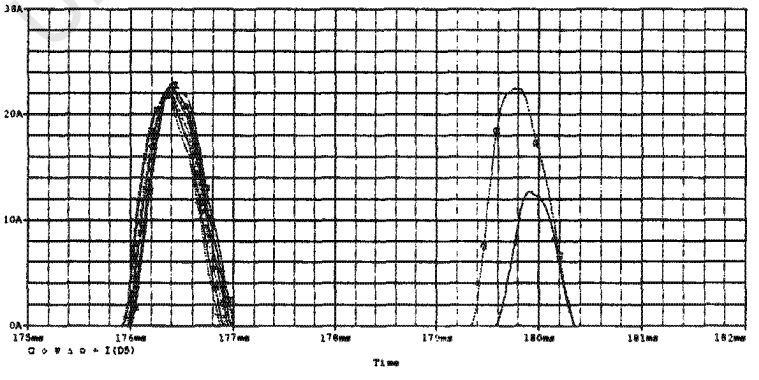

Figure A3.4: Diode D5 current from zero to 5% LVUR

APPENDIX A4

A4.1: Dc-step response for an uncharged cable

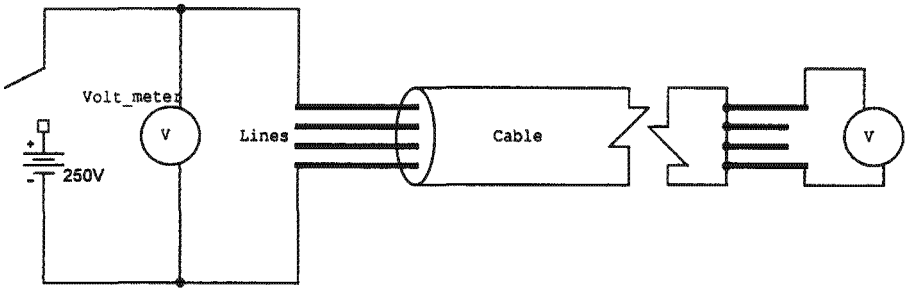

Figure A4.1: Dc-step response test schematic

A4.2: Unbalance voltage supply from the Mains with 2.4% unbalance and 3.8% over voltage.

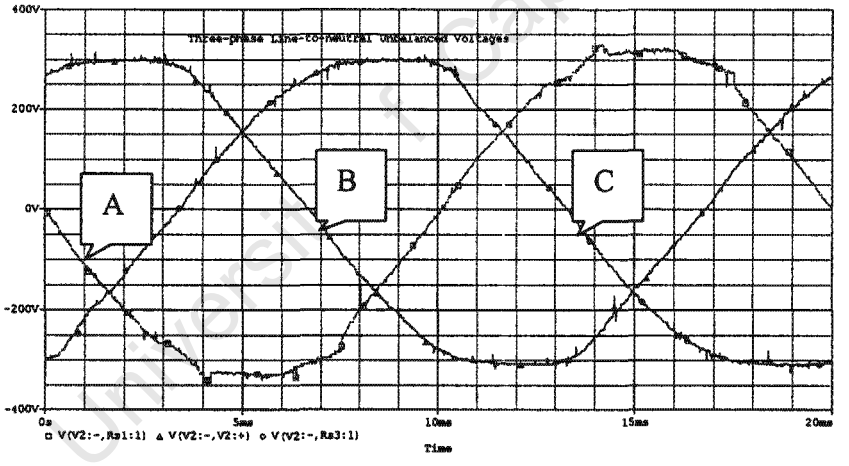

Figure A4.2: Line-to-neutral three-phase unbalanced supply voltage

APPENDICES A5

A5.1: AllWeiler pump specs

PUMP MODEL **32-160**

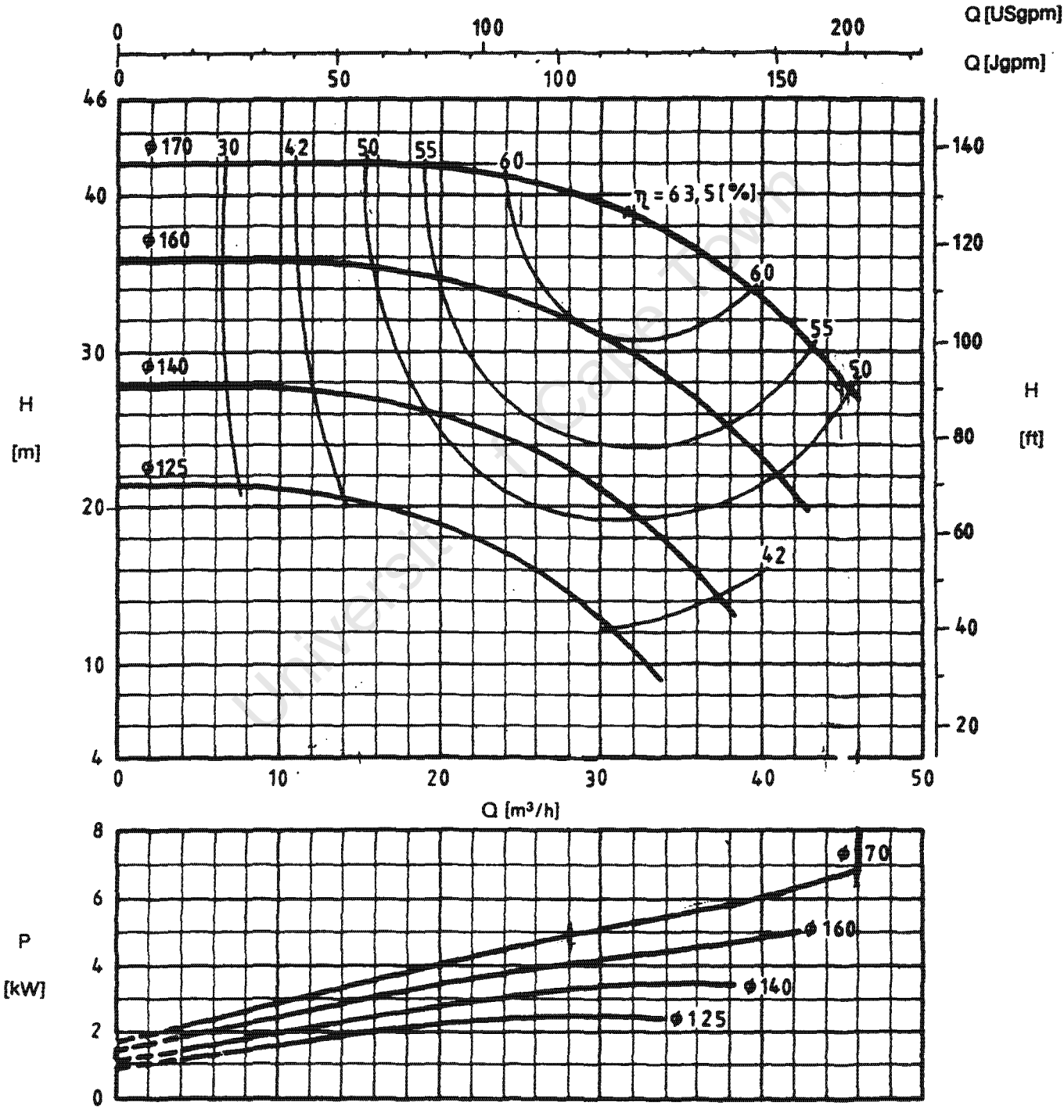

A5.2: Tutuka power station condensate extraction plant specifications

1. Pump type: 400/ 600 Two stage vertical caisson

- Flow :1600m^3/hr
- Head :160m
- Nominal :1500rpm
- Efficiency :80%
- Maximum shut-in head :221m
- Power absorbed :872kW
- NPSH; Net Positive Suction Head :5.6m

2. Induction motor: Cage induction, JKC 450/5

- Manufacturer :GEC machines (Alstom)
- Enclosure :drip proof IP22
- Supply voltage :3.3kV 3-phase-50Hz
- Rated output :1025kW
- Full load current :211A
- Rated speed :1486 rpm

A5.3: User interface input tables

Table A5.1: Parameter input window

	QUANTITY	UNITS	VALUE
1	Liquid density (water =1)	ρ (κγ/μ3)	1000
2	Pump nominal flow	Qn (m^3/h)	200
3	Nominal head of the pump	Hn (m)	70
4	Pump maximum head (at zero flow)	Hmax (m)	84
5	Static head of the system	Hst (m)	5
6	Nominal efficiency of the pump	ηπ (%)	80
7	*Head over open throttle valve*	*Hv (m)*	5
8	Rated power of motor	P1 (kW)	55
9	Supply and motor voltage	V (V)	380
10	Rated motor speed (induction machine)	RPM	2965
11	Motor full load current	A	100
12	Nominal efficiency of the motor	ημ(%)	95
13	Nominal efficiency of the VSD	ηωσδ (%)	98
14	Total operating time per year	Tk (hrs)	7000
15	Price of energy per kWh	Rands	0.35

Table A5.2: Spreadsheet LDC input table

Flow	m^3/h	Time (%)	Hours	Load (%)
30%	480	0	0	30
40%	640	5	350	40
50%	800	15	1050	50
60%	960	20	1400	60
70%	1120	30	2100	70
80%	1280	20	1400	80
90%	1440	10	700	90
100%	1600	0	0	100
Total sum		100	7000	

A5.4: Equipment and costs for the Tutuka Power Station Condensate Extraction Pumps

Table a5.4: Equipment costs for the first case study

Type Number	Description	Nett Price
6SE7141-1HJ62-4BA0	1000 kW 690V MASTERDRIVE CABINET UNIT	1*R 695,946.00
MOTOR	1100 kW 4 POLE 690V INDUCTION MOTOR	1*R 290,444.00
TRANSFORMER	1600kVA 3.3kV/ 690V	1*R 200,000.00
	Sub tolal (VAT excluded)	**R 1,186,390.00**

A5.4: Equipment and cost for the example selected by Southern Pumps SA (Pty) Ltd.

Table a5.5: Equipment log for the second case study

Item	Qty	Description	Nett Price
1	1	380V/ 75kW MASTERDRIVE/ 6-PULSE DIODE	R 53,115.00
2	1	75kW/ 2POLE IP55 cast iron 380/3/50 INDUCTION	R 26,240.00
3	1	STORK MODEL CEN 100-250 CENTRIFUGAL PUMP	R 9,458.00
4	1	FENNER TYPE CLOSED COUPLING	R 3,134.00
		Sub tolal (VAT excluded)	**R 91,947.00**